Investigation of Quark Gluon Plasma-like signals with Lund string interactions

Chakraborty, Smita

2022

Investigation of Quark Gluon Plasma-like signals with Lund string interactions

SMITA CHAKRABORTY
FACULTY OF SCIENCE | LUND UNIVERSITY

Investigation of Quark Gluon Plasma-like signals with Lund string interactions

Investigation of Quark Gluon Plasma-like signals with Lund string interactions

by Smita Chakraborty

LUND
UNIVERSITY

Thesis for the degree of Doctor of Philosophy
Thesis advisors: Prof. Leif Lönnblad
Faculty opponent: Dr. José Guilherme Teixeira de Almeida Milhano

To be presented, with the permission of the Faculty of Science of Lund University, for public criticism in the Lundmarksalen lecture hall at the Department of Astronomy and Theoretical Physics on Friday, the 9th of September 2022 at 10:00.

Organization	Document name
LUND UNIVERSITY Department of Astronomy and Theoretical Physics Box 14A SE–223 62 LUND Sweden	**DOCTORAL DISSERTATION** Date of disputation 2022-09-09 Sponsoring organization
Author(s) Smita Chakraborty	

Title and subtitle

Investigation of Quark Gluon Plasma-like signals with Lund string interactions

Abstract

This thesis investigates the interactions that occur in extreme densities for high-energy collisions of subatomic particles. The theoretical models developed for this purpose are based on the Lund model. The developments have been implemented as a new module called Gleipnir to the Monte-Carlo event generator, PYTHIA. The two models developed are string shoving and rope hadronization, and can now be used for proton-proton, proton-nucleus and nucleus-nucleus collisions.

Paper I presents a novel method to calculate string shoving in all systems. The strings are considered as colour flux-tubes, with colour electric fields with transverse extent. The force between two colour flux tubes is calculated in a special Lorentz frame called the parallel frame. Final state collectivity reproduced by string shoving is investigated in both small and large systems. We conclude that further modifications to string shoving are required to be able to produce a better agreement with experimental data for large systems.

Paper II presents the rope hadronization mechanism using the parallel frame. Rope hadronization would modify the strangeness yields, and this effect can be observed in jets as well. The system of interest is jet-triggered proton-proton collisions, where we probe the yields of strange hadrons and baryons in a jet. We find significant enhancement of strangeness, particularly strange baryons in the jet.

Paper III shows the enhancement in strangeness yields with rope hadronization in all systems, using the techniques introduced in Paper I and Paper II. The formalism produces significant improvements over default Pythia and Angantyr. To be able to reproduce a better agreement to data, further modifications are necessary, such as the inclusion of string shoving mechanism.

Paper IV describes the correction to production vertices of primary hadrons from string interactions for both small and large systems. The impact from string shoving is found to be higher than compared to rope hadronization. This would influence other PYTHIA processes that build on primary hadronic vertices such as hadronic rescattering.

Key words

QCD, Phenomenology, QGP-like signals, Proton-proton collisions, Heavy-ion collisions, Jets

Classification system and/or index terms (if any)

Supplementary bibliographical information	Language
	English
ISSN and key title	ISBN
	978-91-8039-348-5 (print) 978-91-8039-347-8 (pdf)
Recipient's notes	Number of pages: 200 / Price
	Security classification

Investigation of Quark Gluon Plasma-like signals with Lund string interactions

by Smita Chakraborty

LUND
UNIVERSITY

A doctoral thesis at a university in Sweden takes either the form of a single, cohesive research study (monograph) or a summary of research papers (compilation thesis), which the doctoral student has written alone or together with one or several other author(s).

In the latter case the thesis consists of two parts. An introductory text puts the research work into context and summarizes the main points of the papers. Then, the research publications themselves are reproduced, together with a description of the individual contributions of the authors. The research papers may either have been already published or are manuscripts at various stages (in press, submitted, or in draft).

Cover illustration front: Abstract image of two Lund strings between two partons flying out after a collision in the laboratory frame.

Cover illustration back: Plot of strangeness enhancement from research Paper III.

Funding information: The thesis work was funded in part by the Knut and Alice Wallenberg foundation, contract number 2017.0036, Swedish Research Council, contracts number 2016-03291, 2016-05996 and 2017-0034, in part by the European Research Council (ERC) under the European Union's Horizon 2020 research and innovation programme, grant agreement No 668679, and in part by the MCnetITN3 H2020 Marie Curie Initial Training Network, contract 722104.

Faculty of Science, Department of Astronomy and Theoretical Physics

ISBN: 978-91-8039-348-5 (print)
ISBN: 978-91-8039-347-8 (pdf)

Printed in Sweden by Media-Tryck, Lund University, Lund 2022

To my mother

Popular summary in English

All visible matter is made up of stable atoms. As we have discovered in the 20^{th} century, atoms have substructures and consist of nuclei and orbitals of electrons. An atomic nucleus consists of one or more subatomic particles called protons and neutrons. Each proton and neutron (together called *nucleons*) can be further split into quanta of fractional electric charge and with another unique set of charges, called the colour charge. These particles are called *quarks* and they interact via exchanging particles called *gluons*. This unique force is called the strong force. Just as we have electrodynamics describing the physics of electric charges, we have *Quantum Chromodynamics* (QCD) describing the mechanics of the strong force.

The oldest form of matter to have existed in the Universe is called the Quark-Gluon Plasma (QGP). Immediately after the Big Bang, our Universe was filled with very high-energy particles in a small space under immense pressure. Before the Universe started to cool down to form local clusters and galaxies, in the extremely hot and small space, the quarks and gluons were in a fluid/soup form that we will probably never see with our eyes. This is not only because they are extremely small, but also because they were at a very high temperature. This free-flowing collection of particles with high energy density existed for $\sim 10^{-10} - 10^{-5}$ seconds after the Big Bang. This plasma state of matter is known to be a nearly "perfect liquid" owing to its very low viscosity, that is, low resistance to flow.

In particle colliders, such as the Large Hadron Collider (LHC) at CERN, Geneva, scientists collide elementary particles, such as the proton, to understand Nature and how it behaves in extreme environments. These proton-proton collisions are described very well by QCD models that do not involve a QGP phase.

Now we compare the QGP state - the extremely short-lived, high-energy and high density state - to the collisions at the LHC at CERN. The way we try to achieve this state of matter at the LHC is by colliding heavy-ions that have spherical nuclei, such as Xenon or Lead ions. Such collisions create events that can be "Little Bang"s, extremely short-lived copies of our Big Bang, that may create extremely short-lived QGP. As mentioned before, the QGP state is dominated by quarks and gluons, so their interaction is described by QCD. This phase behaves like a fluid in thermal and chemical equilibrium and exhibits an overall collective behaviour. So it might be fitting to be described by a macro approach by using one equation of state to describe the entire system. These models work well for heavy-ion collisions.

On the other hand, we have observed QGP-like footprints in proton-proton collisions - which just does not align with their dynamics at all. Protons are extremely small particles with a radius around $\sim 10^{-15}$ m. In contrast, we have huge nuclei of Xenon and Lead whose radii are 5-7 times larger than that of the proton nucleus, therefore, are extended in space in contrast to protons. Therefore, the question is: how can things like protons that have negligible spatial extent give rise to signals that require spatial extensions as their cause?

Hence, the particle physics community has performed rigorous measurements to match up the observations going from proton-proton collisions to nuclear collisions. QCD is universal, thus the description should not depend on whether we go towards nuclear collisions starting from proton-proton collisions or vice versa. Therefore, a link is missing between the two types of collisions. This is what we try to solve in this thesis.

We work with an established model, called the Lund string model that has successfully described electron-positron (the antiparticle of electron) and proton-proton collisions for many years now. To put it simply, the model says that the force between two quarks can be imagined by a classical string, much like a thin elastic band. The model also has several advanced features.

The Lund model could be further developed for heavy-ion collisions only if we tell the strings how to interact with each other when they are close by. That is what we do in this thesis - redefine the Lund strings' colour field with a shape and size, much like an electric field, and let them interact. We see that doing so gives us similar signals as seen by a fluid-based approach to heavy-ions and proton-proton collisions. This is astonishing since it means that the string approach could be our missing link going from proton-proton to nuclear collisions, which does not require QGP to be formed even in heavy-ion collisions. This challenges the idea of QGP formation. The Lund model hence can have more fundamental properties tied to it than we have seen in the past.

The overarching aim of this thesis is to understand the origin of QGP-like signals in all systems using the Lund model. This work is done in different categories in the 4 publications in this thesis. We review and explain the research done in those 4 papers, more elaborately in the introduction to the thesis.

In midst of what is known, I have sought the unknown.
— Rabindranath Tagore (translated)

Contents

Introduction

To understand the Universe and the components it is made of, humans have devised remarkable probes. Many of them look out in the vast space - stationed on Earth or as a satellite - to search for how the Universe and the astronomical objects in their present form were formed and how they evolved. However, Nature also needs to be studied in the greatest detail. For that, we have built the most precise instruments on Earth, where we create a similar environment as was formed in the first few microseconds after the Big Bang. An example of precision experiments on Earth is the Large Hadron Collider (LHC) in Geneva, Switzerland.

One of the tasks that the LHC performs is to collide the smallest stable particles. Such particles, such as protons, are stable and they are composite particles made of even smaller particles that interact with each other very strongly. It is impossible to observe their unstable constituents on their own in Nature. The only way to 'look' inside them is to collide protons at very high energies to break them apart. The proton, for example, consists of three *quarks*. After the collision between two protons, we look at the resulting ensemble of quarks and *gluons* which hold the quarks together – jointly known as *partons*.

Particle physics & the Standard Model

Particle physics is the branch of physics which describes the subnuclear constituents and their interactions. Although we have been successful in understanding different behaviours of such nuclear and subnuclear particles at different energy scales, there are still big challenges to our current knowledge. The robust foundation of all particle physics research is the Standard Model that has been able to describe most

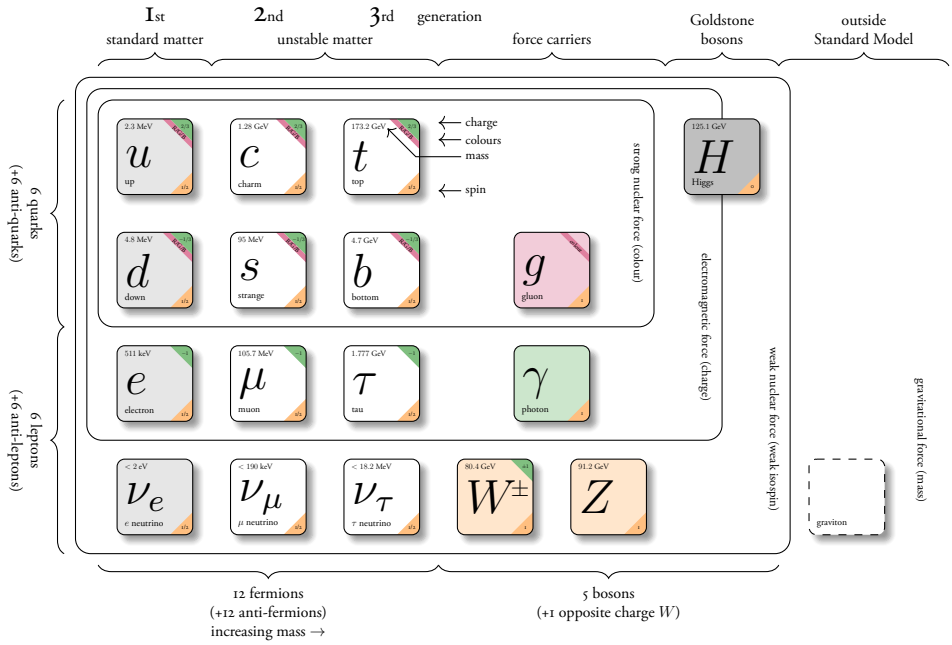

Figure 1: Particles of the Standard Model of Particle Physics. Some of their properties and the forces they interact with are labelled.

components of matter that we observe. In the Standard Model, shown in figure 1, there are 16 *elementary particles* - 12 of them are *fermions* and 4 of them are *gauge bosons*. The fermions are classified into 6 quarks and 6 leptons. The gauge bosons are carriers of the three Standard Model interactions, as shown in Table I. The strengths and range of the different forces are also shown for completeness.

The photon (γ) is the mediator of the electromagnetic force, the gluon (g) is the mediator of the strong force, and the $W^{\pm}$ and Z^0 bosons are the mediators of the weak force. The Higgs boson (H) is responsible for the mass of fermions and W/Z bosons. For each particle, there exists an antiparticle with the same mass but with opposite *quantum numbers*. Quantum numbers are the values of quantized physical properties for particles in the quantum scale. Some particles, such as photons, are their own antiparticle. Now, we should note that not all particles are involved in each of the forces, it is only the particles which have the specific form of *charge* that can interact with the other particles with the same class of charges. Every particle or antiparticle follow *conservation laws* of physical properties of the corresponding force. This is true for Quantum Electrodynamics (QED) which describes the elec-

tromagnetic force between particles with electric charges, and the weak force acting between weakly charged particles, and in Quantum Chromodynamics (QCD).

Only 5% of the Universe's total energy is visible matter [1], and 99% of the visible matter is described by QCD. The Standard Model still has its shortcomings, one of those is the fact that there are observations which it cannot describe. One such example is dark matter, which makes up $\sim 85\%$ of all matter in the Universe and can only be detected due to its gravitational interaction. Yet we do not know the exact way to modify the Standard Model to be able to explain such components of our Universe.

Table 1: The Standard Model Forces

Force	Carrier	Strength	Distance range
Electromagnetic force	photon (γ)	$\frac{1}{137}$	long ($\propto 1/r^2$)
Weak force	W and Z boson	10^{-6}	10^{-17} m
Strong force	gluons (g)	1	10^{-15} m

The subject of this thesis is the physics of the *strong force*, one of the Standard Model forces. Quantum Chromodynamics (QCD) is the theory of *strong interaction* among quarks and gluons, which are particles with a charge called *colour*. The strong force is responsible for holding the protons and neutrons (nucleons) in an atomic nucleus together. The strong interaction is prominent at distances around 10^{-15} m (of the order of the proton radius) and has a varying magnitude depending on the distance between the two interacting particles. This varying behaviour of the strong force can be parameterized by the scaling parameter, which is known as the strong coupling α_s. The value of α_s which determines the strength of the interaction among the different partons is crucial in deciding how we choose to model them. The value of the α_s is lower at high energies (Q^2), which implies that the strong interaction is weaker at such scales, so one can apply perturbative techniques to study the system. This regime is known as the *perturbative* QCD (pQCD) scale. For high values of α_s (at low energy), the strong interaction dominates and quarks cannot be separated due to *confinement*. This is known as the *non-perturbative* QCD (non-pQCD) scale. The difference between these regimes depends on the strength of interaction between the partons in a proton. The variable value of α_s also earns it the name of *running* α_s.

[1] interacts with each other or reflects light.

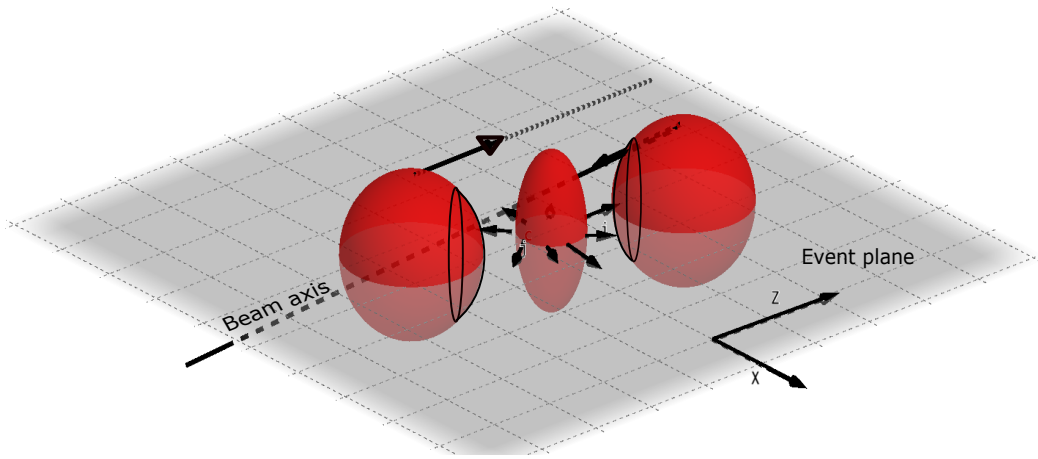

Figure 2: Illustration of a 3-dimensional nucleus-nucleus collision, showing the beam axis and the event plane, further discussed in section 4.

Due to the high values of α_s in the non-pQCD regime at low energy scales of particles, calculating QCD cross-sections becomes difficult. Hence, several models have been devised to explain the behaviour of the particles at these energy scales. One such model is the *Lund string model*, first proposed in 1979. In the Lund model, the colour electric force F between a quark (q) and an antiquark ($\bar{q}$) pair is approximated by a string with $F = \kappa r$, where κ is the string tension and r is the distance between the q and $\bar{q}$. We discuss the Lund model in details in section 2.

Motivation for this thesis

In this thesis, we have studied heavy-ion (HI) collisions or nucleus-nucleus collisions (A-A), such as lead-lead (Pb-Pb) and xenon-xenon collisions (Xe-Xe), in most of the publications. Before we describe the motivation for this thesis, we present briefly how a HI event will look like. For that we return to the processes studied at the LHC and other collider experiments, where they also smash two spherical nuclei of the same element, which we refer to as HI collisions. The evolution of the colliding system in A-A collisions is in contrast to proton-proton (p-p) collisions due to the larger spatial extent of nucleus.

In a typical A-A collision, each of the participating nuclei become “flat pancake”

in the laboratory frame due to Lorentz contraction. Depending on whether such a collision is a direct (central) or a marginal (peripheral) collision, the final-state behaviour of the outgoing particles will vary. One such unique behaviour is the anisotropy in the particle momentum distribution over a large span of space, referred to as the elliptic flow. The origin of this behaviour lies in the initial asymmetry in the geometry of the overlap between the two incoming spherical ions, as shown in the figure 2. Depending on how much is the initial overlap between the nuclei volumes in 3 dimensional space, the pressure gradient in the overlap area will vary. So the almond shape overlap region in 3-d space gives rise to anisotropy in the momentum space, which influences the transverse expansion of the medium. This is considered as one of the signals of the strongly interacting *Quark Gluon Plasma* (QGP) formed in semi-central to peripheral heavy-ion collisions [1] [2]. We will discuss this in more detail in sections 4 and 5.

The Quark-Gluon Plasma has been observed to behave like a *nearly perfect liquid*. This implies that it has special properties such as a very low internal resistance to flow (*i.e.* very small viscosity). An interesting thought experiment to describe QGP's other unique features is to consider a spherical ball of QGP. Now if we shine a torch through this sphere, we would see that the light beam is refracted on the same side as the incident light beam, much similar to reflection but with certain peculiar characteristics. This is because QGP is believed to have a negative refractive index[3] [3].

In this thesis, we focus on how the Lund string model can describe the unique physical observations observed for high-density systems. In the Lund model, there is no QGP phase. In earlier studies, the interactions between Lund strings, which we discuss in section 5, have been observed to play a significant role in hot and dense systems of high-multiplicity p-p collisions. So it became clear that the physics of the p-p collisions is also important for heavy-ion collisions. That is the major aim of this thesis - *to develop and understand the string interactions in both p-p and A-A collisions*. If the string interactions reproduce such observations in high-multiplicity p-p and HI collisions, such as anisotropic flow, that would imply that such effects can be observed without QGP formation.

The main methodology used in this thesis is the development and use of *Monte Carlo event generators*, specifically the PYTHIA event generator. Since the 1970s, the

[2] Also in some central collisions [2].

[3] The refractive behaviour is dependent on the frequency of the electromagnetic waves and the polarization of the EM waves upon refraction from QGP might be changed as well.

endeavour of theoretical physics to describe all observations in pen and paper was superseded by numerical computations . Hence, the age of Monte Carlo event generators started which became popular in both theory and experimental community. In the work done as part of this thesis, we have implemented the string interactions in the Monte Carlo event generator *PYTHIA* and Angantyr, in a new model called *Gleipnir*. Therefore, this thesis might as well be called "Simulating physics with computers", which is already an article written by Richard Feynman [4].

This thesis contains two parts, one is the "Introduction" where we present the background physics for the work done in the second part - the publications. In this introduction to the thesis, we will lay out the foundations of the physics. We will discuss QCD in more detail in section 1, present the Lund string model in section 2, and the PYTHIA event generator in section 3. In section 4, we review heavy-ion collisions and QGP-like signatures in hot and dense systems. Finally, in section 5, we discuss the main components of this thesis – the interactions between Lund strings. We study two string interactions in further detail – string shoving and rope hadronization - while reviewing their contribution to generating QGP-like signals in both small and large systems. Finally, in the outlook, we present some of the open questions that lie ahead in the p-p and heavy-ion community in light of the work done in this thesis.

1 Quantum Chromodynamics

To describe QCD, we start with an analogy to Quantum Electrodynamics (QED). In QED, there is an electric charge, which can be either positive or negative. A negatively charged particle will attract (repel) another positively (negatively) charged particle. Similarly in QCD, we have colour charges. For the strong force or *colour force*, the number of *colour charges* is instead 3, and they are denoted by *red* (r), *blue* (b) and *green* (g) and their corresponding anti-colours, called anti-red ($\bar{r}$), anti-blue ($\bar{b}$) and anti-green ($\bar{g}$). As mentioned in the previous section, the mediator of the strong force is *gluon* which carries both colour and anti-colour charges, in contrast to the photon, therefore experiences the strong force itself. As we notice in Table I, the range over which this force is dominant is around the femtometre scale ($\sim 10^{-15}$ m), which means that only subnuclear particles can interact via the strong force.

In Nature, the stable particles are *colour neutral*, such as protons. Colour neutral

particles can be further categorized into quarks (q), which come in six different flavours: up, down, strange, charm, bottom (or beauty), and top (see figure 1). Every quark flavour has a different mass. The quarks have their corresponding antiparticles called antiquarks ($\bar{q}$). Quarks have colour charge and antiquarks carry anti-colour charge.

Combining a particle with a colour charge, say r with their anti-colour partner $\bar{r}$, gives us a colour neutral or colour-singlet state and hence a stable particle. Such an example is a *meson* which is made up of a pair of quark-antiquark. One can also get a colour neutral state by combining one particle of each colour r, g and b, and similarly for anti-colours. These are called *baryons* and consist of three quarks or three antiquarks. For example, protons consist of 2 *up* quarks and 1 *down* quark.

Now the strong force has two peculiarities. We know that the stable particles are colour neutral. Also, the gluon which is the force mediator is coloured itself and hence interacts with other quarks and gluons, which is not the case for photons. This distinguishes QCD from QED. Therefore, when we try to separate a quark and an anti-quark from each other by pulling them apart, owing to the self-interactions of the gluon field between this $q-\bar{q}$ system, a new pair of quark–antiquark is formed between the original quark–antiquark pair, following mass-energy equivalence $E = mc^2$. This property of quarks that they do not exist in isolation is called *confinement*. Confinement implies that it is impossible to separate the coloured particles from a colour neutral state and is a non-perturbative property (high α_s) of the strong interaction. The other unique behaviour of strong interaction is called *asymptotic freedom*. It refers to the strength of the interaction between two partons being asymptotically weaker at high energy scales and small distances, essentially behaving as non-interacting particles. At large distances, the force between the q and the $\bar{q}$ can be expressed in the form $F = \kappa r$, where r is the distance between the quark-antiquark pair, and κ is the "string tension" between the two quarks. The behaviour of the force can be interpreted as a string between two quarks. This string also has a transverse extension, and can be imagined as a "flux tube" [5–7]. In section 2, we will discuss further how this property is used in the Lund model.

Due to confinement, we cannot study a single quark in isolation to learn about the ways it interacts with other quarks. What we can do instead is to smash two protons with each other at relativistic velocities v (where $v \approx c$, c is the speed of light, to simplify our calculations, we consider $c = 1$). This method is similar to the deep inelastic scattering (DIS) process for $e - p$ collisions, which results in a surge of partons. Often we get partons with higher than average parton energy in such an

event, called *jets*. All partons in an event interact with each other in different strong and weak processes, finally forming mesons and baryons (together called *hadrons*) which are then detected by the different detectors at the experiment.

1.1 Cross sections in QCD

To arrive at the cross sections[4] of a collider experiment, we need to have a theoretical foundation for the evolution from a initial particle state to the final state. The transition of a closed system of particles from an initial state $|k\rangle$ to a final state $|f\rangle$ is described in Quantum Field Theory by the S-matrix which is a *scattering* matrix:

$$|f\rangle = S\,|k\rangle \tag{1}$$

The matrix elements of the S-matrix are given by:

$$S_{fk} = \langle f|\, S\,|k\rangle \tag{2}$$

This can be written in algebraic form:

$$S_{fk} = \delta_{fk} + i(2\pi)^4\delta^{(4)}(p_f - p_k)T_{fk} \tag{3}$$

where δ_{fk} is the Kronecker delta and when it is 1, the state does not change, implying that there has been no interaction. Here, $\delta^{(4)}(p_f - p_k)$ is the delta function ensuring energy-momentum conservation, and T_{fk} is the *transition amplitude* from $|k\rangle$ to $|f\rangle$ state. In addition, $T_{fk}(S_{fk})$ is a function of the 4-momentum and the polarization of particles. Also, from the conservation of probability norm in the interaction, we have $S^\dagger S = 1$. This means that the sum of probabilities of all possible processes at a given energy is equal to unity.

The probability of a final-state is not only given by T_{fk}, but also sum of all possible kinematic configurations for the specific process. This is done by including the Lorentz invariant phase-space [5] :

$$d\Phi_n = \prod_n \frac{d^3p_f}{(2\pi^3)}\frac{1}{2E_f}(2\pi^2)\delta^4\left(\Sigma p_k^\mu - p_f^\mu\right) \tag{4}$$

where the product over n indicates the final-state particles.

[4]Probability of collision for the incoming particles.

[5]Ensemble of all possible states after a collision.

Theoretically, modelling the evolution of a hard collision from the time of collision to the time of observation is a challenging task since we need calculate the perturbative and non-perturbative processes at every increasing time step (or decreasing energy). After a particle collision at the highest virtuality Q^2_{max} or highest energy s, the event evolves with decreasing Q^2 and increasing t (time). It has been seen that the wave-functions of the hadron states have characteristic behaviours at different resolution (Q^2) scales. At high Q^2, the properties of a system or the interaction between partons can be determined from S-matrix theory, while low Q^2 behaviour needs to be phenomenologically modelled with the help of experimental data. Therefore, to determine cross-sections for different processes in hadronic collisions, such as a p-p collision, it is crucial to know the Q^2 scale of the process.

Since hadrons are composite objects, their parton content is given by the valence quarks and antiquarks, along with a sea of gluons and further quark-antiquark pairs. To calculate the cross section of hadronic collisions at a given Q^2, it is useful to relate the hadronic to partonic cross sections of each individual parton colliding. This can be written in terms of partonic cross sections $\hat{\sigma}_{j,k}(\mu_F, \mu_R)$ as:

$$\begin{aligned}
&\sigma_{2\to n} \\
&= \sum_{j,k} \int_0^1 dx_j dx_k f_{j/h_1}(x_j, \mu_F) f_{k/h_2}(x_k, \mu_F) \hat{\sigma}_{j,k}(\mu_F, \mu_R) \qquad (5) \\
&= \frac{1}{2s} \sum_{j,k} \int_0^1 \frac{dx_j}{x_j} \frac{dx_k}{x_k} f_{j/h_1}(x_j, \mu_F) f_{k/h_2}(x_k, \mu_F) \int d\Phi_n |\mathcal{M}_{jk}(\Phi_n; \mu_F, \mu_R)|^2.
\end{aligned}$$

where $\sigma_{2\to n}$ is the hadronic cross section for 2 incoming hadrons scattering to n particle final state. $f_{j/h_1}(x_j, \mu_F)$ is the *parton distribution function* (PDF) of parton j inside hadron h_1. The μ_F variable is the factorization scale and μ_R is the renormalization scale, and are process-dependent quantities. The renormalization scale μ_R is the energy scale (Q^2) at which α_s is determined. Above the factorization scale μ_F, partonic interactions are described by the partonic cross section $\hat{\sigma}_{j,k\to n}$. Below μ_F, the partonic dynamics is described by the PDFs. The factorization scale μ_F separates the *hard* and the *soft* scale in QCD and hence forms a theoretical basis for further calculation of pQCD results. $\int d\Phi_n |\mathcal{M}_{jk\to n}(\Phi_n; \mu_F, \mu_R)|^2$ is the integral of the partonic amplitude squared over n-parton phase-space element $d\Phi_n$.

The different components of the master formula in eq. (5) are described below:

1. $f_{j/h_1}(x_j, \mu_F)$ is the parton distribution function (PDF) of parton j which depends on the light-cone momenta fraction x with respect to the hadron

h_1, (of which parton j is a constituent) and the factorization scale μ_F, and similarly for f_{k/h_2}

2. $\hat{\sigma}_{j,k}(\mu_F, \mu_R)$ is the parton-level cross section of the incoming partons j and k,

3. μ_F is the factorization scale and μ_R is the renormalization scale. μ_F is the scale where PDFs are determined and μ_R is the scale where the coupling constants are determined. Often, we assume $\mu_F = \mu_R$. For scattering processes, we typically have $\mu_F = p_\perp$ of the scale characterizing the process, whereas in case of resonance production, $\mu_F = M$, is the usual choice, where M is the mass of the resonance.

4. $\int d\Phi_n |\mathcal{M}_{jk\to n}(\Phi_n; \mu_F, \mu_R)|^2$ is the integral of the partonic transition amplitude squared over the n-parton phase-space element $d\Phi_n$.
This phase-space element is similar to eq. (4), in terms of j, k is given by the equation:

$$d\Phi_n = \prod_{i=1}^{n} \left[\frac{dp_i}{(2\pi^4)} (2\pi)\delta(p_i^2 - m_i^2)\Theta(p_i^{(0)}) \right] (2\pi^4)\delta^4(p_j + p_k - \sum_{i=1}^{n} p_i) \quad (6)$$

1.2 Parton distribution functions

To construct the rest of the parton evolution dynamics, we need a well-behaved function as the description of the parton density in a hadron. The evolution of these PDFs with changing resolution scale Q^2 is given by the coupled set of differential equations called **Dokshitzer–Gribov–Lipatov–Altarelli–Parisi** (**DGLAP**) equation.

Box 1: The DGLAP equation

When a proton is probed at increasing Q^2, the number of partons increases, but their size decreases. This behaviour is described by the DGLAP equation. This is given by:

$$\frac{\partial}{\partial \log Q^2} \begin{pmatrix} f_{q/h}(x,Q^2) \\ f_{g/h}(x,Q^2) \end{pmatrix} = \frac{\alpha_s(Q^2)}{2\pi} \int \frac{dz}{z} \begin{pmatrix} P_{qq}(x/z) & P_{qg}(x/z) \\ P_{gq}(x/z) & P_{gg}(x/z) \end{pmatrix} \begin{pmatrix} f_{q/h}(z,Q^2) \\ f_{q/h}(z,Q^2) \end{pmatrix} \tag{7}$$

where $P(x/z)$ is the splitting function for a process, say $g \to q\bar{q}$ (for P_{qq}) and $f_{q/h}(x, Q^2)$ is the probability density of finding a quark a carrying the momentum fraction x in hadron h, and similarly for gluons given by $f_{g/h}(x, Q^2)$.

PDFs are the probability distributions that give us the probability of finding a parton with a given momentum fraction z within a hadron, for example a proton. After the hard scattering at maximum Q^2 (Q^2_{max}), the parton ensemble will evolve down to $Q^2 (\approx Q_0^2$ which is the lowest $Q^2)$ will start to *hadronize* to form primary resonances which further decay. Since this is a non-perturbative QCD process (low Q^2 and large α_s), it is difficult to use pQCD approach at this α_s scale. Hence, several hadronization schemes have been proposed over the years, and the overall challenge has been to include both pQCD and non-pQCD in a single model to produce good agreement with the data. We will revisit further discussion of hard scattering and parton evolutions in section 3.

2 Lund string model

The Lund model comes into the picture in non-pQCD for hadronization of partons. The fundamental concept of the Lund model is to consider a string representing colour force between q–$\bar{q}$ pair, much like a physical string with a string tension κ. In this section, we discuss the main features of the Lund string model.

In the Lund model [8, 9], the colour field between a quark and an antiquark is pictured as a one-dimensional massless relativistic string. In space-time, the string ends would move as shown in figure 3. At time $t = 0$ in the centre-of-mass frame, the string is formed between the two massless partons travelling away from each other with equal but opposite momentum E_0 at the speed of light c $(= 1)$. The

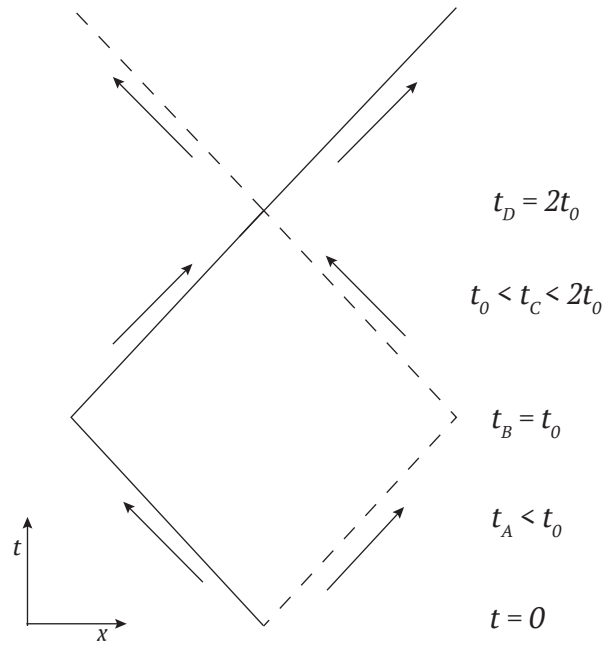

Figure 3: The space-time diagram of the *yo-yo* mode for a massless $q\bar{q}$ pair in its rest frame. The characteristic times of the motion as mentioned in the text are marked.

total energy of the system is therefore $2E_0$. As the string stretches out, the kinetic energy of the q–$\bar{q}$ is transferred into the colour field. At time t_A ($< t_0$), the $q - \bar{q}$ pair is at a distance $\delta x = 2t_A$ apart, leaving each of them with energy $E_0 - \kappa t_A$ and the energy going into the colour field which is $2\kappa t_A$. The transformation of the kinetic energy of the quarks into the colour field is complete at $t_B = t_0 = \frac{E_0}{\kappa}$, where t_0 is a half-cycle of the string kinematics going from one space-time point where the q–$\bar{q}$ meets to the next. Here, they reverse their direction of motion and travel towards each other. Hence, the energy invested in the colour field is being transformed into the momenta of the partons.

Then the $q - \bar{q}$ pair meets again at $t_D = \frac{2E_0}{\kappa}$. After they meet at $t_D = 2t_0$, they exchange their modes of motion and now the parton on the negative x-axis travels to the positive x-axis and vice-versa. So, the string length starts increasing again. This motion of the Lund string is called the *yo-yo* motion, and the partons in the string ends together form a hadronic bound state due to this behaviour. Here we note that the colour field ends at the string ends, in that way this string succeeds in capturing the essence of confinement in strong force.

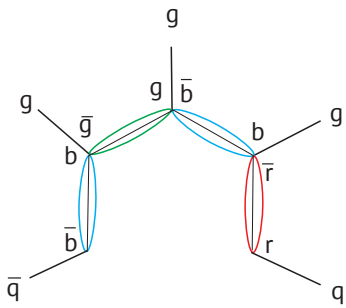

Figure 4: Gluon emissions along a string.

The first formulation of this model was made in the 1970s [8], with subsequent addition of advanced mechanisms, of which some are part of this thesis. One of the other concepts that is closely correlated with the Lund strings is the idea of *colour dipoles* [10]. In PYTHIA, the general way is to think about the string connected from one parton to the other via a series of gluon kinks. This picture can also be depicted in the form of colour dipoles, where then we replace the set of gluons by set of colour dipoles as in figure 4. Hence, if a dipole splits into two dipoles, which is the equivalent to a gluon emission, then that would imply one more gluon kink.

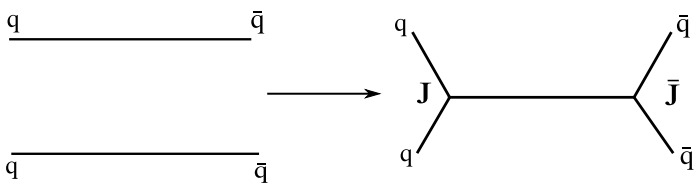

Figure 5: Junction formation between two strings

The string geometry and the yo-yo motion discussed before is the simplest case of Lund strings. Often, more complex string structures can form if kinematically allowed. So strings between 3 quarks may be formed and would appear as a T-junction, called single junction. A more complex case of double junctions is also formed as shown in figure 5. Junction decays also contribute to baryon production, although they are not usually the dominant contributors. There are several challenges in including junctions to extend the works done in this thesis, one of which

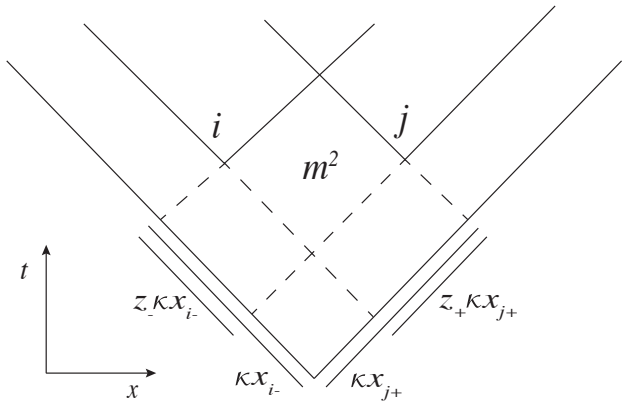

Figure 6: Production of a hadron with mass m, between two breakup vertices i and j on a string, with corresponding lightcone components as mentioned in the text [13].

is to define a junction rest frame. An extended discussion of the problem can be found in references [11] and [12].

2.1 Hadronization of a string

In reality, most of the parton pairs formed have larger mass than stable hadrons hence the string formed between them will *decay* into several hadrons of smaller masses. When the string between a $q - \bar{q}$ pair is maximally extended at $t = t_B$ in figure 3, all the energy is stored as potential energy in the field. When it becomes energetically favourable, a new $q - \bar{q}$ pair is formed which results in a *string break*. We describe the process of the string break in this subsection, closely following the detailed derivation in ref. [13].

In figure 6, the string breaks up in two vertices i and j, thus producing a hadron of mass m. The total energy stored in the string (E_{st}) in lightcone coordinates of the breaking vertices are:

$$E_{\text{st}}^2 = \kappa^2 x_{i-} x_{j+} \tag{8}$$

where $x_\pm = t \pm x$. After two such breakups, we have three string segments. The properties of the new string formed due to breaking at the vertices i and j are selected iteratively from a probability density function. This function is called *Lund*

fragmentation function $f(z)$ where z is the fraction of the lightcone momenta. We will use the coordinates $\Gamma = \kappa^2 x_- x_+$ and $y = \frac{1}{2}\ln\left(\frac{x_+}{x_-}\right)$. We assume that the vertex i can be reached from the left (and j from the right) for a given energy. The fraction of the remaining lightcone momentum taken away by the hadron produced is given by $z_\pm$ and can vary between 0 and 1. Therefore, the mass of the hadron produced is $m^2 = \kappa^2 z_- x_{i-} z_+ x_{j-}$ as seen in the figure 6. The probability of going on the positive lightcone and arriving at the vertex j is

$$H(\Gamma_j) d\Gamma_j dy_j \tag{9}$$

where H is an unknown function. Now, the probability to produce a $q-\bar{q}$ pair with a given momentum fraction to arrive at vertex i (from right to left) is $f(z_+)dz_+$. The combined probability is attained by multiplying the two distributions. Now producing the $q-\bar{q}$ pair from left to right will give us the probability to go from left to right via i and then arrive at j. From figure 6, the relations between the variables in eq. (11) are obtained:

$$\begin{aligned} \Gamma_i &= \kappa^2 x_{i+} x_{i-} = \kappa^2 (1-z_+) x_{j+} x_{i-} \\ \Gamma_j &= \kappa^2 x_{j+} x_{j-} = \kappa^2 x_{j+} (1-z_-) x_{i-}. \end{aligned} \tag{10}$$

These two probabilities should be equal and following eq. (9), we get:

$$H(\Gamma_j) d\Gamma_j dy_j f(z_+) dz_+ = H(\Gamma_i) d\Gamma_i dy_i f(z_-) dz_- \tag{11}$$

If we take the logarithm of the above equation such that $h(\Gamma) = \ln(\Gamma)$ and $g(z) = \ln(zf(z))$, we can write it as:

$$h(\Gamma_j) + g(z_+) = h(\Gamma_i) + g(z_-) \tag{12}$$

Now, differentiating this expression in z_+ and then z_-, the g dependence vanishes, leaving the h dependence. The resulting equation is:

$$\frac{dh(\Gamma_1)}{d\Gamma_1} + \Gamma_1 \frac{d^2 h(\Gamma_1)}{d\Gamma_1^2} = \frac{dh(\Gamma_2)}{d\Gamma_2} + \Gamma_2 \frac{d^2 h(\Gamma_2)}{d\Gamma_2^2} \tag{13}$$

The equation holds true only if both sides are equal to the same constant, say $-b$, which can also be expressed in terms of $h(\Gamma)$:

$$\frac{d}{d\Gamma}\left(\Gamma \frac{dh}{d\Gamma}\right) = -b \implies h(\Gamma) = -b\Gamma + a\log\Gamma + \log C \tag{14}$$

where C, b and a are integration constants. Here, b is the same for all vertices, while a and C may be different. Now, inserting eq. (14) into eq. (12) and rearranging so that all z_- are on one side of the equation and the same for z_+, we get the following expression for $f(z)(= 1/z \exp(g(z)))$:

$$f(z) = N\frac{1}{z}(1-z)^a e^{-bm^2/z} \tag{15}$$

where $z = z_-(z_+)$. For a further discussion of this derivation, we refer to [13]. Using eq. (15), we can arrive at the probability $\mathcal{P}$ of a particular breakup with n final hadrons:

$$d\mathcal{P} \propto \left(N d^2p_i \delta(p_i^2 - m^2)\right) \delta\left(\sum_{i=1}^{n} p_i - P\right) e^{-bA}, \tag{16}$$

where P is the total momentum of the string, A is the area covered by the string before fragmentation, N is a normalization constant, and b is a flavour independent parameter tuned to data. The production vertices for the q–$\bar{q}$ pairs will be located around a hyperbola in space-time with a typical proper-time τ determined by the relation between a and b, via the relation:

$$\langle \tau^2 \rangle = \frac{(1+a)}{bm^2}. \tag{17}$$

The multiplicity per unit rapidity ($\frac{dN}{dy}$) is related to the time τ via the relation:

$$\frac{dN}{dy} \sim \frac{\sqrt{\langle \tau^2 \rangle}\kappa}{m} \tag{18}$$

where y is rapidity. Of the several characteristics of the string hadronization scheme, we note that for a given string, the energy is conserved and the electric charge produced from fragmentation of a string is conserved. From the fragmentation function, we see that a large a controls the suppression of the $z \to 1$ region while b controls the suppression of the $z \to 0$ region.

2.2 Flavour and baryon production in string fragmentation

For the production of $q\bar{q}$ pairs with mass m and transverse momentum $p_\perp$, the production of heavy flavours is suppressed. This is because the $q\bar{q}$ pairs can no longer be formed at the same vertex, and they need to *tunnel* μ/κ distance to be produced, where $\mu^2 = (m^2 + p_\perp^2)$ is the transverse mass of the quark flavour. The suppression is given by the exponential factor $e^{-\pi\mu^2/\kappa}$. So for a quark flavour with mass m_q, the tunnelling probability is given by:

$$\frac{1}{\kappa}\frac{d\mathcal{P}_q}{d^2p_\perp} \propto \exp\left(-\frac{\pi\mu^2}{\kappa}\right) \propto \exp\left(-\pi p_\perp^2/\kappa\right)\exp\left(-\pi m_q^2/\kappa\right). \tag{19}$$

So we see that the mass (flavour) generation and the $p_\perp$ generation for the quark pair separates except for the κ dependence, and allows for independent generation. It is apparent from eq. (19), that heavier flavours would be suppressed, and for strange (s) flavour, the factor can be given as a ratio to the mass of u/d flavour:

$$\rho = \exp\left(-\frac{\pi(m_s^2 - m_u^2)}{\kappa}\right). \tag{20}$$

Since absolute quark masses cannot be precisely determined, the ratio $m_s : m_u$ is introduced as a parameter ρ and is tuned to LEP data [6], while the suppression for charm and bottom are so large, that they cannot be produced at all.

Flavour and spin of the hadrons from the decay of a string is determined independently for each string breakup, depending on several fragmentation parameters. In section 5.3 and references [14, 15] and Paper II [16], we see that when we consider string interactions, the flavour and spin of hadrons produced from a string is influenced by the strings around the string being fragmented.

The Lund string hadronization is the recipe for meson production, but one can also get baryons from Lund strings. Baryons can be formed from a diquark (antidiquark) breakup, which implies that any baryon produced would have an anti-baryon produced adjacent to it. The *popcorn model* allows for intermediate production of mesons between a baryon and an anti-baryon. That can also be thought of in terms of popcorn production of $q\bar{q}$ pairs with wrong colours, as shown in figure 7. It is to be noted that diquark production is suppressed due to their heavier mass due to the tunnelling factor, as explained above.

[6] In PYTHIA settings, the ρ parameter is called `StringFlav:probStoUD`, and has a default value of 0.217.

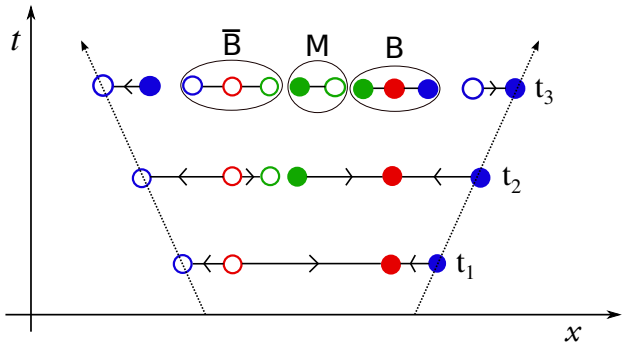

Figure 7: Space-time diagram of the popcorn model of baryon production [15]. At t_1 a $r\bar{r}$ pair is produced by vacuum fluctuation. At t_2 and t_3 there are two consecutive $g\bar{g}$ pairs produced, resulting in string breakups. At t_3, there are additional string breakups due to production of two $b\bar{b}$ pairs near the original $b\bar{b}$ pairs, producing two baryons on either ends and a meson in between.

At t_1, a $r\bar{r}$ pair is produced between the $b\bar{b}$ pair sitting at the string ends, by quantum fluctuation which *does not* break the string. The r quark forms an effective antigreen charge, and similarly the $\bar{r}$ forms an effective green charge, making the field between the pair green, with opposite direction of colour flow. In this green field between the $r\bar{r}$ pair, the string breaks due to production of first a $g\bar{g}$ pair at t_2 and then again at t_3. Also, at t_3, two new $b\bar{b}$ pairs are produced closer to the original $b\bar{b}$ pairs, causing two other string breakups. The several $q\bar{q}$ pairs produced at t_3, would produce one or more mesons ($\boldsymbol{M}$) between the two baryons ($\boldsymbol{B}$ and $\bar{\boldsymbol{B}}$). In this way, the $\boldsymbol{B}$ and $\bar{\boldsymbol{B}}$ pair would have only one flavour in common. For a detailed discussion, we refer to [13]. Baryon production in PYTHIA is implemented as diquark production with popcorn correction introducing additional parameters, which are tuned to data.

Now we turn to discussing how a soft gluon emission fits into this model. The emission of a quark is equivalent to formation of a new string. However, emission of soft gluons gives rise to a unique structure of the Lund string and the corresponding string evolution is originally referred to as the *dance of the butterfly* [8].

These complex space-time regions spanned by the gluon strings are referred to as *plaquettes*. The soft gluon will form two new string pieces with the original string. These soft gluons will lose their energy very fast and give rise to a new straight string piece, as described more in Paper I and Paper IV. These have non-trivial contribution to non-pQCD effects such as string interactions. They are further discussed in reference to string shoving and rope implementation in Paper IV. Now that we have reviewed the fundamentals of the Lund string model, in the next section 3, we present how an event is generated in the PYTHIA Monte Carlo event generator.

3 Monte Carlo Event Generation in PYTHIA

The basis of Monte Carlo Event Generators (MCEG) is the Monte Carlo algorithm. In this technique, one evaluates the integral of a function $f(x)$ by generating new values of the distribution for a physical process. As the integral of the distribution, $I = \int_{x_2}^{x_1} f(x)dx$ can be written as an average $(x_2 - x_1)\langle f(x)\rangle$, this average can be calculated by generating N random numbers from a uniform distribution:

$$I \approx I_N \equiv (x_2 - x_1)\frac{1}{N}\Sigma_{i=1}^{N} f(x_i). \tag{21}$$

The efficiency of the random number generation can be improved by using *importance sampling*. Here, we can generate the random number following a different arbitrary distribution $G(x)$ which has a simpler form than the complicated distribution $f(x)$ (as is the case for many stages in the parton evolution) and fulfills $G(x) > f(x)$ for all values of x.

Box 2: Benefits of MC algorithm

The value computed by this method improves with the number of times the function is sampled. The usefulness of this recipe, however is not apparent until we increase the number of variables or dimensions (d). For a given number of trials (N), errors in schemes such as Simpson's rule, increases with d according to $\mathcal{O}(1/N^{4/d})$. However, the error in MC integration is independent of the number of dimensions and it scales like $\mathcal{O}(\sqrt{N})$.

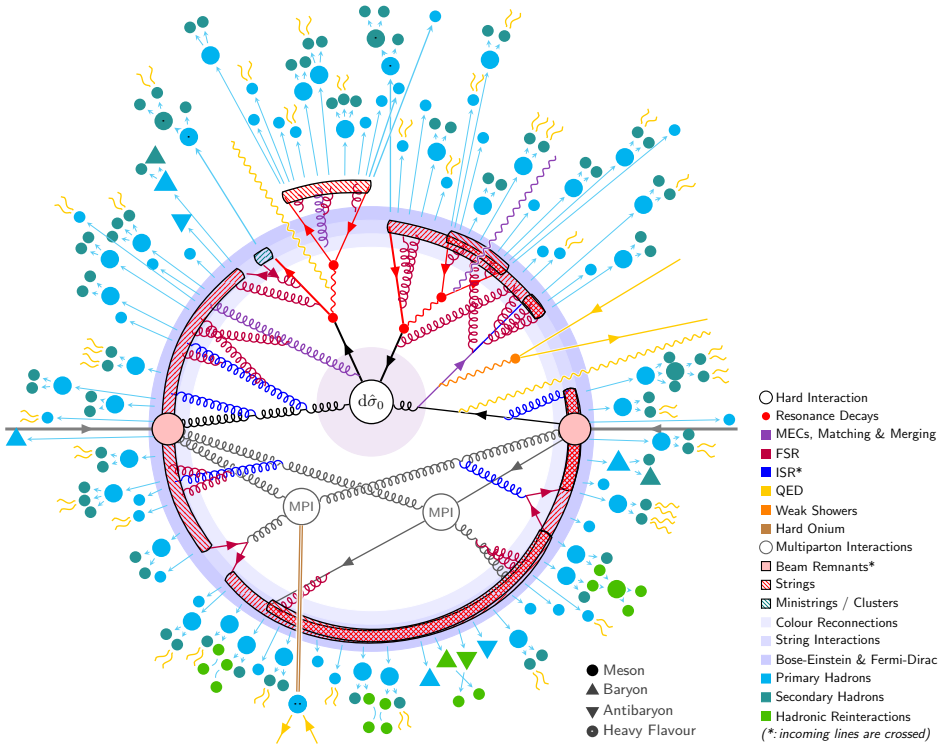

Figure 8: Illustration of processes occurring in a p-p $\rightarrow t\bar{t}$ event, as modelled by PYTHIA event generator. Figure from ref. [17]. The major processes, most of which are described in the text, are labelled.

To model a complete event in PYTHIA MCEG, the first step is to construct the hard scattering process at the highest Q^2 (Q^2_{max}) in terms of elementary partons. After the hard scattering, to model the incoming beams in terms of composite objects, we make use of the parton distribution functions (PDFs). Additional radiations from outgoing partons may occur, called *parton showers*, with the evolution in Q^2 scale, and when it reaches Q^2_0, the system enters non-pQCD regime and starts hadronizing. During hadronization, strings are formed among outgoing quarks and gluons. These strings hadronize via several breakups obeying the Lund fragmentation function given by eq. (15). There are also additional decays after hadronization, and further scatterings. These successive stages in the end spans the entire available phase space for an event. In this section, we go through the main components of an event generation in further detail, some of which are shown in figure 8.

3.1 Hard process

The initial scattering of the two incoming partons is called a hard scattering. To start with, we consider that the initial states are well separated and hence do not interact. With time evolution, as the particles travel towards each other, the interaction between their wave-functions become non-negligible and scattering takes place, as discussed in section 1.1. The scattering process produces two or more outgoing particles, with well-separated wavefunctions into the future. At least one incoming parton from each of the two incoming showers will enter the scattering process. This hard scattering process can be a perturbative QCD process or electroweak process. In PYTHIA, there are several phase-space cuts applied to evade infrared singularities for calculating cross sections of hard processes.

3.2 Initial and final state parton showers

The incoming partons may branch in several consequent splittings. This is called the *initial-state radiation* (ISR). The outgoing partons may also branch further similar to ISR, which is called *final-state radiation* (FSR). The partons shower branchings obey the DGLAP equations as given in eq. (7) in section 1.2. For example for $q \to qg$ splitting, the energy carried by the each of the daughter partons is given by the splitting function of the corresponding process. The *splittings* are further ordered from highest to lowest virtuality (Q^2), which means that ISR happens back in time (backward evolution) and FSR occurs in future time (forward evolution).

3.2.1 Splitting functions

A parton can further radiate, giving rise to partons with momentum fractions z and $(1-z)$ at every step. Such processes have splitting kernels which are fixed for a specific process, for example of g splitting into gg, for which this function $f_{g\to gg}$ at the leading order has the form:

$$\mathcal{P}_{g\to gg}(z) = 6\left(\frac{1-z}{z} + \frac{z}{(1-z)_+} + z(1-z) + \left(\frac{11}{12} - \frac{n_f}{18}\right)\delta(1-z)\right) \tag{22}$$

The splitting functions for $q \to qg$, $q \to gq$ and $g \to q\bar{q}$ splittings are given by:

$$\begin{aligned}
\mathcal{P}_{q\to qg}(z) &= \frac{4}{3}\left(\frac{(1+z^2)}{(1-z)_+} + \frac{3}{2}\delta(1-z)\right) \\
\mathcal{P}_{q\to gq}(z) &= \frac{4}{3}\left(\frac{1+(1-z)^2}{z}\right) \\
\mathcal{P}_{g\to q\bar{q}}(z) &= \frac{1}{2}(z^2+(1-z)^2),
\end{aligned} \tag{23}$$

where n_f is the number of light quark flavours. In the $1/(1-z)_+$ denominators, the + subscript denotes that this is a distribution given by:

$$\int_0^1 dx \frac{f(x)}{(1-x)_+} = \int_0^1 dx \frac{f(x)-f(1)}{(1-x)} \tag{24}$$

which regularises the singularity at $x = 1$.

3.2.2 Sudakov form factor

The distribution of partons based on parton branching is given by the function

$$d\mathcal{P}(z,Q^2) = \frac{\alpha_s}{2\pi}\frac{dQ^2}{Q^2}\mathcal{S}(Q^2_{\text{max}},Q^2)P(z)dz \tag{25}$$

where $P(z)$ is the splitting function and $\mathcal{S}(Q^2)$ is the zero-emission probability sometimes called the Sudakov form factor. This factor is given by:

$$\mathcal{S}(Q^2_{\text{max}},Q^2) \equiv \exp\left(-\int_{Q^2}^{Q^2_{\text{max}}}\frac{dQ'^2}{Q'^2}\int dz\frac{\alpha_s}{2\pi}P(z)\right). \tag{26}$$

The interpretation of the Sudakov factor $\mathcal{S}$ is the probability of a given particle to not radiate a secondary particle between the range Q^2 and Q^2_{max}. As it can be seen, that $\mathcal{S}$ ranges from 0 to 1.

3.3 Multiparton interactions

In PYTHIA, soft QCD processes are modelled on the basis of an effective theory approach called Regge theory. In this method, the force carriers are called *pomerons* and *reggeons*. Apart from elastic scattering where two hadrons colliding emerge intact, there can also be inelastic scatterings, that can be either diffractive or non-diffractive. A diffractive process can be a single diffractive process where either of the participating nucleons dissociates into multiple particles, or a double diffractive process where both of the participating nucleons dissociates into multiple particles with a large rapidity gap in between. In PYTHIA, a non-diffractive process is where the hadrons dissociates and form a common system, which cannot be categorized into further subsystems.

Since the inelastic non-diffractive events dominate the perturbative jet activity, the multiparton interactions in an average event would be given predominantly by non-diffractive events. The integrated cross section for hard scattering is given by:

$$\sigma_{\text{hard}}(p_{\perp\text{min}}) = \int_{p^2_{\perp\text{min}}}^{s/4} \frac{d\sigma_{\text{hard}}}{dp^2_\perp} dp^2_\perp \tag{27}$$

where σ is the $2 \rightarrow 2$ cross section similar to eq. (5). As the differential cross section $d\sigma_{\text{hard}}$ diverges roughly with $dp^2_\perp/p^4_\perp$, the integrated form σ_{hard} in eq. (27) diverges for low $p_{\perp\text{min}}$ values. It means that for small $p_\perp$ ranges, σ_{hard} exceeds the total non-diffractive cross section, which indicates that $\sigma_{\text{hard}} > \sigma_{\text{ND}}$ as evidence for additional partonic $2 \rightarrow 2$ scattering processes.

The incoming hadrons comprise of several partons which can also interact in additional subprocesses, called *multiparton interactions* (MPI). In PYTHIA, for a p-p event with $2 \rightarrow 2$ scattering process, the MPI cross section function is regulated using a tunable paramter $p_{\perp 0}$:

$$\frac{d\sigma_{2\rightarrow 2}}{dp^2_\perp} \propto \frac{\alpha_s^2(p^2_\perp)}{p^4_\perp} \rightarrow \frac{\alpha_s^2(p^2_\perp + p^2_{\perp 0})}{(p^2_\perp + p^2_{\perp 0})^2} \tag{28}$$

where $p_\perp$ is the transverse momentum of the outgoing partons [18, 19]. This can then be used to determine the approximate number of MPIs for average inelastic non-diffractive hadron-hadron collision, which is given by:

$$\langle n_{\text{MPI}} \rangle (p_{\perp 0}) = \frac{\sigma_{2\rightarrow 2}(p_{\perp 0})}{\sigma_{\text{ND}}} \tag{29}$$

In PYTHIA, the ISR showers and MPI are treated together, where the current approach introduces some tunable parameters to regulate the cross sections.

3.4 Angantyr

The Angantyr framework in PYTHIA8 [20] generates heavy-ion events with the underlying philosophy of the PYTHIA MPI machinery. The principal scheme of Angantyr is to model a collision between a projectile nucleus and a target nucleus by constructing nucleon-nucleon (NN) sub-collisions based on Glauber calculations [21, 22]. Their interactions are modified by accounting for diffractive events as fluctuations in the nucleon substructure and also fluctuations in the NN interaction probabilities. After the number and type of NN sub-collisions have been determined, the resulting final states are modelled with the MPI-based machinery for minimum bias p-p collisions in PYTHIA. The diffractive events have large rapidity gaps, which are not spanned by strings. This determines the string configurations for further processes such as string interactions which is the subject for this thesis.

3.4.1 Nucleon-nucleon sub-collision

Angantyr is based on the wounded nucleon formalism where the wounded or participating nucleons N_{w}, including non-diffractively and diffractively excited nucleons. This includes both fluctuations in nucleon position and nucleon wavefunction. Angantyr collides two nuclei based on the philosophy of the old Fritiof model [23–25]. In the wounded nucleon formalism [26], each wounded nucleon follows a single particle emission function $F(\eta)$ which adds up to be give the total final-state multiplicity $\frac{dN_{\mathrm{ch}}}{d\eta}$, which is given by:

$$\frac{dN_{\mathrm{ch}}}{d\eta} = w_p F(\eta) + w_t F(-\eta) \tag{30}$$

where w_p (w_t) is the total number of wounded nucleons from left (right). PYTHIA's single diffractive scattering, which includes the MPI framework, is used to determine the form of $F(\eta)$. The strings formed among these participant nucleons are hadronized following the Lund fragmentation model discussed in section 2.

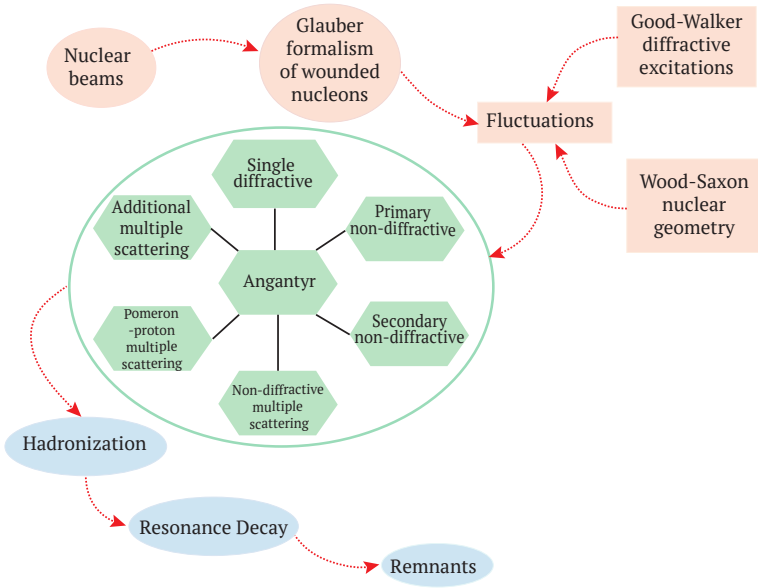

Figure 9: Workflow in Angantyr to generate a complete heavy-ion event, with the different processes labelled in their successive order. The various scattering processes into which a nucleon-nucleon subcollision can be categorized into are labelled as part of the Angantyr step.

3.4.2 Distinction of diffractive and non-diffractive collisions in Angantyr

Wavefunction fluctuations (diffractive events) in Angantyr for both the target and projectile nucleons are used to categorize the interactions as either single diffractive, double diffractive or non-diffractive processes (see sec 3.3 for definitions) [14].

A nucleon in the projectile nucleus can interact non-diffractively with many other nucleons in the target nucleus or vice versa, each of which are separate sub-collisions. In Angantyr, a NN sub-collision is either labelled as a primary or secondary non-diffractive collision or diffractive collision. A NN sub-collision which is labelled as primary non-diffractive, is generated as a non-diffractive p-p collision. A secondary non-diffractive process, where one of the nucleons have already been wounded in a ND interaction with another nucleon, is generated using a modification of the PYTHIA diffractive process. If a NN sub-collision does not qualify as non-

diffractive, there are further checks to determine if either of them is diffractive.

Sucessive processes and the role of PYTHIA's MPI-based minimum bias machinery in Angantyr is illustrated in figure 9. Therefore in Angantyr, one can use the basic PYTHIA machinery to give a fully-formed proton-ion/ion-ion collision. This framework is of particular importance not only for heavy-ion phenomenology but also for electron-ion collisions in the future [7], such as the upcoming Electron-Ion Collider (EIC) facility at Brookhaven National Laboratory, New York.

3.5 String interactions

In Angantyr, strings hadronize independently. This fails to reproduce certain HI observables such as strangeness enhancement (we discuss more in section 4.2). Therefore, some other string mechanisms which can reproduce such effects can be included, some of which we have developed in this thesis. These processes occur before or as hadronization sets in. One such process is string interactions, e.g. *string shoving* mechanism. One of the recent developments to the Lund model is that the strings have a colour field of Gaussian profile that extend over a finite width R [27, 28]. When two such strings lie close to each other, their fields repel each other. This gives the primary hadrons formed from such strings a transverse push. This phenomenon can contribute to final-state collective flow in high-multiplicity p-p, p-A and A-A collisions. This phenomenon is the subject of Paper I and Paper IV.

The other string interaction is *rope hadronization* [16, 29]. This leads to formation of joined colour entities that are created by stacking of strings that lie close to each other. Such entities, called *ropes*, have the characteristic behaviour where each string within a rope influences the string tension κ of the neighbouring strings. The modified κ_{eff} in turn modifies more than 10 tunable fragmentation parameters via eq. (19), influencing the hadronization in PYTHIA. This enhances the production of strange flavours in high-multiplicity p-p and nuclear collisions. We extend this model to heavy-ion collisions in Paper II. We discuss string shoving and rope hadronization in details in section 5.

In MC generators, we use the assumption of infinitely many colours in QCD, $N_c \to \infty$ instead of $N_c = 3$ to form strings. This makes handling of gluon emissions easier, since every gluon emission has a new colour and they do not interfere with each other. If $N_c = 3$ would be used, as is the case is for QCD, it would add

[7] Currently PYTHIA/Angantyr cannot model $e - A$ collisions.

more ambiguity to gluon emissions while forming string configurations, making event generation challenging in several ways. For $N_c = 3$ configuration, partons can change their string configurations owing to change in colour flow between two nearby partons, which is known as *colour reconnection* (CR). Colour reconnection changes the effective length of a string depending on how the strings are rearranged, usually with the effect of shortening strings pieces. One of the implications of colour reconnection are junctions which can result in baryon enhancement [11], as mentioned in section 2. In case of Angantyr as of now, though colour reconnection within a NN sub-collision can occur, colour reconnection among separate sub-collisions in is lacking.

3.6 Hadronization, decay and hadronic rescattering

In addition to the primary hard scattering, there are several semihard interactions between the other partons of two incoming hadrons as mentioned in subsection 3.3. After the partons participating in the hard scattering are taken away from the incoming particles, the remainder is called the beam remnant and can form strings with the other partons in the event. The strings among final-state quarks hadronize at low Q^2 to form primary hadrons. Phenomenological models, such as the introduced Lund string hadronization in section 2 or the cluster hadronization in Herwig [30] are heavily used for hadronization.

Primary hadrons and some resonances are formed directly from string hadronization. They can further decay to form secondary hadrons and may scatter among themselves, which is called *hadronic rescattering* [31]. This can give rise to formation of excited hadronic states after rescattering both in p-p collisions and nuclear collisions and collective flow in A-A collisions.

Until this section we have covered the founding concepts that are used in modern MC generators and in PYTHIA/Angantyr, and have been used in this thesis. Now in the next section, we will discuss nuclear collisions and QGP-like signals which are the main foundations of the main observables for this thesis and finally turn to string interactions in further details in section 5.

4 Nuclear collisions and QGP-signals

We now arrive at nuclear collisions, which is similar to colliding N number of protons and neutrons due to isospin symmetry of QCD (N is the total mass number of both the projectile and the target nuclei). Since the nucleus has a well-defined shape, the initial overlap region can be quantified by the physical entity called *centrality*. Centrality refers to the sense of how "central" these collisions can be. The extent of centrality is counter-intuitive to the measure of the actual overlap between the ions, which is because if the collision is 80% central, then it is a peripheral collision, and if it is 0% central, then it is a head-on collision. 100% centrality indicates that the two nuclei have missed each other and no collision has occurred.

Nuclear collisions have their peculiarities compared to p-p collisions and e^+-e^- collisions. This is because a nucleus has a larger mass and volume [8], and as a result extreme densities can be formed in A-A collisions. In a typical A-A collision, two Lorentz-contracted planes of matter collide to give rise to thousands of final-state particles. For comparable energies in p-p, what is new here is that the system can now form a dense and high energy *environment* in a head-on (central) collision. Since the average number of charged particles in a heavy-ion collision is nearly 100 times greater than in p-p collisions, it implies that the number of multiparton interactions also increases significantly. These final-state particles in HI collision, are sensitive to the effects of the bulk properties of matter and exhibit collective effects. The final-state of A-A collisions is also characterized by significant hadronic rescattering.

In the introduction, we discussed that matter at low energy densities is composed of electrons, protons, and neutrons. When this system is heated, we might produce thermal excitations that include strongly interacting light-mass particles such as the pion. As discussed before, inside the protons, neutrons, and other strongly interacting particles are quarks and gluons. If the matter has a high enough energy density, the protons, nucleons, and other particles overlap and are squeezed so tightly that their constituents are free to roam the system without being confined inside the hadrons. At such a high density, parton deconfinement occurs and the system enters a plasma state called a Quark–Gluon Plasma (QGP). Therefore, in heavy-ion collisions, QGP is expected to form within the dense initial state.

[8] For a given nucleus, its volume is proportional to $r_0^3 \times A$, where r_0 is the proton radius and A is the mass number of the nucleus

As the energy density becomes very large, the interactions between the quarks and gluons become weak. This is a consequence of the asymptotic freedom of strong interactions, that at short distances the strong interactions become weak as explained in section 1. The hot and dense initial state formed in an HI collision expands under its own pressure and cools during expansion. Around the critical temperature of ≈ 156 MeV a cross-over transition takes place which confines the quarks into the hadrons, known as *chemical freeze-out*. After this stage, the hot and dense hadronic state still expands and cools undergoing rescattering, until it reaches *kinetic freeze-out*, at which stage the momentum of the particles reaches equilibrium. In the dense hadronic state between chemical and kinetic freeze-out, hadrons can interact via elastic and pseudo-elastic scattering causing a change in their momentum. Thus, resonances that have lifetimes comparable to that of this state (in the range of $\sim 1 - 10$ fm/c) are sensitive probes for the evolution of the hot-dense state.

The physics of nuclear collisions has traditionally been described using statistical models and hydrodynamics as the system is large and strongly coupled. This relates to the fact that in A-A events, the transverse system size is of the order of a few fm and therefore 10 times larger than a typical p-p collision. However, the picture of QGP evolution with hydrodynamics is in sharp contrast to the Lund model for A-A collisions. For starters, there is no concept of temperature in Lund strings, and the phases of chemical and kinetic freeze-out in the hydrodynamic picture are replaced with that of hadronization via string fragmentation.

A characteristic behaviour of the hot and dense initial states is the modification of high Q^2 processes (such as jets) by low Q^2 partons. Other high Q^2 processes, such as flavour production [9] would be influenced as well. Such effects depend on the chemical and kinetic freeze-out phases and their individual time spans. These observations pertain to the experimental observations of *jet quenching*, strangeness enhancement and modification in charmonium yields in heavy-ion events. Also, particle correlations over large spans of pseudorapidity ($\Delta\eta > 1$) is a characteristic behaviour of these systems. These observations are collectively referred to as the *QGP-like signals* across both small and large systems. In this section, we present the theoretical description of the three major QGP-like signals. These physical properties become our testing ground in section 5.

[9] Heavy flavours have higher mass so they have to be handled differently than u and d quarks.

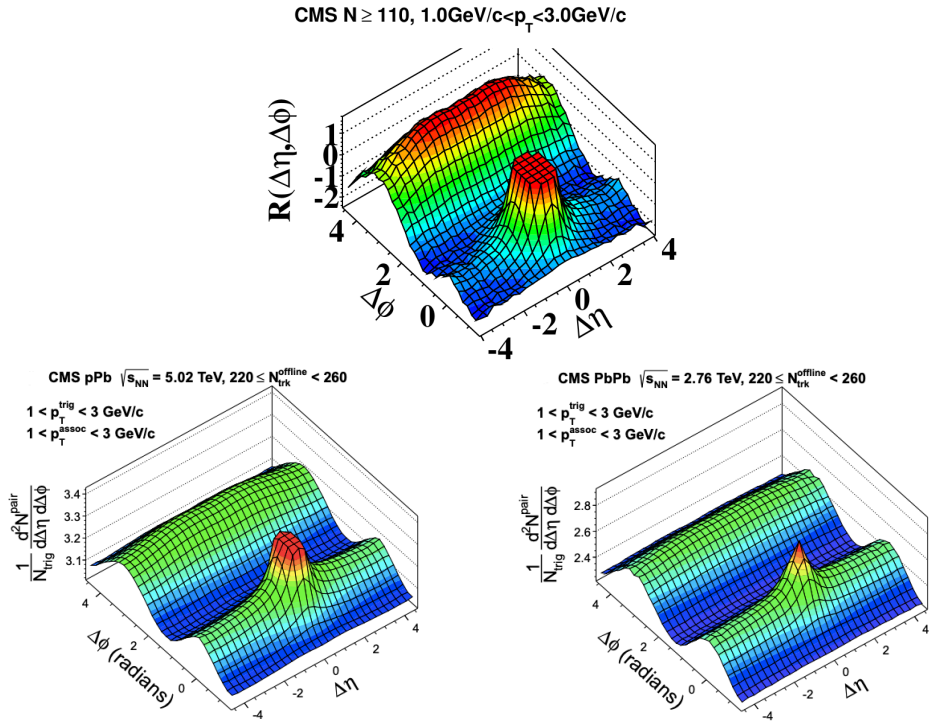

Figure 10: Plot from CMS collaboration showing the long-range near-side 2D two-particle correlation function $R(\Delta\eta, \Delta\phi)$ for p-p collision at $\sqrt{s}$=7 TeV (top), p-Pb collision at $\sqrt{s_{\rm NN}}$=5.02 TeV (bottom left) and Pb-Pb collision at $\sqrt{s_{\rm NN}}$=2.76 TeV (bottom right) at the LHC [32, 33].

4.1 Final-state collectivity

As mentioned in the introduction, the in-plane elliptic flow is the signature of the anisotropic particle-momentum distribution in relativistic nuclear collisions. This collective flow is sensitive to early asymmetries in the geometry of the system, as it occurs between final state particles separated by large rapidity span. Due to the rapid expansion of medium after the A-A collision, which decreases the spatial asymmetry with time, such collective effect can only arise in the first fm/c ($c = 1$) due to causality. Such flow measurements are made following the Fourier expansion of the Lorentz-invariant distribution of momenta of outgoing particles. The Fourier coefficients v_n in the expansion convey the magnitude of *anisotropic flow*.

In A-A collisions, the plane spanned by impact parameter vector and the beam direction is called the *reaction plane*. The azimuthal angle of the reaction plane is

given by Ψ_{RP}. The azimuthal distribution of particles as a function of the angle relative to the reaction plane is anisotropic. Hence, a Fourier expansion of the Lorentz-invariant distribution of outgoing particles is given by:

$$E\frac{d^3N}{dp^3} = \frac{1}{2\pi}\frac{d^2N}{p_T dp_T dy}\left(1 + \Sigma_{n=1}^{\infty} v_n(p_T, y)\cos[n(\phi - \Psi_{\mathrm{RP}})]\right) \tag{31}$$

where v_n are the Fourier coefficients averaged over all particles in an event, given by

$$v_n = \langle \cos[n(\phi - \Psi_{\mathrm{RP}})]\rangle. \tag{32}$$

The sine terms are absent due to symmetry with respect to the reaction plane. The v_n terms are also known as n^{th} *harmonic differential flow*. They are also functions of rapidity y and transverse momentum p_T. v_1 is known as the directed flow and v_2 is known as the elliptic flow. Often the particle distribution is studied using the function $R(\phi) = \frac{dN}{d\phi}$, which is a periodic function representing the azimuthal distribution, where the azimuthal angle ϕ is in the range $[0, 2\pi]$.

Surprisingly, the long-range near-side correlations were also observed in high-multiplicity p-p collisions, for the first time in 2010 by the CMS collaboration [32], and later by RHIC and ALICE collaborations. This is shown in figure 10 where the 2D two particle correlation function is plotted against azimuthal angle $\Delta\phi$ and pseudorapidity $\Delta\eta$ for p-p, p-Pb, and Pb-Pb collision systems from CMS collaboration [10]. This could imply that collective behaviour is also possible in small systems, but the source of this signal is debatable due to the negligible anisotropic structure in p-p collisions.

To extract v_n experimentally, often sophisticated background subtraction is performed on signals. Now we discuss how to determine v_n in an event. *Event plane* (EP) in a nuclear collision gives the orientation of the reaction plane. It is determined by the geometry of two nuclei during each collision. Since extracting Ψ_{RP} is not possible from experiments, several measurement techniques have been devised for calculating v_n. One of them is the event plane method (see Box 3), another is the multi-particle cumulant (MPC) method. In the event plane method, the observed v_n with respect to the Ψ_n^{EP} given by

$$v_n = \frac{\langle \cos\left(n[\phi - \Psi_n^{\mathrm{EP}}]\right)\rangle}{\sqrt{\langle \cos\left(n[\Psi_{n,p}^{\mathrm{EP}} - \Psi_{n,m}^{\mathrm{EP}}]\right)\rangle}} \tag{33}$$

[10] We use the center-of-mass (CM) energies per nucleon pair in A-A collisions, which is denoted by $\sqrt{s_{\mathrm{NN}}}$.

using eq. (35) in Box 3. Here, $\Psi^{\rm EP}_{n,p}$ is calculated over p particles, and similarly over m for $\Psi^{\rm EP}_{n,m}$. In the MPC method, v_n is given by:

$$\langle v_n^{2k} \rangle = \langle \cos[n(\phi_1 + ... + \phi_k - \phi_{k+1} - ... - \phi_{2k})] \rangle \tag{34}$$

We use this approach in Paper I and we will discuss the results from our work in section 5.2.

Box 3: Event-plane method in A-A collisions

In this method, the azimuthal angle of the reaction plane is derived from the observed event plane angle using anisotropic flow itself [34]. This can be done for each harmonic n of the Fourier expansion. The event flow vector $\boldsymbol{Q}_n$ is a 2d vector in the transverse plane:

$$Q_{n,x} = \sum_i w_i \cos(n\phi_i) = \boldsymbol{Q}_n \cos(n\Psi^{\rm EP}_n)$$
$$Q_{n,y} = \sum_i w_i \sin(n\phi_i) = \boldsymbol{Q}_n \sin(n\Psi^{\rm EP}_n),$$

where ϕ_i is the lab azimuthal angle and w_i is the weight for the particle i. The *event plane angle* $\Psi^{\rm EP}_n$ is the azimuthal angle of $\boldsymbol{Q_n}$:

$$\Psi^{\rm EP}_n = \tan^{-1}\left(\frac{Q_{n,y}}{Q_{n,x}}\right)/n. \tag{35}$$

4.2 Modification in flavour yields

Due to deconfinement and thermal production in the dense state after a heavy-ion collision, the yields of flavour hadrons, specifically strange (s) hadrons are modified. Hence, modification in these flavours are direct signals of the formation of a deconfined medium in high-multiplicity p-p and HI collisions. Strangeness enhancement as a signature of QGP formation was predicted in 1982 [35]. This was later observed in several experiments such as NA49 [36] and more recently by ALICE [37] and STAR [38].

Enhancement in the production of strange flavour hadrons is measured by the ratio of the yield of strange mesons and baryons to that of pions in all systems. The enhancement amount is calculated comparing this ratio to that in low multiplicity p-p collisions. In Paper II, we investigate the strangeness enhancement in jet-triggered events in p-p collisions due to rope hadronization mechanism in PYTHIA/Angantyr. In Paper III, we test the rope hadronization mechanism for p-p, p-A and A-A collisions and find that rope hadronization gives rise to strangeness enhancement in all

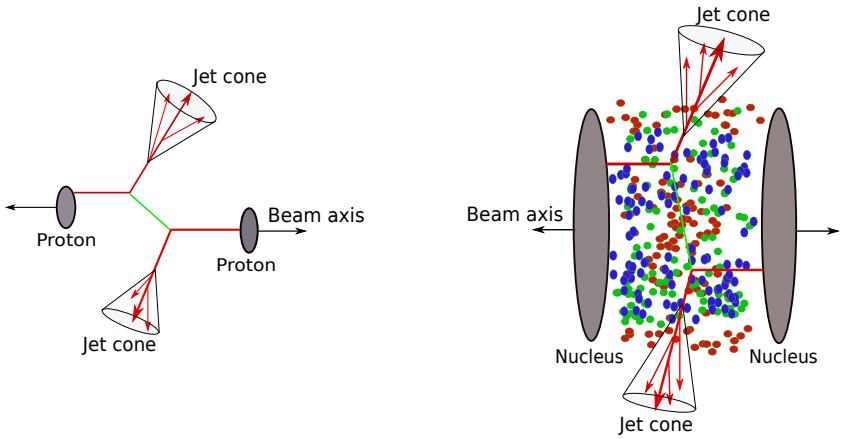

Figure 11: Reconstructed jets in a p-p event (left) and an A-A event showing the presence of dense environment (right). The green line stands for interaction between two partons from each of the nucleons.

systems. However, as we discuss in section 5.3, the enhancement in A-A requires further corrections from other string interactions, which is the subject of Paper IV.

In addition to modification in strangeness yields, charmonium suppression as a QGP-signal was theorized in the late 1980s [39, 40]. The correlation between both strangeness enhancement and modification of charmonium yield has also been observed experimentally [41].

4.3 Jet modification

In high-density collisions, an evolving hard parton traverse the dense partonic environment interacting with the medium, which causes its energy loss. If such a parton is qualified as a jet after reconstruction, then the energy loss it suffered is known as jet quenching. If there is a spread in the jet cone, it is called jet broadening [42]. These two effects are final-state effects. Difference in environments for reconstructed jets between p-p and A-A collisions is shown in figure 11.

In light of ultra-relatisvistic heavy-ion collisions, jet quenching was first hypothesised by Bjorken in 1982 [43]. It has been observed in STAR and PHENIX at BNL

[44, 45]. These observations are absent in p-p and p-A collisions but present in A-A collisions (see Table 2). Jet modification is traditionally measured using the nuclear modification factor, denoted by $R_{\rm AA}$. Any any given observable Φ_{AA} can be compared to its corresponding p-p counterpart (Φ_{pp}) using the definition:

$$R_{\rm AA}(\sqrt{s_{\rm NN}}, p_\perp, y, m, b) \propto \frac{\text{hot, dense QCD medium}}{\text{QCD vacuum}} \propto \frac{\Phi_{AA}}{\Phi_{pp}} \tag{36}$$

where b is the impact parameter. For nuclear modification factor, without medium effects, the high-$p_\perp$ particle yields grow proportional to the number of hard partonic interactions, which is proportional to the number of sub-collisions ($N_{\rm coll}$) in an A-A event. This dependence can be written as:

$$dN_{\rm AA}(b) = \langle N^{\rm AA}_{\rm coll}(b)\rangle dN_{\rm pp} \tag{37}$$

In case of high-$p_\perp$ production, the effects of the medium on the yield of a hard probe in A-A reaction is given by the nuclear modification factor:

$$R_{\rm AA}(p_\perp, y, b) = \frac{\frac{d^2N_{\rm AA}}{dp_\perp dy}}{\langle N^{\rm AA}_{\rm coll}\rangle \frac{d^2N_{\rm pp}}{dp_\perp dy}} \tag{38}$$

This factor measures the deviation of A-A at b from a superposition of NN collisions ($R_{\rm AA} = 1$). After dividing by the $N_{\rm coll}$ factor, if $R_{\rm AA} > 1$, it suggests enhancement, and in case of $R_{\rm AA} < 1$ suggest suppression. Further reviews of jet quenching phenomena can be found in refs. [46–48].

So far existing data suggests that jet quenching has not been observed in p-p [49]. On the other hand, strangeness enhancement is significant in high-multiplicity p-p collisions [37]. Hence the observational gaps in p-p, p-A and A-A collisions where in some systems QGP-like signals are observed and not others is an open question to both theory and experiments. We summarise the observational status of QGP-like signals in the different collision systems in the table below:

Table 2: Observation status of QGP-signals from p-p to A-A collisions

	High-multiplicity p-p	p-A	A-A
Final state collective flow	✓	✓	✓
Strangeness enhancement	✓	✓	✓
Jet quenching	✗	✗	✓

In addition to the initial geometry and modification of high Q^2 processes (such as jets), the crucial question in the community is whether such high energy densities give rise to *new forms of matter* which later hadronizes to form higher yields of heavier particles. In particular, this can be a QGP phase or a *Colour Glass Condensate* (CGC) phase or a combination of both. The CGC state is a dense condensate of gluons, where the associated fields evolve very slowly relative to natural time scales in HI evolution and are disordered [50]. In Paper I, we present how our string shoving model (sec. 5.2) differs from CGC.

In this thesis, our objectives is to probe the impact of string interactions on the observables described here, specifically final state collectivity and strangeness enhancement. Now that we have reviewed each of these signals, in the next section, we discuss novel string interactions in the Lund string model. These mechanisms may give rise to QGP-like signals in all systems. They are the centerpieces of this thesis and have been implemented and explored in the publications.

5 String interactions in the Lund model

Angantyr generates both p-p and HI events based on the impact parameter distribution of nucleons in an event. Other density-dependent interactions in the system is absent in Angantyr, therefore QGP-like signals, such as collective flow, are not reproduced. In the Lund string framework, such observations can be produced in nuclear systems only by including the interactions between strings.

String interactions are central to give rise to QGP-like effects since these interactions influence the final-state particle properties in different ways, based on the initial density of the collision. Since such interactions are absent in Angantyr, a jet in a nuclear collision will not suffer any modification of its physical properties. This is in disagreement with experimental data. This gap is bridged by string interaction mechanisms such as string shoving and rope hadronization, which is what we focus on in this section.

In all of our works, we calculate all string interactions by looking at pair-wise interactions. The calculation of such interactions between two strings in the laboratory frame is a complex problem. In the lab frame, most strings in ion-ion collisions are neither parallel to the beam axis nor to each other. That leads us to the next question - which reference frame do we consider to calculate such interactions for every string pair in an event?

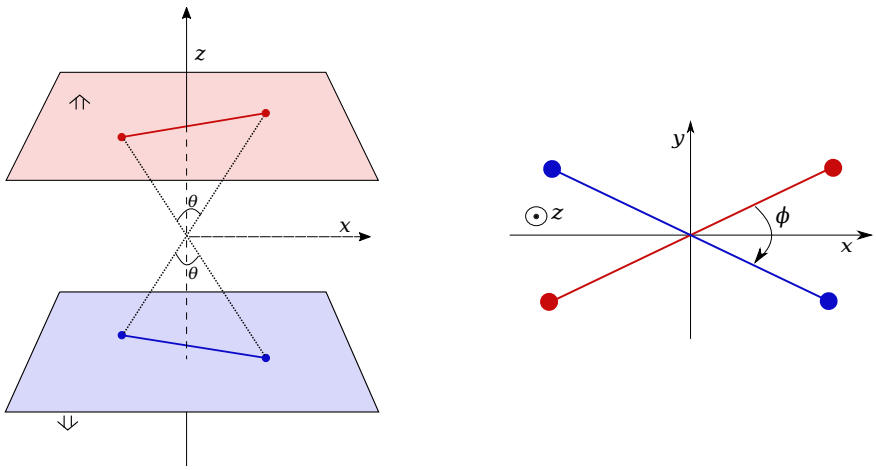

Figure 12: 3D diagram of the special Lorentz frame, called the *parallel frame* [16]. The string pair lie in parallel planes with respect to each other, each with the opening angle θ and the skewness angle ϕ between their projections.

5.1 The parallel frame formalism

Imagine a head-on collision of two nucleons. What follows next is an enormous burst of partons while parton showers evolve in both initial and final states, as shown in figure 8 in section 3. As these partons fly apart, strings are formed, which also interact with each other. Such interactions could occur via the colour electric fields pushing each other (that is, string shoving), and by the formation of colour ropes and their subsequent hadronization. If we are to calculate only the interaction force in this case, we need to devise a reference frame where, for any given pair of strings, they are in a *geometrically symmetric configuration*. This need is handled by the special Lorentz frame called the *parallel frame*, into which every possible pair of string pieces can be boosted where they lie in parallel planes with respect to each other. This is shown in figure 12. We calculate the shoving force and the rope hadronization based on the spatial overlap between two strings in this frame.

The usefulness of the parallel frame is apparent in the dense environments of ion-ion collisions. Most strings lie haphazardly over the pseudorapidity (η) span of the collider, and very few of them are parallel to the beam axis. There are also high-$p_\perp$ partons in A-A collisions and the strings connecting them are not parallel to the beam axis. The first implementation of string shoving, where only parallel strings were considered in high-multiplicity p-p collisions [20], does not handle

A-A collisions completely. There shoving effects were not calculated for high-$p_\perp$ partons due to the same reason. So for high-density collisions, we need a generic frame to include *all* the strings formed in an event.

Now that we know that we need a reference frame which we can construct such that the geometrical symmetry in the system is maximized. Since we are talking about three-dimensional space, we try to keep the two strings symmetric to each other in the spatial coordinates. The partons are assumed to be massless, so they move with the velocity of light c. Thus only the angles between the strings, called skewness angle ϕ and the opening angle θ for each string is required to find the relation between the momenta and spatial configuration.

For any four partons, p_1, p_2, p_3 and p_4, the relation between the four-momenta and transverse momenta in the parallel frame is given by the equation below in terms of η and the azimuthal angle ϕ:

$$\begin{aligned}
p_1 &= p_{\perp 1}\left(\cosh\frac{\eta}{2};\quad \cos\frac{\phi}{2},\quad \sin\frac{\phi}{2},\quad \sinh\frac{\eta}{2}\right),\\
p_2 &= p_{\perp 2}\left(\cosh\frac{\eta}{2};-\cos\frac{\phi}{2},-\sin\frac{\phi}{2},\quad \sinh\frac{\eta}{2}\right),\\
p_3 &= p_{\perp 3}\left(\cosh\frac{\eta}{2};\quad \cos\frac{\phi}{2},-\sin\frac{\phi}{2},-\sinh\frac{\eta}{2}\right),\\
p_4 &= p_{\perp 4}\left(\cosh\frac{\eta}{2};-\cos\frac{\phi}{2},\quad \sin\frac{\phi}{2},-\sinh\frac{\eta}{2}\right).
\end{aligned} \tag{39}$$

The $p_{\perp i}$ can be derived from the six invariant masses s_{ij} (given no two momenta are completely parallel):

$$\begin{aligned}
p_{\perp 1}^2 &= \frac{s_{12}}{4}\sqrt{\frac{s_{13}s_{14}}{s_{23}s_{24}}},\quad p_{\perp 2}^2 = \frac{s_{12}}{4}\sqrt{\frac{s_{23}s_{24}}{s_{13}s_{14}}},\\
p_{\perp 3}^2 &= \frac{s_{34}}{4}\sqrt{\frac{s_{13}s_{23}}{s_{14}s_{24}}},\quad p_{\perp 4}^2 = \frac{s_{34}}{4}\sqrt{\frac{s_{14}s_{24}}{s_{13}s_{23}}},
\end{aligned} \tag{40}$$

and the angles η and ϕ are given by:

$$\begin{aligned}
\cosh\eta &= \frac{s_{13}}{4p_{\perp 1}p_{\perp 3}} + \frac{s_{14}}{4p_{\perp 1}p_{\perp 4}},\\
\cos\phi &= \frac{s_{14}}{4p_{\perp 1}p_{\perp 4}} - \frac{s_{13}}{4p_{\perp 1}p_{\perp 3}}.
\end{aligned} \tag{41}$$

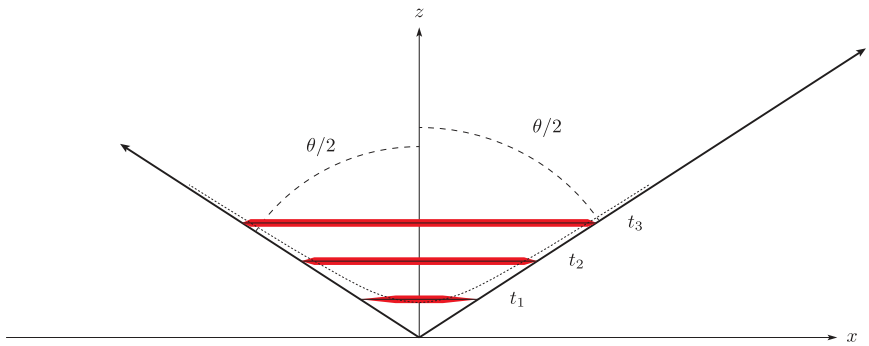

Figure 13: Evolution of a string to maximum radius R in several time steps $t_1 < t_2 < t_3$ in the z–x plane, in the parallel frame [28]. The red region marks the transverse extent of the string.

As can be seen from the above equation, the four-momenta of these 4 partons are symmetric in the parallel frame. The string pieces, at all times, are approximately straight lines and lie in parallel planes in the three-dimensional space. Further discussion of the parallel frame formalism is presented in Paper I.

5.2 String shoving

The cornerstone in the string-shoving formalism is that each string is a colour electric field with a spatial extent. These fields are approximated with a Gaussian profile in our work in Paper I [28] that closely follows the results from lattice calculations, e.g. [7]. The colour electric field in a cylindrical string of radius R can be expressed as:

$$E = N\exp\left(\frac{\rho^2}{2R^2}\right) \tag{42}$$

where N is a normalization factor, and ρ is the transverse distance from the centre of the string (in cylindrical coordinates). The form of the force per unit length generated between two such cylindrical strings which are lying parallel with respect to each other and to the beam axis, is then:

$$f(\rho) = \frac{dE_{\text{int}}}{d\rho} = \frac{g\kappa\rho}{R^2}\exp\left(-\frac{\rho^2}{4R^2}\right) \tag{43}$$

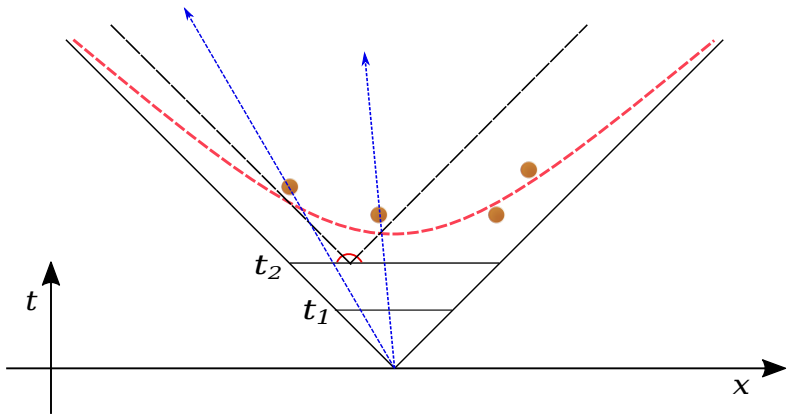

Figure 14: Space-time spread of a $p_\perp$ generated (red semicircle) at t_2 due to shoving, along a lightcone on a string [28]. The dashed red line marks the fragmentation hyperbola and the blue lines mark lines of constant η.

where κ is the string tension, ρ is the transverse separation between the centres of the strings, R is the radius of each of the cylindrical string, and g is a tunable parameter of the order of 1. One can note here that g corresponds to the fraction of the total string energy E_{st} carried by the electric field. The other part of E_{st} is carried by the magnetic current, which holds the string together.

In an Abelian field, when two such strings overlap, there will be repulsion between their colour fields[11] half the time, and attraction for the other half, depending on whether the fields are parallel or anti-parallel to each other. Now, every string is spanned between either a triplet (3) or an anti-triplet ($\bar{3}$) state. Therefore, in the case of non-Abelian QCD, we would only arrive at the attraction between two anti-parallel strings in the resultant singlet case, and in the case of two parallel strings, for the resultant anti-triplet case. To be more detailed, parallel strings combine to result in two states: $3 \otimes 3 = \bar{3} + 6$, while for anti-parallel strings, the resulting states are: $\bar{3} \otimes 3 = 8 + 1$. This implies that in the anti-parallel case, there is attraction only if the strings are in the same colour state, and for the parallel state, attraction occurs only when they are in different colour states. By weighting these states by the probability of occurrence of these states, it can be seen that, in the majority of cases, overlapping strings push each other. For a more detailed account of the colour multiplet dependence of shoving, see ref. [51]. It is to be noted that the strength of the shoving force can be modified by colour reconnections (see section

[11]From now onward, it is implied that we refer to colour electric field when we say colour field.

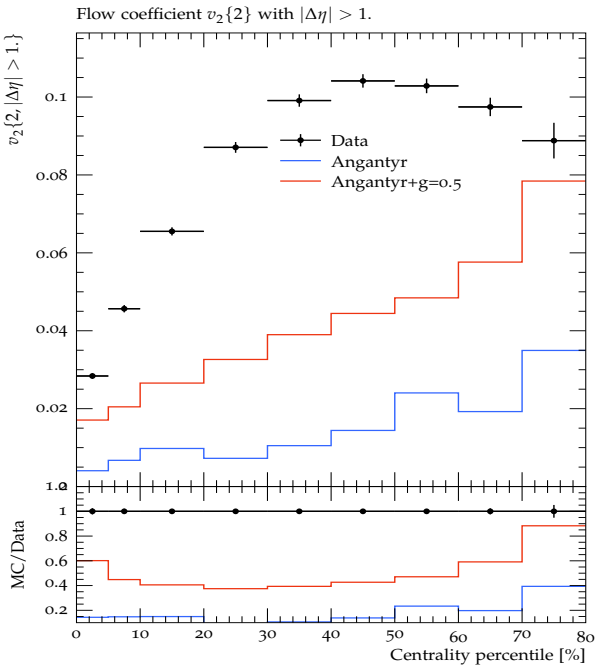

Figure 15: $v_2\{2\}$ response in Pb-Pb collisions at $\sqrt{s_{\mathrm{NN}}} = 5.02$ TeV with string shoving with $R = 1$ fm and $g = 0.5$, compared to default Angantyr. Plot from Paper I [28].

3.5), as it rearranges the colour flow in the new configuration of strings.

The shoving force between a pair of string pieces in the parallel frame results in a discretized and small ($\sim$ 20 MeV) $p_\perp$ push on each string piece. When such a $p_\perp$ is generated, it spreads in a lightcone (as it moves with c) as illustrated in figure 14. For a particular string piece, this force adds up over time steps during its evolution until hadronization. After hadronization, the accumulated push $\Sigma p_\perp$ for each string piece is distributed to the primary hadron formed from such a string piece, as shown in figure 14. Detailed mathematical construction of the colour fields and the Monte Carlo implementation of string shoving can be found in Paper I.

We already have seen in previous work, that string shoving produces final-state $v_2\{2\}$ in high-multiplicity p-p collisions [27]. Using that study as motivation, we applied this novel formalism to both small and large systems in this work. The main finding from Paper I is that even though string shoving is an important process in all systems, the overall collectivity in the final state of p-A and A-A collisions is not enough to account for the total collective effects as seen in experimental data. This

is shown for $v_2\{2\}$ in Pb-Pb collision in figure 15. It should be noted that this does not dismiss string shoving as a source of collective flow in large systems. As mentioned at the end of section 2.2, there are further corrections to the shoving force, due to the presence of soft gluons in the string, which were not taken into account in this implementation. These gluons would give rise to plaquettes, which are higher order string regions, and they would further contribute to the shoving force between a string pair. The impact of these corrections is further discussed in Paper IV.

5.3 Rope hadronization

String shoving does not result in large separation among all strings, so there is some degree of overlap among strings at the time of hadronization. Rope formation starts due to the overlap of the colour fields of strings after string shoving has occurred. Ropes are formed among overlapping colour flux tubes when their end-point partons combine to form higher colour multiplets, as seen from lattice calculations [52]. The string tension κ is modified due to the formation of such ropes, indicating that the energy per unit length between the endpoint multiplets is increased. Whether the overlap between such strings is parallel or anti-parallel, depending on the relative direction of the colour flow, also determines how much the string tension is modified. Below we present a brief discussion of our rope hadronization mechanism.

A rope formed between m colour charges and n anti-colour charges can form a colour multiplet denoted by $\{p, q\}$, due to the combination of triplets $\{1, 0\}$ and anti-triplets $\{0, 1\}$. We always have $p \leq m$ and $q \leq n$. For this colour state, the multiplicity is given by:

$$N = \frac{1}{2}(p+1)(q+1)(p+q+2). \tag{44}$$

From lattice calculations, it is found that the total tension of this rope is proportional to the second Casimir operator C_2 for the multiplet $\{p, q\}$[52]. This can be expressed as:

$$\kappa^{\{p,q\}} = \frac{C_2(p,q)}{C_2(1,0)}\kappa^{\{1,0\}} = \frac{1}{4}(p^2+pq+q^2+3p+3q)\kappa^{\{1,0\}}, \tag{45}$$

where $\kappa^{\{1,0\}} = \kappa$ is the string tension in a single string.

When a breakup occurs in a string forming a rope, the higher colour multiplets $\{p, q\}$ are reduced to lower colour multiplets $\{p-1, q\}$ or $\{p, q-1\}$. Therefore, the energy due to the modified string tension κ_{eff} is released following the relation eq. (46), for the transformation $\{p+1, q\}$ multiplet $\mapsto \{p, q\}$ multiplet:

$$\frac{\kappa_{\text{eff}}}{\kappa} = \frac{\kappa^{\{p+1,q\}} - \kappa^{\{p,q\}}}{\kappa} = h = \frac{2p+q+2}{4} \tag{46}$$

This released energy is available for tunnelling via eq. 19. This would give rise to a *higher number of heavy flavour quarks, particularly enhancing strange hadrons and baryons*. This is the most important effect of rope hadronization in PYTHIA/Angantyr. The h factor also modifies other flavour parameters in PYTHIA. To give an example of one such parameter, let us consider x [12] which gives the suppression of diquarks with strange quark content relative to diquarks without strange quarks [13]. This parameter x scales with the enhancement factor h as:

$$x \mapsto \tilde{x} = x^{\frac{1}{h}}. \tag{47}$$

Box 4: Effect of κ_{eff} on general observables

Even with the introduction of rope hadronization, the overall charged particle multiplicity N_{ch} of an event is approximately unchanged. This implies that the total number of strings is unchanged compared to events where rope formation does not occur.

Other parameters determining spin selection during hadronization are also influenced by κ_{eff}. One example of this is the parameter y which gives the suppression of spin 1 diquarks relative to spin 0 diquarks. This also scales as $\tilde{y} = y^{1/h}$.

[12] which is `StringFlav:probSQtoQQ` in the PYTHIA settings.

[13] In addition to the factor ρ for each extra s-quark.

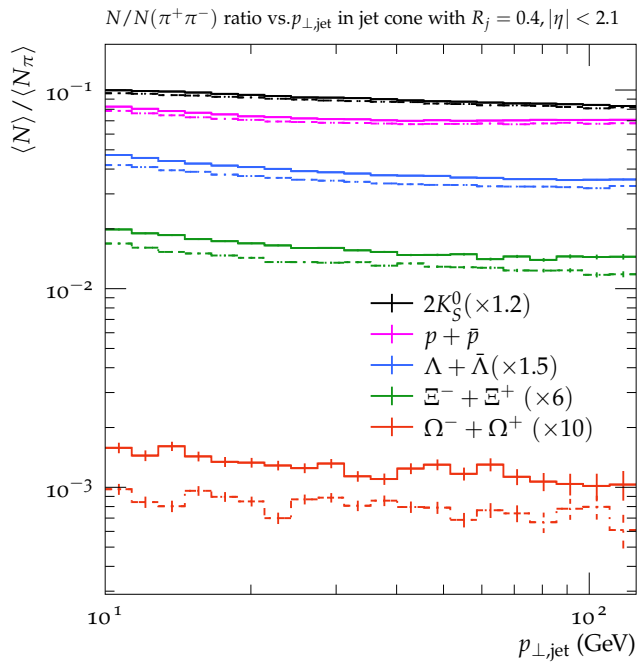

Figure 16: Strangeness and baryon enhancement in reconstructed jets using anti-k$_T$ in p-p collisions at $\sqrt{s} = 13$ TeV with string radius $R = 1$ fm. Plot from Paper II [16].

We have applied this formalism to study strangeness yields in jet-triggered events in p-p collisions in Paper II [16], as well as the general enhancement in minimum bias events in both small and large systems in Paper III [53]. Recall that one of the advantages of the parallel frame discussed in section 5.1, is that it can be used to study jets. This is what we do in Paper II, and find that rope hadronization can cause higher strangeness and baryon yields in jets in p-p collisions. This is shown in figure 16 where the result is shown for strange hadrons and their anti-particles. Going further, this study can also be done for p-A and A-A collisions in Angantyr.

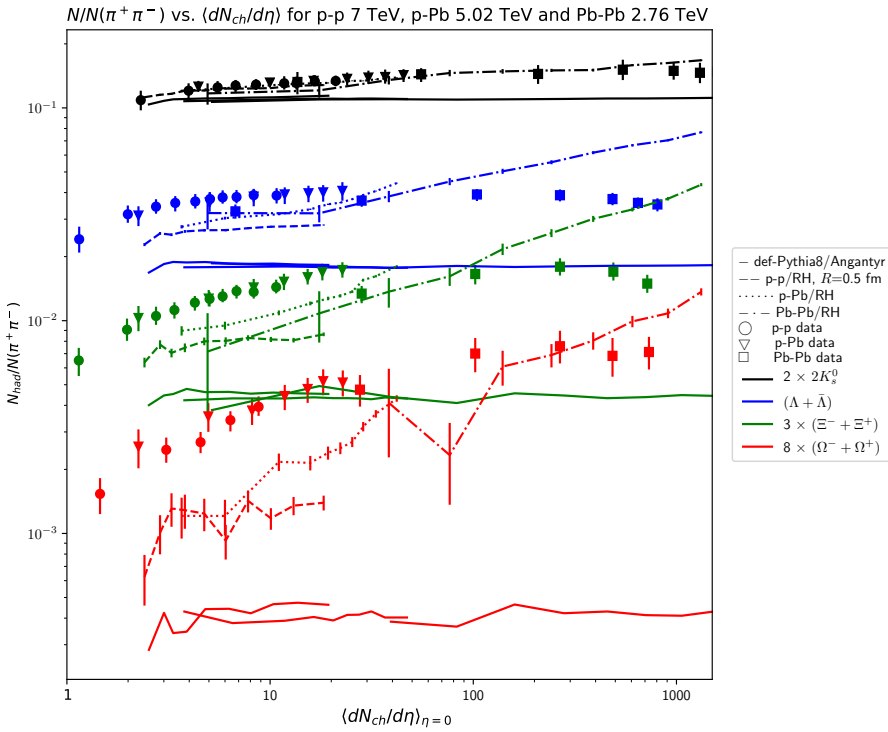

Figure 17: Enhancement in strangeness in p-p at $\sqrt{s} = 7$ TeV, p-Pb $\sqrt{s_{\rm NN}} = 5.02$ TeV and Pb-Pb $\sqrt{s_{\rm NN}} = 2.76$ TeV collisions for string radius $R = 0.5$ fm. RH stands for rope hadronization. Plot from Paper III [53].

The other advantage of the parallel frame is that *all* strings in an event can be considered for string interactions. This important aspect plays a major role in Paper III, where we study strangeness enhancement in all systems. The main result from Paper III is shown in figure 17. We found that the enhancement in strangeness increases coherently on the average $\frac{dN_{\rm ch}}{d\eta}$, going from small to large systems in PYTHIA/Angantyr. There is a huge improvement in strangeness production by rope hadronization over default PYTHIA for p-p, p-Pb and Pb-Pb collisions, mostly noticed for baryons and mutli-strange baryons such as Λ, Ξ and Ω. However, in high multiplicities in Pb-Pb collision, the yields overshoot experimental data. This linear rise may be countered by the inclusion of string shoving discussed in the previous section, and we discuss this aspect further in Paper IV.

5.4 Gleipnir

Gleipnir is the MC module built on PYTHIA/Angantyr to calculate effects due to string interactions. The workflow of Gleipnir is constructed such that it can be applied to all collision systems. Building a single framework for both small and large systems is both a physical and computational challenge. The parallel frame, therefore, simplifies this task by providing a common reference frame.

Some other mechanisms which are not part of this thesis will influence QGP-like effects discussed in section 4. One such example is the final-state colour swing [54]. The colour swing [54] is a perturbative phenomenon where colour dipoles in a parton shower are rearranged based on if there is a single or multiple gluon exchange between them. The effect is that of a new configuration of possibly shorter strings, which are available for hadronization. This is similar to previously discussed colour reconnection in section 3.5, the difference being that colour swing is performed at the perturbative level [14].

In the current version of Gleipnir[15], so far string shoving and rope hadronization have been implemented for all systems [16, 28, 53].

Table 3: Steps in event generation in Gleipnir in PYTHIA/Angantyr

$\tau \approx 0$ fm $\rightarrow$	No transverse extension of strings
$\tau \approx 0.5$ fm $\rightarrow$	Parton showers and colour reconnection end, string shoving sets in
$\tau \approx 1$ fm $\rightarrow$	Strings are at maximum radius, maximum shoving force between overlapping strings
$\tau \approx 2$ fm $\rightarrow$	Hadronization via ropes
$\tau > 2$ fm $\rightarrow$	Hadronic rescattering

The main idea in Gleipnir is that we first get an ensemble of colour dipoles after the parton showers, including effects such as colour reconnection. We then calculate the string interactions among such strings, which evolve in "radius" from their time of formation ($R = 0$ fm) to reach an equilibrium radius R (~ 0.5 fm). The

[14] A new implementation based on the parallel frame formalism is currently being done.

[15] At the time of writing, Gleipnir is not yet a public code.

timeline of all the steps for $R = 0.5$ fm is shown in Table 3. First string interaction to set in is string shoving, succeeded by rope hadronization. Since we use the parallel frame for all pairs of strings, the effects are calculated at the proper time in the parallel frame. This implies that rope hadronization does not "set in" at the same time for all the strings in the lab frame.

For small systems, such as in e^+-e^- collisions, very few strings are formed. They evolve without significant interaction and hence have negligible shoving force and rope effects in the hadronic final states. In contrast, for p-p collisions in the higher multiplicity regime, the density of strings is high. As string interaction effects are larger in dense environments, the effects are magnified in high-multiplicity p-p and A-A collisions.

To conclude, in our bottom-up approach using the parallel frame, the interaction for *every* pair of string piece is calculated. This can be done for both small and large systems. Given this common framework for all systems, the differences in the evolution of the system become more apparent. However, there are other mechanisms and different ways in which the origin of the QGP-like signals in the Lund string picture can be probed, some of which we have discussed in this introduction.

6 Outlook

The thesis aims to gain insights into the origin of QGP-like signals in all systems. Below we present some possible developments to that end, arising from the work done in each publication as a part of this thesis.

In Paper I, we construct the string shoving mechanism in PYTHIA and Angantyr [28]. We present the arguments behind the physical picture in the parallel frame and the MC implementation. We observe that even though string shoving generates enough final-state flow in p-p, in Pb-Pb, string shoving does not reproduce the entire $v_2\{2\}$ signal, as discussed in section 5.2. There are some corrections to the shoving force calculations, that can be included to produce a more consistent prediction.

In Paper II, we present the novel implementation of rope hadronization in Gleipnir [16] using the parallel frame. As such we can now simulate jets in p-p with rope effects and we observe enhanced strangeness in jet-triggered high-multiplicity p-p collisions, as discussed in section 5.3. In future, such effects can also be compared

with experimental data for all systems.

In Paper III, we present our rope hadronization results for strangeness enhancement for small and large systems in minimum bias. The novel implementation of rope hadronization gives a significant improvement compared to default PYTHIA and Angantyr in all systems, particularly in A-A collisions and for multi-strange baryon production. We discussed the main results in section 5.3, and observe a linear rise in the highest multiplicity in A-A collisions. More consistent results may be produced if string shoving is included.

In Paper IV, we present corrections to the primary hadronic vertices in PYTHIA and Angantyr due to the modified string tension κ (due to rope hadronization) and $p_\perp$ in the production vertices due to string shoving. This is the first step towards merging Gleipnir and hadronic rescattering in PYTHIA and Angantyr. We observe a significant effect due to shoving on the distribution of the vertices and in future, this effect may be implemented at the string level, so that rope hadronization effects are more accurately produced.

Apart from the work presented in this thesis, there are several ideas on how these questions can be tackled in the Lund string model, and some broader questions in the heavy-ion community. We present some of those in this section that are interesting in future research.

Origin of final state collectivity in all systems

The study performed in Paper I show that string shoving contributes to final-state collective flow in all systems. However, it does not produce enough collective flow in ion-ion collisions. So there might be a single or a combination of alternate mechanisms in the string model that can give rise to collective effects as seen in data. This could mean that string shoving and hadronic rescattering together might produce collective flow in all systems. Also, some of the other mechanisms contributing to this effect could be a perturbative ones within the Lund model, such as colour reconnection.

Particle yield correlations

Associated production of particles, such as the production of strange and vector mesons with heavy baryons, can also provide insights into particle production pro-

cesses in hot and dense environments. This has been studied in some experiments and can be explored in PYTHIA/Angantyr.

R_{AA} in p-p collisions

Since the distinction between jets and "medium" in p-p collisions is a challenge, the definition for R_{AA} given in section 4.3 is not suitable for p-p collisions. We would need well-defined physical observables in p-p phenomenology to understand and observe jet modification, to be able to compare to large systems.

Investigation for QGP-like effects in e^+-e^- collisions

Effects such as string shoving and rope hadronization will influence final states in e^+-e^- collisions as well, but these effects are rare. There have been some searches for collective effects in e^+-e^- collisions with archived data or at low luminosities [55, 56], so far without any observable effects. In experiments such as the Future Circular Collider-ee, these effects would be more probable due to an increase in the number of Z particles ($\mathcal{O}(10^{12})$). This is an exciting domain to be explored.

We will still need more tools to know more about the perturbative contribution to QGP-like effects in nuclear collisions and e-A collisions. If we have a look at the recent and future timeline of the relevant physics research, several significant events in the broader community and some developments in the Lund model are upcoming:

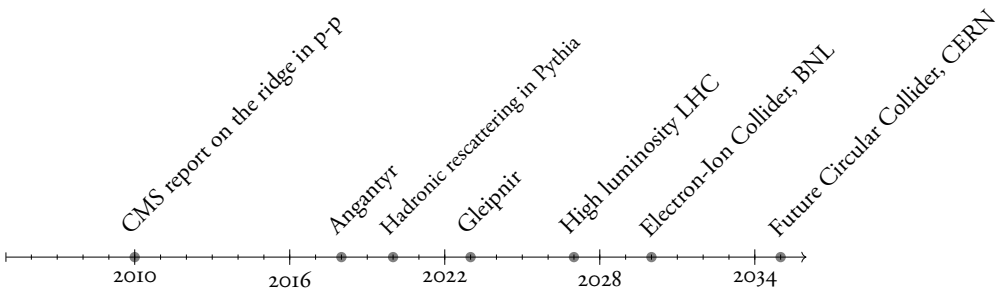

If we condense the fundamental aspects discussed in this introduction in the light of the above timeline, we can highlight some of the big questions:

- In nuclear collisions, how do the several approaches, such as CGC and kin-

etic theory and the string model, differ and what can be learnt from the differences among these various approaches?

- Can high luminosity LHC show us the phase space where the small and large systems will split up and might have unique features in dense environments?
- What are some physical effects and probes that will help us understand EIC and Future Circular Collider era physics better with the Lund model?

These are some of the outstanding questions that we are excited to gain further insights into in the future.

7 References

[1] J.-Y. Ollitrault, "Anisotropy as a signature of transverse collective flow," *Phys. Rev. D* **46** (1992) 229–245.

[2] H. Heiselberg, "Event-by-event physics in relativistic heavy ion collisions," *Phys. Rept.* **351** (2001) 161–194, nucl-th/0003046.

[3] A. Amariti, D. Forcella, A. Mariotti, and G. Policastro, "Holographic Optics and Negative Refractive Index," *JHEP* **04** (2011) 036, 1006.5714.

[4] R. P. Feynman, "Simulating physics with computers," *Int. J. Theor. Phys.* **21** (1982) 467–488.

[5] P. Cea, L. Cosmai, F. Cuteri, and A. Papa, "Flux tubes at finite temperature," *JHEP* **06** (2016) 033, 1511.01783.

[6] P. Cea, L. Cosmai, F. Cuteri, and A. Papa, "Flux tubes in the SU(3) vacuum: London penetration depth and coherence length," *Phys. Rev. D* **89** (2014), no. 9 094505, 1404.1172.

[7] M. Baker, P. Cea, V. Chelnokov, L. Cosmai, F. Cuteri, and A. Papa, "Isolating the confining color field in the SU(3) flux tube," *Eur. Phys. J. C* **79** (2019), no. 6 478, 1810.07133.

[8] Andersson, Bö and Gustafson, G. and Ingelman, G. and Sjöstrand, T., "Parton Fragmentation and String Dynamics," *Phys. Rept.* **97** (1983) 31–145.

[9] B. Andersson, G. Gustafson, and B. Söderberg, "A General Model for Jet Fragmentation," *Z. Phys. C* **20** (1983) 317.

[10] G. Gustafson and U. Pettersson, "Dipole Formulation of QCD Cascades," *Nucl. Phys. B* **306** (1988) 746–758.

[11] J. R. Christiansen and P. Z. Skands, "String Formation Beyond Leading Colour," *JHEP* **08** (2015) 003, 1505.01681.

[12] C. Bierlich and J. R. Christiansen, "Effects of color reconnection on hadron flavor observables," *Phys. Rev. D* **92** (2015), no. 9 094010, 1507.02091.

[13] B. Andersson, *The Lund model*, vol. 7. Cambridge University Press, 7, 2005.

[14] C. Bierlich, G. Gustafson, and L. Lönnblad, "Diffractive and non-diffractive wounded nucleons and final states in pA collisions," *JHEP* **10** (2016) 139, 1607.04434.

[15] C. Bierlich, S. Chakraborty, G. Gustafson, and L. Lönnblad, "Hyperfine splitting effects in string hadronization," *Eur. Phys. J. C* **82** (2022), no. 3 228, 2201.06316.

[16] C. Bierlich, S. Chakraborty, G. Gustafson, and L. Lönnblad, "Jet modifications from colour rope formation in dense systems of non-parallel strings," 2202.12783.

[17] C. Bierlich *et. al.*, "A comprehensive guide to the physics and usage of PYTHIA 8.3," 2203.11601.

[18] T. Sjöstrand, S. Mrenna, and P. Z. Skands, "PYTHIA 6.4 Physics and Manual," *JHEP* **05** (2006) 026, hep-ph/0603175.

[19] T. Sjöstrand, S. Ask, J. R. Christiansen, R. Corke, N. Desai, P. Ilten, S. Mrenna, S. Prestel, C. O. Rasmussen, and P. Z. Skands, "An introduction to PYTHIA 8.2," *Comput. Phys. Commun.* **191** (2015) 159–177, 1410.3012.

[20] C. Bierlich, G. Gustafson, L. Lönnblad, and H. Shah, "The Angantyr model for Heavy-Ion Collisions in PYTHIA8," *JHEP* **10** (2018) 134, 1806.10820.

[21] R. J. Glauber, "Cross-sections in deuterium at high-energies," *Phys. Rev.* **100** (1955) 242–248.

[22] R. J. Glauber and G. Matthiae, "High-energy scattering of protons by nuclei," *Nucl. Phys. B* **21** (1970) 135–157.

[23] B. Andersson, G. Gustafson, and B. Nilsson-Almqvist, "A Model for Low p(t) Hadronic Reactions, with Generalizations to Hadron - Nucleus and Nucleus-Nucleus Collisions," *Nucl. Phys. B* **281** (1987) 289–309.

[24] B. Andersson, G. Gustafson, and H. Pi, "The FRITIOF model for very high-energy hadronic collisions," *Z. Phys. C* **57** (1993) 485–494.

[25] H. Pi, "An Event generator for interactions between hadrons and nuclei: FRITIOF version 7.0," *Comput. Phys. Commun.* **71** (1992) 173–192.

[26] A. Bialas, M. Bleszynski, and W. Czyz, "Multiplicity Distributions in Nucleus-Nucleus Collisions at High-Energies," *Nucl. Phys. B* **111** (1976) 461–476.

[27] C. Bierlich, G. Gustafson, and L. Lönnblad, "Collectivity without plasma in hadronic collisions," *Phys. Lett. B* **779** (2018) 58–63, 1710.09725.

[28] C. Bierlich, S. Chakraborty, G. Gustafson, and L. Lönnblad, "Setting the string shoving picture in a new frame," *JHEP* **03** (2021) 270, 2010.07595.

[29] C. Bierlich, G. Gustafson, L. Lönnblad, and A. Tarasov, "Effects of Overlapping Strings in pp Collisions," *JHEP* **03** (2015) 148, 1412.6259.

[30] J. Bellm *et. al.*, "Herwig 7.0/Herwig++ 3.0 release note," *Eur. Phys. J. C* **76** (2016), no. 4 196, 1512.01178.

[31] T. Sjöstrand and M. Utheim, "A Framework for Hadronic Rescattering in pp Collisions," *Eur. Phys. J. C* **80** (2020), no. 10 907, 2005.05658.

[32] **CMS** Collaboration, V. Khachatryan *et. al.*, "Observation of Long-Range Near-Side Angular Correlations in Proton-Proton Collisions at the LHC," *JHEP* **09** (2010) 091, 1009.4122.

[33] **CMS** Collaboration, S. Chatrchyan *et. al.*, "Multiplicity and Transverse Momentum Dependence of Two- and Four-Particle Correlations in pPb and PbPb Collisions," *Phys. Lett. B* **724** (2013) 213–240, 1305.0609.

[34] A. M. Poskanzer and S. A. Voloshin, "Methods for analyzing anisotropic flow in relativistic nuclear collisions," *Phys. Rev. C* **58** (1998) 1671–1678, nucl-ex/9805001.

[35] J. Rafelski and B. Müller, "Strangeness Production in the Quark - Gluon Plasma," *Phys. Rev. Lett.* **48** (1982) 1066. [Erratum: Phys.Rev.Lett. 56, 2334 (1986)].

[36] **NA49** Collaboration, D. Varga, "Recent results on strangeness production from CERN experiment NA49," in *36th Rencontres de Moriond on QCD and Hadronic Interactions*, pp. 295–298, 2001. hep-ex/0105035.

[37] **ALICE** Collaboration, J. Adam *et. al.*, "Enhanced production of multi-strange hadrons in high-multiplicity proton-proton collisions," *Nature Phys.* **13** (2017) 535–539, 1606.07424.

[38] **STAR** Collaboration, G. Agakishiev *et. al.*, "Strangeness Enhancement in Cu+Cu and Au+Au Collisions at $\sqrt{s_{NN}} = 200$ GeV," *Phys. Rev. Lett.* **108** (2012) 072301, 1107.2955.

[39] S. J. Brodsky and A. H. Mueller, "Using Nuclei to Probe Hadronization in QCD," *Phys. Lett. B* **206** (1988) 685–690.

[40] N. Armesto and A. Capella, "A Quantitative reanalysis of J / psi suppression in nuclear collisions," *Phys. Lett. B* **430** (1998) 23–31, hep-ph/9705275.

[41] F. Becattini, L. Maiani, F. Piccinini, A. D. Polosa, and V. Riquer, "Correlating strangeness enhancement and J/psi suppression in heavy ion collisions at s(NN)**1/2 = 17.2-GeV," *Phys. Lett. B* **632** (2006) 233–237, hep-ph/0508188.

[42] R. Baier, Y. L. Dokshitzer, A. H. Mueller, S. Peigne, and D. Schiff, "Radiative energy loss of high-energy quarks and gluons in a finite volume quark - gluon plasma," *Nucl. Phys. B* **483** (1997) 291–320, hep-ph/9607355.

[43] J. D. Bjorken, "Energy Loss of Energetic Partons in Quark - Gluon Plasma: Possible Extinction of High p(t) Jets in Hadron - Hadron Collisions,".

[44] **STAR** Collaboration, J. Adams *et. al.*, "Evidence from d + Au measurements for final state suppression of high p(T) hadrons in Au+Au collisions at RHIC," *Phys. Rev. Lett.* **91** (2003) 072304, nucl-ex/0306024.

[45] **STAR** Collaboration, J. Adams *et. al.*, "Transverse momentum and collision energy dependence of high p(T) hadron suppression in Au+Au collisions at ultrarelativistic energies," *Phys. Rev. Lett.* **91** (2003) 172302, nucl-ex/0305015.

[46] Y. Mehtar-Tani, J. G. Milhano, and K. Tywoniuk, "Jet physics in heavy-ion collisions," *Int. J. Mod. Phys. A* **28** (2013) 1340013, 1302.2579.

[47] M. Connors, C. Nattrass, R. Reed, and S. Salur, "Jet measurements in heavy ion physics," *Rev. Mod. Phys.* **90** (2018) 025005, 1705.01974.

[48] A. Majumder and M. Van Leeuwen, "The Theory and Phenomenology of Perturbative QCD Based Jet Quenching," *Prog. Part. Nucl. Phys.* **66** (2011) 41–92, 1002.2206.

[49] **ALICE** Collaboration, A. Kotliarov, "Search for jet quenching effects in high-multiplicity proton-proton collisions at $\sqrt{s}$ = 13 TeV," *PoS* **LHCP2021** (2021) 183.

[50] L. D. McLerran and R. Venugopalan, "Computing quark and gluon distribution functions for very large nuclei," *Phys. Rev. D* **49** (1994) 2233–2241, hep-ph/9309289.

[51] S. Chakraborty, "String shoving effects on jets in p-p collisions," in *10th International Conference on Hard and Electromagnetic Probes of High-Energy Nuclear Collisions: Hard Probes 2020* , 9, 2020. 2009.00559.

[52] G. S. Bali, "Casimir scaling of SU(3) static potentials," *Phys. Rev. D* **62** (2000) 114503, hep-lat/0006022.

[53] C. Bierlich, S. Chakraborty, G. Gustafson, and L. Lönnblad, "Strangeness enhancement across collision systems without a plasma," 2205.11170.

[54] E. Avsar, G. Gustafson, and L. Lönnblad, "Small-x dipole evolution beyond the large-N(c) imit," *JHEP* **01** (2007) 012, hep-ph/0610157.

[55] A. Badea, A. Baty, P. Chang, G. M. Innocenti, M. Maggi, C. Mcginn, M. Peters, T.-A. Sheng, J. Thaler, and Y.-J. Lee, "Measurements of two-particle correlations in e^+e^- collisions at 91 GeV with ALEPH archived data," *Phys. Rev. Lett.* **123** (2019), no. 21 212002, 1906.00489.

[56] **Belle** Collaboration, Y. C. Chen *et. al.*, "Measurement of Two-Particle Correlations of Hadrons in e+e- Collisions at Belle," *Phys. Rev. Lett.* **128** (2022), no. 14 142005, 2201.01694.

8 List of publications

This thesis is based on the following publications, referred to by their Roman numerals:

Paper I

Setting the string shoving picture in a new frame
C. Bierlich, **S. Chakraborty**, G. Gustafson and L. Lönnblad
Journal of High Energy Physics **2021, 270 (2021)**
e-Print: 2010.07595 [hep-ph]
MCnet-20–22, LU-TP-20–48

In this publication, we present a novel method to calculate string shoving in all systems. The strings are considered as colour flux-tubes, with colour electric fields with transverse extent. The force between two colour flux tubes is calculated in a special Lorentz frame called the parallel frame. The final state collectivity reproduced by string shoving is investigated in both small and large systems.

The string shoving formulation follows from a previous work of my collaborators. The theoretical formulation of the parallel frame was done by Gösta Gustafson and re-calculated by myself. For the Monte-Carlo implementation, I wrote the code for the parallel frame formulation, while Leif Lönnblad wrote the overall Gleipnir framework. I produced all preliminary and main results while Leif Lönnblad handled the tuning value of a parameter.

In the publication, I wrote the model description and implementation with Leif Lönnblad and the parts on heavy-ion results and discussion. Rest of the manuscript was revised in collaboration.

Paper II

Jet modifications from colour rope formation in dense systems of non-parallel strings
C. Bierlich, **S. Chakraborty**, G. Gustafson and L. Lönnblad
To be published in *SciPost Physics*
e-Print: 2202.12783 [hep-ph]
MCnet-22–02, LU-TP-22–09

In this publication, we present the implementation of rope hadronization mech-

anism using the parallel frame. Rope hadronization would modify the strangeness yields, and this modification can be observed in jets as well. The system of interest is jet-triggered proton-proton collisions, where we probe the yields of strange hadrons and baryons in a jet. We find significant enhancement of strangeness, particularly Ω baryon in the jet.

The rope hadronization formulation follows from a previous work of my collaborators and the work done in Paper I. The theoretical development was done in collaboration. I wrote the code for rope hadronization implementation with Leif Lönnblad. I handled the analyses for minimum bias in all systems and the jet analysis for proton-proton collisions which is the focus of the paper.

The manuscript was drafted by myself. The Monte-Carlo implementation section was written in collaboration with Leif Lönnblad. Rest of the sections were revised in collaboration.

Paper III

Strangeness enhancement across collision systems without a plasma
C. Bierlich and **S. Chakraborty**, G. Gustafson and L. Lönnblad
In review, *Physics Letters B*
e-Print: 2205.11170 [hep-ph]
MCnet-22–11, LU-TP-22–25

In this letter, we show the enhancement in strangeness yields with rope hadronization in all systems. The formalism produces significant improvements over default Pythia and Angantyr.

The parallel frame and rope hadronization formulations used in this publication build on the implementation done in Paper I and Paper II respectively. I handled the analyses for all three systems and produced the main results of this letter. The manuscript was drafted by myself and revised in collaboration.

Paper IV

Impact of string interactions on the space-time evolution of hadronic vertices
S. Chakraborty and L. Lönnblad
To be submitted to *European Physical Journal C*
e-Print: 2207.14186 [hep-ph]
MCnet-22–12, LU-TP-22–50

The interface between the different string interactions, and processes such as hadronic rescattering would need further adjustments to be able to reproduce more consistent results. This is what we address in this publication. We introduce corrections to the production vertices of the primary hadrons both in the transverse momentum component of the production vertices and the string tension used during hadronization. I analysed and produced the preliminary results for all systems, while Leif Lönnblad produced the final results. The paper was written in collaboration.

9 Further published works

Publications not included in this thesis, listed according to their chronological order:

Paper VI

String shoving effects on jets in p-p collisions
S. Chakraborty
Proceedings of Science **HardProbes2020 (2021) 134**
e-Print: 2009.00559 [hep-ph]

This paper is a conference proceeding from the Hard Probes conference, held online in June 2020. I produced the results and wrote the paper.

Paper VII

Cracking hadron and nuclear collisions open with ropes and string shoving in PYTHIA8
S. Chakraborty
To be published in *SciPost Proceedings*
e-Print: 2109.12359 [hep-ph]

This paper is a conference proceeding from the International Symposium on Multiparticle Dynamics conference, held online in July 2021. I produced the results and wrote the paper.

Paper VIII

Hyperfine splitting effects in string hadronization
C. Bierlich, **S. Chakraborty**, G. Gustafson and L. Lönnblad
European Physical Journal A **82 (2022) 3, 228**
e-Print: 2201.06316 [hep-ph]

This paper provides the tuned values of fragmentation parameters used in baryon and flavour production during hadronization in PYTHIA 8. Christian Bierlich tuned the parameters and wrote the paper, while I checked the strangeness and baryonic yields for p-p, p-Pb and Pb-Pb collisions (not included in the paper) with the tuned

values and produced few figures.

Paper IX

A comprehensive guide to the physics and usage of PYTHIA 8.3
C. Bierlich, **S. Chakraborty** et. al. PYTHIA collaboration
In review, *SciPost Physics Codebases*
e-Print: 2203.11601 [hep-ph]

The PYTHIA 8.3 manual, describing the physics of the current and latest implementations, with major developments. I wrote parts of the string interactions section and provided the figures for those sections. Revision and proof-reading of the manuscript was done in collaboration.

10 Acknowledgements

At the time of writing, due to Covid-19 pandemic and visa restrictions, I have not met my family over the last 3 years. Even with the geographical separation and timezone difference, they have always provided me unconditional support, so before anything else I want to express my gratitude to them for taking care of themselves and of me throughout the pandemic.

I want to start by thanking my supervisor Leif Lönnblad for the opportunity to perform research in theoretical particle physics specifically in heavy-ions. I have gained insights from his vast experience in event generators and his intuition for particle physics phenomenology. I would like to thank my other advisor Gösta Gustafson and collaborator, Christian Bierlich for the good collaboration over the years. My concepts of QCD and the Lund model have taken shape and benefited to a great extent from our brainstorming sessions.

It has been a marvellous experience discussing and learning physics from many colleagues and seniors spread around the World, both online and in person, and finding inspiration in their work. I am grateful to the MCnet collaboration for the excellent learning opportunities and the primary funding for this position. I am also thankful to all PYTHIA collaborators and to the CLASH group with the experimentalists at Lund. I have learned a lot through our many discussions and dialogues. Thanks should also go to the MCnet student postdoc committee, it has been a great pleasure to work together with other PhDs and postdocs across the World.

I would like to thank Korinna Zapp for her support. Her extensive and critical comments on the introduction and the excellent discussions that has helped shape the introduction to this thesis on several points. I would also like to thank Marianne Sommarin for her support and encouragement. Thanks to Carsten Peterson for always being welcoming and for sharing his wisdom from his spectacular academic experiences. I am also grateful to Stefan Prestel for sharing his excellent knowledge of event generators and for cheering my work.

Many thanks to Najmeh Abiri for being a great friend. Harsh Shah helped a lot with figuring out the administrative side of this new country, so my sincere thanks for that. Special thanks to Johannes Bellm for being a source of optimism, and to Christine Rasmussen for being a great friend and providing encouragement. I would like to thank Marius Utheim for being a very supportive colleague and a good

friend. I am also thankful to Jarkko Peuron, for being a wonderful office-mate and colleague, also for his comments on the very first draft of the introduction to this thesis. I wish the best to all my fellow PhDs – Andrew, Chiara, Harsh, Mårten, Mattias, Robin, Timea and Torbjörn – on your work.

I would like to acknowledge our administrative officers, Lena Magnuosson for being positive, Caroline, Eva, Mandana and Louise for their assistance. Thanks to our former librarian, Marianne Madsen for being so helpful throughout my PhD.

All the years in Lund have been particularly exceptional due to the active University affairs. Special thanks to my friend and fellow astronomer, Brian Thorsbro for encouraging me into the Lunds Doktorandkår world and Simon Schmidt for being the perfect co-chair of LDK. I greatly enjoyed working together with both of you. Thanks also to Malin Rantzer for being a wonderful colleague. To the rest of the LDK team, during and after my time as the chair, it has been quite a journey, and I wish you all the best.

I would like to thank my friends Leif and Weibke, Baptiste and Elena for the many good times and for their cheerful company. Special thanks to my friends Komal and Jonathan, Swati and Naveen for their warm support and company.

At last but not the least, I would like to thank my Bachelor's degree lecturer, Dr. Dhruba Banerjee, for your encouragement since my time as a Bachelor's student to this day. I am grateful to Goonja, who shared similar aspirations but never got the chance to fulfill them. I have felt her absence throughout all these years since October 2018, and will cherish our childhood memories always.

I would like to thank my fiancé Benjamin, for your exceptional support and understanding and encouragement. In the end, I am very grateful to my mother, for patiently hearing through my physics rants and for being my endless inspiration and support, this journey would not have happened otherwise.

Paper I

I

Setting the string shoving picture in a new frame

Christian Bierlich, Smita Chakraborty, Gösta Gustafson, and Leif Lönnblad

Journal of High Energy Physics **2021**, 270 (2021)
e-Print: 2010.07595 [hep-ph]
MCnet-20–22, LU-TP-20–48

Abstract

Based on the recent success of the Angantyr model in describing multiplicity distributions of the hadronic final state in high energy heavy ion collisions, we investigate how far one can go with a such a string-based scenario to describe also flow effects measured in such collisions.

For this purpose we improve our previous so-called *shoving* model, where strings that are close in space–time tend to repel each other in a way that could generate anisotropic flow, and we find that this model can indeed generate such flows in AA collisions. The flow generated is not quite enough to reproduce measurements, but we identify some short-comings in the presented implementation of the model that, when fixed, could plausibly give a more realistic amount of flow.

1 Introduction

High energy proton-proton and heavy ion (HI) collisions are frequently analysed assuming very different dynamical mechanisms. Models based on string formation or cluster chains and subsequent hadronization, implemented in event generators like PYTHIA [1, 2], HERWIG [3, 4], or SHERPA [5, 6], have been very successful in describing particle production in e^+e^- annihilation, DIS, and pp collisions. In contrast many features in HI collisions have been described assuming the formation of a thermalized quark–gluon plasma (QGP), in particular collective flow [7, 8, 9, 10, 11, 12] and enhancement of strange particles [13]. However, lately the difference between pp and nuclear collisions has become much less clear. Both collective effects and increased strangeness production have been observed in high multiplicity pp events (see *e.g.* [14] and [15]). This has raised the question whether a plasma can be formed in pp collisions, or alternatively, if these effects in HI collisions also can be described in a scenario based on strings.

For pp collisions the conventional picture includes multi-parton subcollisions, and at high energies the scattered partons are mainly gluons, which form colour connected gluon chains. This picture corresponds to multiple pomeron exchange (including pomeron vertices), with a gluon chain pictured as a cut BFKL pomeron ladder. It is also consistent with models based on reggeon theory, *e.g.* the models by the groups in Tel Aviv [16], in Durham [17], or by Ostapchenko [18]. The gluons here also hadronize forming strings or cluster chains.

For high energy nucleus collisions many features can contribute to the observed collective effects, and they are often combined to the following scenario: At high energy the gluons in a nucleus form a "color glass condensate" (CGC) [19, 20]. This state is described by a classical colour field, where the strength is saturated due to unitarity, with a "saturation scale" $Q_s \sim (1/\alpha_s)(x/x_0)^{-\lambda}$. When two nuclei collide the overlapping non-Abelian fields form a "glasma"; for reviews of the CGC and the glasma see *e.g.* refs. [21, 22, 23]. The glasma state contains parallel longitudinal colour-electric and colour-magnetic fields, associated with induced magnetic charges in the projectile and target remnants. These fields also build up a topological charge giving rise to CP-violating effects [24, 25]. The glasma is unstabel, and in this scenario it turns rapidly into a QGP, which soon thermalizes, see *e.g.* ref. [26]. This transition is often motivated referring to "Nielsen–Olesen instabilities" in the QCD Fock vacuum [27, 28], or "Weibel instabilities" in an electro-magnetic plasma [29].

All features in this scenario may not be necessary to get the observed collective effects. Thus correlations between the coordinate space and the momentum space

in the CGC, expressed in a Wigner wavefunction, can result in collective flow in pA collisions, also without thermalization [30]. A completely different angle at the problem, is offered by the dipole evolution model DIPSY [31, 32], which includes saturation in a way similar to the CGC, but does not in itself show momentum space anisotropies compatible with flow, though the geometries generated – even for pp collisions [33] – are more or less compatible with the expectations if final state interactions are to transport initial state geometries to the final state. This is even true for more involved flow observables in both pp and pA collisions, and also holds promise for generating geometries at a future electron–ion collider [34]. The relation between initial asymmetry and collective flow in AA collisions, in case of incomplete thermalization, has also been studied by Drescher *et al.* in ref. [35]. In this article we are not able to clarify which steps in the above chain are responsible for which observable. Instead we will here limit ourselves by comparing the string scenario for nucleus collisions with a process, in which there is a hot thermalized expanding quark-gluon plasma.

We note that in high multiplicity pp events, the density of strings is quite high. The width of a string-like flux tube is estimated to be of the order of $1/\Lambda_{QCD}$, which implies that the flux tubes will overlap in space. Recently we have demonstrated, that in pp collisions both collectivity and strangeness enhancement can be explained as consequences of a higher energy density in systems of overlapping strings or "ropes". This gives both a transverse pressure, which can cause long range collective flow [36], and enhanced strangeness following from the higher energy release in the breakup of a rope [37]. We also note that string-based models have successfully described the general particle distributions in nuclear collisions. Early models were Fritiof (working well for not too high energies) [38] and HIJING [39], and the PYTHIA event generator for pp was recently generalized to AA collisions in the Angantyr model [40] (now included in PYTHIA8). These results open up for a unified description of pp, pA, and AA collisions, with a smooth transition from dilute to dense systems, and we will in this paper propose the generalization of the shoving model for pp in ref. [36] to a string-based model for collective flow in AA collisions. The generalization of the model for strangeness enhancement will, however, be postponed to a later publication.

The particle distribution is in (symmetric) nucleus collisions characterized by an approximately boost invariant central plateau. This feature is quite natural if the hadrons are produced from boost invariant strings stretching between the projectile and target remnants. An essential feature is here that the relativistic string, like a homogeneous electric field, has no momentum in the longitudinal direction, and thus no longitudinal pressure and also *no longitudinal expansion*. The increased

energy density in overlapping parallel strings will, however, lead to a transverse pressure and a transverse expansion. The energy increase due to the overlap will be comparatively moderate, and the energy density dE/dz therefore roughly constant in time up to the hadronization at (proper) time $\tau = 1.5-2$ fm. From this moment the hadrons move out with rapidities approximately equal to the hyperbolic angle $\eta_{st} \equiv (1/2)\ln[(t+z)/(t-z)]$ corresponding to the place where they were "born"[1] (see section 3).

A boost invariant plateau is also expected for an initial glasma state, if the longitudinal colour–electric and –magnetic fields are stretched out in a similar longitudinal way. But if the glasma is rapidly transformed into a thermalized plasma, then this plasma will expand longitudinally and dilute with an energy density falling like τ^{-1} or faster, before freeze-out or hadronization time [41]. A fast thermalization therefore must have a correspondingly higher initial density. A quantitative estimate of this difference is presented in section 2.1.

As we will see in section 5.2, the expansion of the string system gradually approaches hydrodynamic flow, for very high initial string densities, although this expansion is constrained to the two transverse dimensions. As discussed above this implies that the energy density is not significantly reduced. We also note that the number of strings is not increased during the evolution. Therefore there is no transition to a more continuous medium, at some intermediate time before hadronization. For events with very high multiplicities we also imagine, that the hadronization may be followed by a phase with hadronic rescattering, as discussed *e.g.* in refs. [42, 43, 44].

The energy density in a flux tube is of the same order of magnitude as in the vacuum condensate, which in the bag model is estimated to 0.55 MeV/fm^3 [45]. It was shown in ref. [28] that the QCD Fock vacuum is unstable, and an added longitudinal colour-electric field will generate a Higgs potential. This implies that the QCD vacuum has many similarities with a superconductor, in which a magnetic field is confined in vortex lines. The properties of the vacuum is therefore important for the interaction between strings. Lattice calculations show that a flux tube between a quark and an antiquark is characterised by a strong longitudinal colour–electric field surrounded by a colour–magnetic current induced in the vacuum condensate [46, 47], but very small magnetic fields [48, 49]. In the string model therefore the energy density in the vacuum condensate is high enough to counteract a longitudinal magnetic field. On the other hand, as the energy density in the glasma may be

[1]This space–time coordinate is conventionally called η, but should not be mixed up with pseudorapidity $= (1/2)\ln[(p+p_z)/(p-p_z)]$. To avoid confusion we will below use the notation η_{st} for the space–time coordinate.

quite high, it is reasonable to expect that the energy in the vacuum condensate here can be neglected, as is normally done, and explicitly stated in ref. [26]. This implies that CP-violating effects are not expected in the string scenario, and experimental evidence for CP-violation would support the formation of a glasma phase. The properties of the vacuum condensate and colour flux tubes are further discussed in section 2.2 and 2.3.

We have earlier presented some preliminary studies in ref. [36], where we used a simplified so-called *shoving* model to describe how strings in a pp collision repel each other to create the so-called near-side ridge, first found in pp by CMS at the LHC [14]. The simplified model had a number of short-comings. One was that it only treated strings that were parallel to the beam direction, using an upper cut on the transverse momentum of the partons stretching the string. Another was that the force between the strings was manifested in terms of many very soft gluons, which was technically difficult to handle in the PYTHIA8 hadronization implementation, and also somewhat difficult to reconcile within the string model as such.[2]

In this work we will present a more advanced model, where all string pieces in an event can interact, not only in pp, but also in AA and basically in any other collision system. Furthermore the problem with producing too many additional soft gluons is circumvented by applying the force in terms of tiny transverse momentum nudges given directly to the produced hadrons in the hadronization. Even though the new model does not produce extra soft gluons, it still has some problem dealing with soft gluons already present, stemming from the perturbative phase in PYTHIA8 , that complicates the string motion, and currently this restricts the amount of shoving that can be achieved.

The layout of this paper is as follows. In section 2 we further elaborate on the differences between a string based and a thermalized scenario. We first study quantitatively the difference in initial energy density. The lower density in the string picture implies that the features of the QCD vacuum condensate become important in the string scenario. The properties of this condensate, and the similarity between a string-like colour flux tube and a vortex line in a superconductor, is discussed in sections 2.2 and 2.3.

In section 3 we then look at how the QCD string is described in the Lund string fragmentation model. Our new shoving model is presented in section 4 giving some details of how one finds a Lorentz frame where any two string pieces always lie in parallel planes, and how we there can discretize the shoving into tiny transverse nudges between them, which are then applied to the hadrons produced. We study the behaviour of the new model in sections 5 and 6. First we apply it to a toy

[2]For a discussion about very soft gluons in the Lund model see *e.g.* [50].

model for the geometry of the initial partonic state of an AA collision to show that we can qualitatively describe some of the flow effects found there. Then we apply the new model to a more realistic initial state generated by the Angantyr model [40] for AA collisions in PYTHIA8 , and find that the quantitative description of flow effects in AA collisions is still lacking. Finally in section 7 we present our conclusion and present some ideas for improvement of our new model that may achieve an improved description of experimental measurements.

2 Differences between a thermalized and a non-thermalized scenario

As mentioned in the introduction the most important differences between the string and plasma scenarios are the lower initial energy density in the string case, and the consecutive importance of the vacuum condensate and the properties of colour flux tubes.

2.1 Initial energy density and possible plasma transition

For a string the energy density dE/dz along the string is given by the string tension $\kappa \approx 0.9$ GeV/fm. When the string is stretched out it does not get thinner. The new string pieces get their energy from the reduced kinetic energy of the quark at the end of the string (or an energy-carrying gluon on the string). When overlapping strings shove each other, they are boosted transversely, but the interaction energy is relatively small compared to the original energy of the strings. Thus the energy per unit length of the string system is only moderately modified. The expansion of the string system is then limited to the two transverse dimensions, and the total energy density is roughly constant until hadronization at proper time $\tau_H = 1.5 - 2$ fm (see section 3). After hadronization the boost invariant hadron system expands longitudinally with constant density in rapidity, dE/dy. In the center this expansion implies that $\Delta z = \tau \Delta y$. At hadronization time the energy density in the string system has to agree with the density in the final state hadrons, which implies

$$dE/dz|_{strings} \approx (dE/dy|_{hadrons})/\tau_H. \quad (1)$$

In contrast a thermalized plasma is expanding both transversely and longitudinally. To end in an (almost) boost invariant hadron distribution, the initial plasma also has to be boost invariant, and thus expand with approximately constant energy, dE/dy, per unit rapidity. As early discussed by Bjorken [41], this implies that the

density in the z-coordinate, dE/dz, is falling like τ^{-1} or faster. Also after freeze-out and hadronization the hadron system expands with the same density per unit rapidity, which thus is approximately constant from the time of thermalization, τ_T. This implies that

$$dE/dz|_{therm} \approx (dE/dy|_{hadrons})/\tau_T. \quad (2)$$

From these results we conclude that the initial energy density in the plasma has to be higher by approximately a factor τ_H/τ_T, when compared to the corresponding density in a string system. This result is independent of the way the plasma is formed.

In an initial glasma phase the energy density may initially have been even higher. The energy density and the time for thermalization in the glasma state are difficult to estimate theoretically, and are frequently presented in lattice units or arbitrary units (*e.g.* in ref. [26]). The density is, however, given in physical units for the IP-Glasma model presented by Schenke *et al.* in refs. [51, 52]. For central PbPb collisions at 2.76 TeV the initial energy density, $dE/\tau dy \approx dE/dz$, integrated over the transverse plane, is estimated to about 55,000 GeV/fm. With a transverse area about 150 fm^2, this gives an initial energy per unit volume $dE/d^3x \approx 370$ GeV/fm^3. While the fields initially are dominated by the longitudinal colour-electric and -magnetic components, at $\tau = 0.1$ fm the longitudinal and transverse fields are approximately equally strong, and the energy density has dropped to $dE/\tau dy \approx 20,000$ GeV/fm, or $dE/d^3x \approx 130$ GeV/fm^3. The energy density is then falling proportional to $1/\tau$, corresponding to a boost invariant expansion, with approximately constant $dE/dy \approx 2,000$ GeV. This can be compared to results for central PbPb collision at LHC, where the charged particle density dN_{ch}/dy is of the order 2,000 (*c.f.* the data from ALICE shown in figure 16). Including neutrals gives approximately 3,000 particles per unit rapidity. Assuming an average transverse mass ~ 0.5 GeV, this gives the energy density $dE/dy \approx 1,500$ GeV, not too far from the result by Schenke *et al.*.

In the string scenario the energy density dE/dz would be approximately constant up to hadronization time $\tau_H = 1.5 - 2$ fm. The LHC results discussed above would then give the initial density $dE/dz = 750 - 1000$ GeV/fm or $dE/d^3x = 5 - 7$ GeV/fm^3. This result also roughly agrees with the estimated number of strings obtained in the Angantyr model.

A similar result is obtained for RHIC energies, although somewhat less dramatic. The result presented in ref. [52] for $\sqrt{s} = 200$ GeV and $b = 9$ fm (centrality ≈ 40 %) is an average density $dE/\tau\, dy \approx dE/dz \approx 300$ GeV/fm or $dE/d^3x \sim 8$ GeV/fm^3. The experimental result for this centrality is $dN_{ch}/dy \approx 150$ [53, 54]. Adding neutrals, and again assuming an average transverse mass ~ 0.5 GeV, this

gives $dE/dy \approx 110$ GeV, which would agree with result by Schenke *et al.*, if the thermalization time is about 0.35 fm. An estimate for the string scenario, where the strings hadronize at $\tau = 1.5 - 2$ fm, would here instead give the density 1.7 GeV/fm^3.

The conclusion from these examples is, that the initial energy density needed in the glasma may be one or two orders of magnitude larger than in the string scenario. This also implies that, while the energy density in the vacuum condensate can be safely neglected in the glasma, it is essential in the string scenario. We also want to point out that any mechanism producing an expanding plasma phase, would also need a high initial density. We finally note that the above discussion (based on several papers by Schenke *et al.*) concerns a boost invariant glasma corresponding to infinitely thin pancakes and thus an infinite rapidity range. In a more recent analysis McDonald, Jeon, and Gale have studied a generalization with finite extension in the longitudinal direction, and this also finite energy and rapidity range [55]. The resulting energy densities for PbPb collisions at LHC are similar to those by Schenke *et al.* for $\tau > 0.1$ fm, but much higher for smaller τ-values. For the infinite rapidity case the density in the transverse fields approach 0 for $\tau \to 0$, while for the finite rapidity analysis these densities grow like $1/\tau^2$.

2.2 The vacuum condensate and dual QCD

As discussed above, the initial energy density is relatively low in the non-thermal scenario, and the properties of the vacuum condensate is important for the formation of colour-electric flux tubes (strings). The QCD vacuum was early studied in several papers by N.K. Nielsen, H.B. Nielsen and P. Olesen. In ref. [27] it was shown that the QCD Fock vacuum (with zero fields) is unstable. If a small homogeneous colour-magnetic field is added, it will grow exponentially. However, as shown in the accompanying paper [28], if the externally added field is in a given direction colour space, it will induce fields in the orthogonal directions in colour space. (For simplicity the authors studied SU(2) Yang–Mills theory.) Higher orders in this induced field then develop a Higgs potential, analogous to the potential describing the condensate in a superconductor. This implies that the exponential growth will be stopped, and the initial Fock vacuum will fall into a non-perturbative ground state with negative energy. [3]

[3]It is often argued that the Nielsen–Olesen instability contributes to a rapid transition from a glasma to a plasma. Nielsen and Olesen showed that the Fock vacuum is a local maximum, and thus unstable. However, it is not obvious to us how this effect motivates a fast transition when a perturbation is added to the (stable) real vacuum.

In a normal superconductor a magnetic field is compressed in vortex lines or flux tubes, and magnetic charges would be confined. The pure Yang–Mills theory is symmetric under exchange of electric and magnetic fields. Quarks with colour-electric charge are confined, and the Copenhagen vacuum is also known to have non-trivial vortex solutions of electric type (see *e.g.* refs. [56, 57]). Thus the QCD vacuum behaves as a *"dual superconductor"*, with exchanged roles for the electric and the magnetic fields. For a review of the "Copenhagen vacuum", see *e.g.* [58].

It was further demonstrated by 't Hooft that the ground state in a pure SU(3) Yang–Mills theory can have two different phases, with either colour-electric or colour-magnetic flux tubes, but not both [59]. In the first phase colour-electric charge is confined, and extended colour-magnetic strings are not possible, while the opposite is true in the second phase. The fact that quarks are confined obviously shows that the QCD vacuum is of the first kind.

Although the pure Yang–Mills theory is symmetric under exchange of electric and magnetic fields, Maxwell's equations for electromagnetism are asymmetric, due to the absence of magnetic charges. Exchanging electric and magnetic fields is obtained by replacing the field $F^{\mu\nu}$ by the dual field tensor $\widetilde{F}^{\mu\nu} \equiv \epsilon^{\mu\nu\kappa\lambda} F_{\kappa\lambda}$. The electric and magnetic currents would then be given by

$$j^{\mu}_{el} = \partial_{\nu} F^{\nu\mu}, \;\; j^{\mu}_{magn} = \partial_{\nu} \widetilde{F}^{\nu\mu}. \tag{3}$$

Expressing the field $F^{\mu\nu}$ as derivatives of a vector potential A^{μ} implies, however, that the magnetic current is identically zero. As a consequence magnetic charges can only be introduced by adding extra degrees of freedom. Dirac restored the symmetry between electric and magnetic charges by adding a "string term", an antisymmetric tensor $G_{\mu\nu}$ satisfying $\partial_{\nu} G^{\nu\mu} = j^{\mu}_{magn}$. The electromagnetic field is then given by

$$\begin{aligned} F_{\mu\nu} &= \partial_{\mu} A_{\nu} - \partial_{\nu} A_{\mu} - \widetilde{G}_{\mu\nu}, \\ \widetilde{F}_{\mu\nu} &= \widetilde{\partial_{\mu} A_{\nu}} - \widetilde{\partial_{\nu} A_{\mu}} + G_{\mu\nu}. \end{aligned} \tag{4}$$

A consistency constraint is then a quantization of electric (e) and magnetic (g) charges: $e \cdot g = 2\pi n$ with n an integer.

The features of a vacuum behaving as a dual superconductor was early discussed in a series of papers by Baker, Ball, and Zachariasen; for a review see ref. [60]. In a dual superconductor a colour-electric flux tube has to be kept together by a colour-magnetic current. Instead of expressing the extra degrees of freedom in terms of Dirac's string term, Baker *et al.* treated $F^{\mu\nu}$ and $\widetilde{F}^{\mu\nu}$ as independent fields.

(In the non-trivial vacuum condensate they are related by a non-local magnetic permeability.) Higher order corrections then induce a Higgs potential in the $\widetilde{F}$ field, analogous to the induced field in the Nielsen–Olesen instability.

The fields $F^{\mu\nu}$ and $\widetilde{F}^{\mu\nu}$ studied by Baker *et al.* are non-Abelian. A problem is here that, although a bound $q\bar{q}$ pair must be a colour singlet, and the energy density has to be gauge invariant, this is not the case for the colour-electric and -magnetic fields. 't Hooft has, however, shown that the essential confining features can be described by an Abelian subgroup $U(1)^2$ to SU(3) [61]. More recent studies of dual QCD are based on this "Abelian dominance". This is also supported by lattice calculations performed in the maximal Abelian gauge, which exhibit a confining phase related to the condensation of magnetic monopoles [62, 63]. For overviews of Abelian projections (or Abelian gauge fixing) see also refs. [64, 65].

2.3 A single QCD flux tube in equilibrium

A normal superconductor can be described by the Landau–Ginzberg (LG) equations, see *e.g.* ref. [66] and appendix A. Here the vacuum condensate is formed by Cooper pairs and influenced by a Higgs potential. In the interior of the superconductor a magnetic field is kept inside flux tubes or vortex lines by an electric current, and magnetic monopoles would be confined. The flux in such a vortex line (and the charge of a possible monopole) is quantized in multiples of $2\pi/q$, where $q = 2e$ is the charge of a Cooper pair.

A vortex line or a flux tube is characterized by two fundamental scales: the penetration depth λ and the coherence length ξ. These scales are the inverse of, respectively, the mass attained by the gauge boson and the mass of the Higgs particle. At the boundary between a superconducting and a normal phase, if $\lambda \gg \xi$ the parameter λ determines how far the magnetic field penetrates into the condensate (from which it is expelled by the Meissner effect). Similarly if $\xi \gg \lambda$, then ξ determines the rate at which the condensate goes to zero at the boundary. When $\xi > \lambda$ (or more exactly $\xi > \sqrt{2}\,\lambda$), both the condensate and the field are suppressed over a range $\xi - \lambda$. This is a type I superconductor, and it implies that the surface provides a positive contribution to the energy. In equilibrium the surface then tends to be as small as possible. If in contrast λ is larger than ξ (type II superconductor), the condensate and the field can coexist over a range $\sim \lambda - \xi$, and the surface provides a negative contribution to the energy, favouring a large surface. (The properties of a classical superconductor are discussed in somewhat more detail in appendix A.)

As discussed above, the QCD vacuum has important similarities with a superconductor. There are, however, also important differences between a non-Abelian

flux in QCD and an Abelian field in a non-relativistic superconductor. The infrared problems in QCD contribute to the difficulties to estimate the properties of a QCD flux tube. The total energy, given by the string tension, is fairly well determined from the spectrum of quarkonium bound states, and approximately equal to 1 GeV/fm. The total flux and also the width of the tube are, however, less well known. One problem is that it is not obvious how much of the string tension is in the field, how much is in destroying the condensate, and how much is in the current keeping the flux together inside the tube. Another problem is that, although the flux is given by the running strong coupling, the scale is not well specified. Also for a fixed total flux, the energy stored in the linear colour-electric field depends on the (not well known) width of the tube. The field energy is $\sim A\,E^2 \sim \Phi^2/A$, where Φ is the total flux and A the transverse area of the tube. We here briefly discuss three approaches to estimate the properties of a QCD flux tube:

i) The bag model: The simplest model for a QCD flux tube is the MIT bag model [45]. Here the vacuum condensate is destroyed within a radius R around the center of the tube. Inside the tube there is a homogeneous longitudinal colour-electric field $E = \Phi/(\pi R^2)$, where Φ is the total flux. The energy per unit length of the tube is then

$$\kappa = \pi R^2 \left[(\Phi/\pi R^2)^2/2 + B \right], \tag{5}$$

where the bag constant B is (minus) the energy density in the condensate.

Equilibrium is obtained by minimizing κ, which gives $\pi R^2 = \Phi^2/2B$ and $\kappa = 2\pi R^2 B$. Here half of the energy is in the field, and half comes from destroying the vacuum condensate inside the tube. With $\kappa \approx 1$ GeV/fm and $B \approx (145\ \mathrm{MeV})^4$ [45], we find $R \approx 1.7$ fm, or $\sqrt{\langle \rho^2 \rangle} \approx 1.2$ fm. (Here ρ is the radial distance in cylinder coordinates.)

ii) Dual QCD: In the approach by Baker *et al.* the fields **D** and **H** are derivatives of a dual potential C_μ. In the vacuum condensate the magnetic permeability μ is non-local, and the fields $\mathbf{E} = \mu\mathbf{D}$ and $\mathbf{B} = \mu\mathbf{H}$ are treated as independent fields (note that $\mu\epsilon = 1$) related to a tensor field $\widetilde{F}^{\mu\nu}$. This tensor field interacts via a Higgs potential, forming a vacuum condensate which confines the colour-electric field **D**. In ref. [60] the LG parameter $\kappa_{LG} = \lambda/\xi$ is estimated to ≈ 0.75, when fitting the model to the string tension and the energy in the vacuum condensate. This is quite close to the borderline, $1/\sqrt{2}$, between type I and type II superconductors. It implies that the surface energy is small, and the authors conclude that the behaviour is not far from a flux tube in the bag model. The

width $\sqrt{\langle\rho^2\rangle}$ is estimated to 0.95 fm. A more recent review over dual QCD is found in ref. [67], which also discusses results from lattice calculations.

iii) Lattice QCD: Lattice calculations are natural tools to solve infrared problems, and several groups have presented studies of flux tubes using different methods; for some recent analyses see refs. [68, 48, 69, 46, 47, 49, 70]. Such analyses are, however, not without problems. One problem is that the strings have to be rather short, in order to have a good resolution. A good resolution is important for the determination of the behaviour for small ρ. Besides the colour-electric field, the features of the flux tube also depends on the properties of the vacuum condensate.

Some studies find that the vacuum acts like type II superconductor, *e.g.* refs. [48, 70], but a majority of recent studies conclude instead that it should be of type I, *e.g.* refs. [68, 69, 47]. In most analyses the electric field is fitted using Clem's ansatz [71] for the condensate (the order parameter) $\psi \propto f\, e^{-i\phi}$, where $f = \rho/\sqrt{\rho^2+\xi_v^2}$. Here ρ is the radius in cylinder coordinates, and the parameter ξ_v is varied to minimize the string energy. As discussed in more detail in appendix A, this ansatz satisfies one of LG's two equations. Minimizing the string tension then gives the electric field

$$E \propto K_0(\sqrt{\rho^2+\xi_v^2}/\lambda). \tag{6}$$

Here K_0 is a modified Bessel function, and the scale parameter λ equals the penetration depth in the LG equations. The parameter ξ_v is tuned to fit the shape of the lattice result for small ρ-values, where it suppresses the logarithmic singularity in K_0. The result is related, but not equal to the coherence length in the superconductor. An important problem is, however, that the ansatz in eq. (6) is expected to work well for type II superconductors, where it gives an approximate solution also to the second of LG's two equations. It does, however, not work for type I superconductors, where the second LG equation can be quite badly violated. This is a problem for those studies, which find fits which correspond to κ_{LG}-values in the type I-region, where the fitted values of λ and ξ no longer represent the initial parameters in the LG equations. This problem is also discussed further in appendix A.

Another problem is how to translate the width of the field from lattice units to the physical scale in fm. This problem is discussed in a review by Sommer in ref. [72]. In earlier studies it was common to adjust the energy in the colour-electric field, $\int 2\pi\rho\, d\rho E^2/2$, to the string tension, known to be ≈ 1 GeV/fm. Also, as noted above, it is uncertain how much of the string tension is due to the field, how much is due to breaking the condensate, and how much is due to the current which keeps the flux together. In the bag model or the dual QCD estimate mentioned

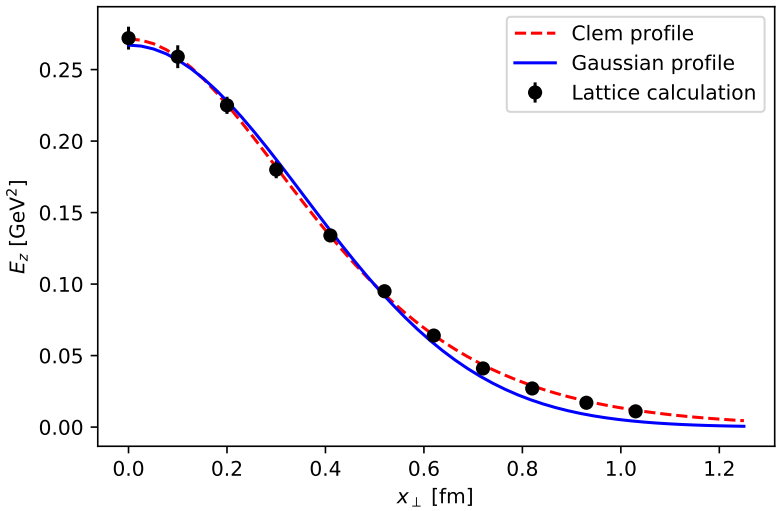

Figure 1: Profile of the electric field from the lattice calculation in ref. [68] compared to the fit by Clem [71] and a Gaussian distribution.

above, about half of the string energy is in the field, and half is due to the condensate. Adjusting the field to represent the full string tension is therefore likely to overestimate the field strength and thus underestimate its radius.

Another way to determine the scale, used in the lattice analyses mentioned above, is to study the transition of the $q\bar{q}$ potential from small to larger separations r, *e.g.* using a fit of the type $V(r) = A/r + Br + C$, see *e.g.* refs. [73, 74]. The parameters can here be adjusted *e.g.* to a phenomenological fit to quarkonium spectra. This method is, however, also uncertain. In the review by Sommer, mentioned above, it is concluded that "the connection of the phenomenological potentials to the static potential $V(r)$ has never been truly quantitative".

Although there are uncertainties in the determination of the LG parameter using Clem's approximation, it does give a good description of the *shape* of the longitudinal field obtained in the lattice calculations. As an example we show in figure 1 the result in ref. [68]. We here note that the profile is also quite well represented by a Gaussian distribution. Due to the uncertainties in determining the value of κ_{LG} and the physical scale, we will below approximate the field by a Gaussian determined by two tunable parameters, which are related to the radius of the field and to the fraction of the string tension related to the colour-electric field energy.

3 The Lund string hadronization

In the Lund string hadronization model, described in ref. [75], it is assumed that the dynamics of a single flux tube, and its breakup via quark pair production, is insensitive to the width of the tube. It is then approximated by an infinitely thin "massless relativistic string". Essential features of the Lund hadronization model are first $q\bar{q}$ pair production via the Schwinger mechanism, and secondly the interpretation of gluons as transverse excitations on the string. This last assumption implies that the hadronization model is infrared safe and insensitive to the addition of extra soft or collinear gluons.

i) Breakup of a straight string We here first describe the breakup of a straight flux tube or string between a quark and an antiquark. For simplicity we limit ourself to the situation with a single hadron species, neglecting also transverse momenta. For a straight string stretched between a quark and an anti-quark, the breakup to a state with n hadrons is in the model given by the expression:

$$d\mathcal{P} \propto \prod_{i=1}^{n} \left[N d^2 p_i \delta(p_i^2 - m^2) \right] \delta^{(2)} \Big(\sum p_i - P_{\text{tot}} \Big) \exp\left(-bA\right). \tag{7}$$

Here p_i and P_{tot} are two-dimensional vectors. The expression is a product of a phase space factor, where the parameter N expresses the ratio between the phase space for n and $n-1$ particles, and the exponent of the imaginary part of the string action, bA. Here b is a parameter and A the space–time area covered by the string before breakup (in units of the string tension κ). This decay law can be implemented as an iterative process, where each successive hadron takes a fraction z of the remaining light-cone momentum ($p^{\pm} = E \pm p_z$) along the positive or negative light-cone respectively. The values of these momentum fractions are then given by the distribution

$$f(z) = N \frac{(1-z)^a}{z} \exp(-bm^2/z). \tag{8}$$

Here a is related to the parameters N and b in eq. (7) by normalization. (In practice a and b are determined from experiments, and N is then determined by the normalization constraint.)

In applications it is also necessary to account for different quark and hadron species, and for quark transverse momenta. The result using Schwinger's formalism for electron production in a homogeneous electric field gives an extra factor

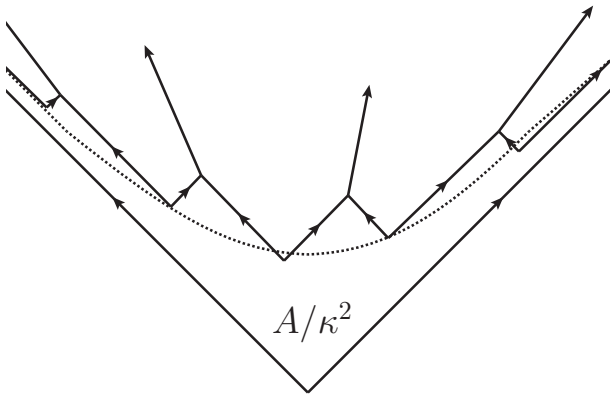

Figure 2: Breakup of a string between a quark and an anti-quark in a $x - t$ diagram. New $q\bar{q}$ pairs are produced around a hyperbola, and combine to the outgoing hadrons. The original q and $\bar{q}$ move along light-like trajectories. The area enclosed by the quark lines is the coherence area A in eq. (7), in units of the string tension κ. The notion of the "hadronization time" is not well defined. It could be the time when the new $q\bar{q}$ pairs are produced, or when they meet for the first time to form a hadron (or something in between).

$\exp(-\pi(\mu^2 + p_\perp^2)/\kappa)$, where μ and $p_\perp$ are the mass and transverse momentum for the quark and anti-quark in the produced pair. For details see *e.g.* ref. [75].

The result in eq. (8) is in principle valid for strings stretched between partons produced in a single space–time point, and moving apart as illustrated in the space–time diagram in fig. 2.

The expression in eq. (7) is boost invariant, and the hadrons are produced around a hyperbola in space–time. A Lorentz boost in the x-direction will expand the figure in the $(t + x)$ direction and compress it in the $(t - x)$ direction (or *vice versa*). Thus the breakups will be lying along the same hyperbola, and low momentum particles in a specific frame will always be the first to be produced in that special frame.

The typical proper time for the breakup points is given by

$$\langle \tau^2 \rangle = \frac{1+a}{b\kappa^2}. \tag{9}$$

This does, however, not necessarily correspond to the "hadronization time", which might also be defined as the time when a quark and an anti-quark meet for the first time to form a hadron.

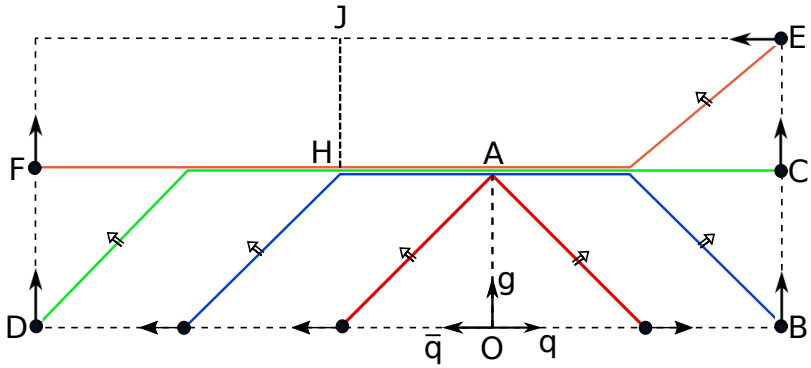

Figure 3: A $q - g - \bar{q}$ system moving out from a single point O with energies 2, 2, and 3 units of energy respectively. The position of the string is shown at four consecutive times, marked by red, blue, green, and purple colour respectively.

With parameters a and b determined by tuning to data from e^+e^- annihilation at LEP, and κ equal to 0.9-1 GeV/fm, eq. (9) gives a typical breakup time 1.5 fm, while the average time for the hadron formation is 2 fm. The typical hadronization time can therefore be estimated to 1.5-2 fm. This is important to keep in mind, as this value sets an upper limit on the time available for strings to interact.

ii) Hadronization of gluons An essential component in Lund hadronization is the treatment of gluons. Here it is assumed that the width of the flux tube can be neglected, and that its dynamics can be approximated by an infinitely thin "massless relativistic string".[4] A quark at the endpoint of the string, carrying energy and momentum, moves along a straight line, affected by a constant force given by the string tension κ, reducing (or increasing) its momentum. A gluon is treated as a "kink" on the string, carrying energy and momentum and also moving along a straight line with the speed of light. A gluon carries both colour and anti-colour, and the string can be stretched from a quark, via a set of colour-ordered gluons, to an anti-quark (or alternatively as a closed gluon loop). Thus a gluon is pulled by two string pieces, and retarded by the force 2κ. When it has lost its energy, the momentum-carrying kink is split in two corners, which move with the speed of light but carry no momentum.

A simple example is shown in figure 3. It shows a quark, a gluon, and an anti-

[4]For the dynamics of such a Nambu–Goto string, see *e.g.* ref. [76].

quark moving out from a single point, called O in the figure. They move outwards at right angles with energies 2, 2, and 3 units respectively. After 1 unit of time (equal to κ^{-1} energy units) the gluon has arrived at point A and lost all its energy. The gluon is then replaced by two corners connected by a straight section. The quark has lost its energy in point B. In the rest frame of the attached string piece it now turns back, gaining momentum in the opposite direction. In the figure frame it is turning $90°$, and after meeting the string corner at C, it is instead pulled back and loosing energy. The anti-quark turns around in a similar way at point D. If the string does not break up in hadrons, the string evolution will be reversed. The kinks meet at point H, and the whole system collapses to a point J. (Note that this system is not in its rest frame.)

We note that although the string pieces initially move with a transverse velocity $1/\sqrt{2}$, after some time most of the string is at rest (the horizontal string pieces in figure 3. A soft gluon will soon stop and be replaced by a straight section stretched as if it were pulled out between the quark and the anti-quark. This implies that the string hadronization model is infrared safe; a soft gluon will only cause a minor modification on the string motion. The same is also true for a collinear gluon [75]. For a string with several gluons there will also be several new straight string pieces, which become more and more aligned with the directions of the endpoints, as described in ref. [77]. Therefore a string stretched over many rapidity units, and with several soft gluon kinks, will be pulled out in a way much more aligned with the beam axis, before it breaks into hadrons.

4 The string shoving picture

In the following we will describe the details in our new implementation of the string shoving model. First we recap the main idea as applied to two straight parallel string pieces, then we consider the interaction between two arbitrary string pieces, and describe a special Lorentz frame in which the shoving can be properly formulated. Finally we describe how we discretize the shoving into small fixed-size *nudges* and how these are ordered in time and applied to the final state hadrons.

4.1 Force between two straight and parallel strings

The force between two straight and parallel strings was discussed in ref. [36], We here shortly reproduce the treatment presented there. Just after the production of a string stretched between a quark and an anti-quark, the colour field is necessarily compressed, not only longitudinally but also transversely. They then expand trans-

versely with the speed of light until they reach the equilibrium radius $R_S \sim 0.5$-1 fm.

As illustrated in figure 1, the electric field E obtained in lattice calculations, and fitted to the Clem formula, eq. (6), is also well approximated by a Gaussian

$$E = N \exp(-\rho^2/2R^2). \tag{10}$$

The normalization factor N can be determined if the energy in the field (per unit length), given by $\int d^2\rho\, E^2/2$, is adjusted to a fraction g of the string tension κ. This gives $N^2 = 2g\kappa/(\pi R^2)$. As discussed in section 2.3, the simple bag model would give $g = 1/2$. Due to the uncertainties in determining the properties of the flux tube, we will treat R and g as tunable parameters.

When the colour-electric fields in two nearby parallel strings overlap, the energy per unit length is given by $\int d^2\rho\, (\mathbf{E}_1 + \mathbf{E}_2)^2/2$. For a transverse separation $d_\perp$ this gives the interaction energy $2\kappa g \exp(-d_\perp^2/(4R^2))$. Taking the derivative with respect to $d_\perp$ then gives the force per unit length

$$f(d_\perp) = \frac{g\kappa d_\perp}{R^2} \exp\left(-\frac{d_\perp^2}{4R^2}\right). \tag{11}$$

For a boost invariant system it is convenient to introduce hyperbolic coordinates

$$\tau = \sqrt{t^2 - z^2}, \quad \eta_{st} = \ln((t+z)/\tau). \tag{12}$$

Near $z = 0$ we get $\delta z = t\,\delta\eta_{st}$, and the force in eq. (11) gives $dp_\perp/dt\,\delta z = f(d_\perp)$. Boost invariance then gives the two equations

$$\frac{dp_\perp}{\tau d\tau\, d\eta_{st}} = f(d_\perp), \quad \frac{d^2 d_\perp}{d\tau^2} = \frac{f(d_\perp)}{\kappa}. \tag{13}$$

We have here assumed that the flux tubes are oriented in the same direction, leading to a repulsion. We have also argued in terms of an Abelian field, which means that if the fields are oppositely oriented there would be an attenuation of the fields rather than a repulsion. Since QCD is non-Abelian, the picture is slightly more complex, but the calculations are still valid. In case of two triplet fields in opposite directions, we get with probability 8/9 an octet field, which also leads to a repulsion when compressed. Only with probability 1/9 we get a singlet field, and in this case the strings are assumed to be removed through "colour reconnection", as described in ref. [37]. Also for strings in other colour multiplets the string-string interaction is dominantly repulsive. This is not in conflict with the Abelian approximation, as discussed in section 2.3. A $q\bar{q}$ string is a colour singlet, where the quark is

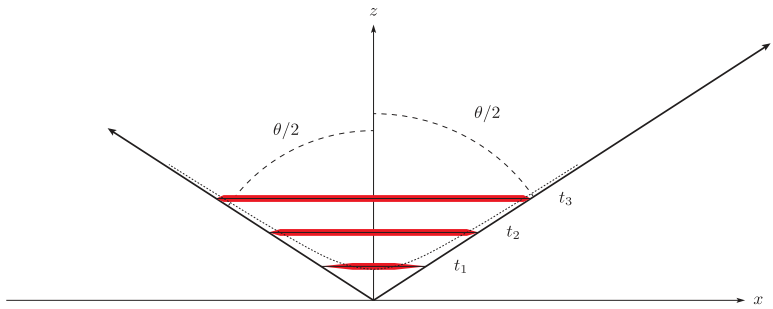

Figure 4: The time-evolution of a string piece between two partons in an arbitrary Lorentz frame. The system is rotated so that the momenta (the magnitude of which are indicated by the lengths of the arrows) of the of the partons are in the $x - z$ plane with equal but opposite angle w.r.t. the z-axis. The horizontal lines indicate the extension of the string horizontally and transversely at different times steps. The dotted curve indicates the hyperbola where in x the proper time of the sting piece is equal to R_S for a given $z = t \cos \frac{\theta}{2}$.

a coherent mixture of red, blue, and green (with corresponding anti-colours for the anti-quark). Similarly the endpoint of an octet string has a coherent combination of the 8 different colour charges.

4.2 String motion and the parallel frame

For a string piece between two (massless) partons, the motion and expansion of the sting is very simple in the rest frame of the two partons. If the partons have momenta along the x-axis, the position of the string ends are simply $x_\pm(t) = (t; \pm t, 0, 0)$, where we note that the ends move by the speed of light irrespective of the momentum of the partons.

If we instead go to an arbitrary Lorentz frame we can also obtain a simple picture by rotating the partons so that they lie in the $x - z$ plane with the same but opposite angle $\theta/2$ with the z-axis, as shown in figure 4. Here the string ends still move by the speed of light and the position of string ends are given by $x_\pm(t) = (t;\, \pm t \sin \frac{\theta}{2},\, 0,\, t \cos \frac{\theta}{2})$. A straight relativistic string is boost invariant and has no longitudinal momentum (similar to a homogeneous electric field). The energy and transverse momentum are given by $dE/dz = \kappa/\sqrt{1 - v^2}$ and $dp_\perp/dz = v_\perp\, dE/dz$. The string in figure 4 is therefore still a straight line; it is just boosted transversely with velocity $v = \cos(\theta/2)$.

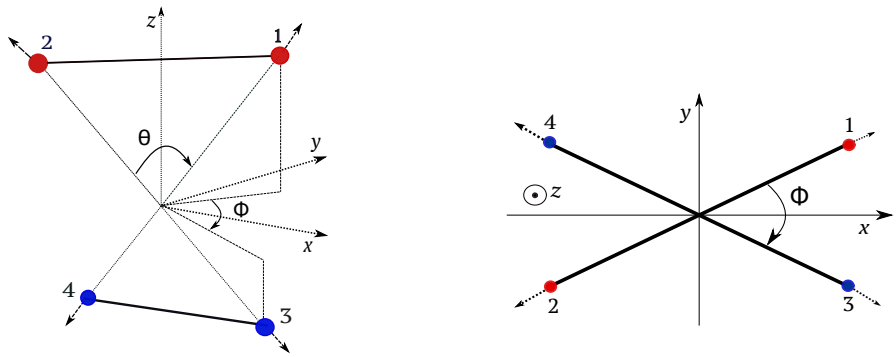

Figure 5: Schematic diagrams of two strings in their parallel frame. On the left, θ is the opening angle between the partons constituting each string, while on the right we show the skewness angle, ϕ in the projection on the $x-y$-plane of the two string pieces.

If we now want to study the interaction between two arbitrary string pieces, it is not possible to find a Lorentz frame where both these are always parallel to the x-axis, but it turns out that it is possible to find a frame where both always lie in parallel planes, perpendicular to the z-axis. To see this, we first we rotate the string piece in figure 4 an angle $\phi/2$ around the z-axis. Then we want another string piece with angle $\pi - \theta/2$ w.r.t. the the z-axis but rotated an angle $-\phi/2$. We then have the situation shown in figure 5 where the four partons have momenta (using pseudorapidity instead of the polar angle, to simplify the notation)

$$\begin{aligned}
p_1 &= p_{\perp 1}\left(\cosh\frac{\eta}{2};\quad \cos\frac{\phi}{2},\quad \sin\frac{\phi}{2},\quad \sinh\frac{\eta}{2}\right),\\
p_2 &= p_{\perp 2}\left(\cosh\frac{\eta}{2};-\cos\frac{\phi}{2},-\sin\frac{\phi}{2},\quad \sinh\frac{\eta}{2}\right),\\
p_3 &= p_{\perp 3}\left(\cosh\frac{\eta}{2};\quad \cos\frac{\phi}{2},-\sin\frac{\phi}{2},-\sinh\frac{\eta}{2}\right),\\
p_4 &= p_{\perp 4}\left(\cosh\frac{\eta}{2};-\cos\frac{\phi}{2},\quad \sin\frac{\phi}{2},-\sinh\frac{\eta}{2}\right).
\end{aligned} \tag{14}$$

Here we have six unknown quantities and, for four massless momenta we can construct six independent invariant masses, s_{ij}. This means that for any set of four massless particles we can (as long as no two momenta are completely parallel) solve

for the transverse momenta

$$p_{\perp 1}^2 = \frac{s_{12}}{4}\sqrt{\frac{s_{13}s_{14}}{s_{23}s_{24}}},\;\; p_{\perp 2}^2 = \frac{s_{12}}{4}\sqrt{\frac{s_{23}s_{24}}{s_{13}s_{14}}},$$
$$p_{\perp 3}^2 = \frac{s_{34}}{4}\sqrt{\frac{s_{13}s_{23}}{s_{14}s_{24}}},\;\; p_{\perp 4}^2 = \frac{s_{34}}{4}\sqrt{\frac{s_{14}s_{24}}{s_{13}s_{23}}}, \tag{15}$$

and the angles

$$\cosh\eta = \frac{s_{13}}{4p_{\perp 1}p_{\perp 3}} + \frac{s_{14}}{4p_{\perp 1}p_{\perp 4}}, \tag{16}$$
$$\cos\phi = \frac{s_{14}}{4p_{\perp 1}p_{\perp 4}} - \frac{s_{13}}{4p_{\perp 1}p_{\perp 3}}. \tag{17}$$

We note that there is a mirror ambiguity in the solution, but apart from that we can now construct a Lorentz transformation to take any pair of string pieces to the desired frame, which we will call their *parallel frame*.

The sketches in figure 5 show the case where the four partons are produced in the same space–time point, which in general is not the case. The partons from the shower and MPI-machinery in PYTHIA8 are all assigned a space–time positions $(0; bx, by, 0)$ in the lab frame assuming the standard picture that at t = 0 they are packed together at z = 0 and only with transverse separation. When a pair of string pieces are Lorentz transformed into their parallel frame, we assume that their respective production points are a simple average of the positions of the parton ends, giving us a $p_0^a = (t_0^a; x_0^a, y_0^a, z_0^a)$ for the string piece moving along the z-axis and the corresponding p^b for the piece going in the other direction. From this we get for any given time, t, in the parallel frame that the string piece travelling along the z-axis has the length, $2(t - t_0^a)\sin\frac{\theta}{2}$, and lies in a plane transverse to the z-axis. The string piece travelling in the opposite z direction will similarly have a length $2(t - t_0^b)\sin\frac{\theta}{2}$, which may be different, but the string will still always lie in a plane perpendicular to the z-axis. The endpoints of the two strings as a function of time then become

$$p^{a\pm}(t) = \left(t;\, x_0^a \pm (t - t_0^a)\sin\frac{\theta}{2}\cos\frac{\phi}{2},\, y_0^a \pm (t - t_0^a)\sin\frac{\theta}{2}\sin\frac{\phi}{2},\, z_0^a + (t - t_0^a)\cos\frac{\theta}{2}\right)$$
$$p^{b\pm}(t) = \left(t;\, x_0^b \pm (t - t_0^b)\sin\frac{\theta}{2}\cos\frac{\phi}{2},\, y_0^b \mp (t - t_0^b)\sin\frac{\theta}{2}\sin\frac{\phi}{2},\, z_0^b - (t - t_0^b)\cos\frac{\theta}{2}\right) \tag{18}$$

We see now that the distance between the two planes will change linearly with time as $\Delta_z(t) = z_0^a - z_0^b - t_0^a + t_0^b + 2t\cos\frac{\theta}{2}$.

Besides the string motion we are also interested in the radius of the string. As indicated in figure 4 this radius is not constant along the string, but depends on the proper time of a point on the string. As the partons are assumed massless, the endpoints of the string always have zero proper time and the colour field there has not had time to spread out transversely. Looking at a point on the x-axis, $\bar{x}$, we can easily find the proper time

$$\tau(t,\bar{x}) = \sqrt{(t-t_0)^2\sin^2\frac{\theta}{2} - (\bar{x}-x_0)^2 - \left((\bar{x}-x_0)\tan\frac{\phi}{2} - y_0\right)^2}. \quad (19)$$

The radius of the string will then vary linearly with τ, from zero in the ends until it reaches the final equilibrium radius, $R_S = \tau_S \lesssim 1$ fm. After this the string's width is fixed (as is indicated in figure 4) until it ultimately brakes, which on the average happens at $\tau_H \lesssim 2$ fm. In our implementation we have chosen to only allow the shoving to take place between string pieces at points in the parallel frame where both strings have proper times between τ_S and τ_H.

Clearly there may also be shoving between string pieces where they have not yet reached their maximum radius, R_S. From the derivation of eq. (11) we see that the force will be larger and the range will be smaller. In our current implementation it is possible to set $\tau_S < R_S$ to allow for shoving also in these region, but the force is still given for $R = R_S$ in eq. (11). This can therefore only give an indication of the effect, and we have to postpone a quantified study to a later publication.

The shoving naturally stops when the string breaks, but there is a grey-zone after the string breaks and before the hadrons are fully formed where one could imagine that the string pieces in the hadrons being formed will still repel each other. Also, after the hadrons are fully formed we expect final state interactions between them. In this article we will not investigate final-state hadron interactions, although it is able to produce a sizable flow signal in PbPb collisions with Angantyr initial conditions [43], and has recently been implemented in PYTHIA8 [42]. As indicated by the discussion about the inherent ambiguity in defining a "hadronization time" in section 3, defining a transition between a string-dominated final state at early times, and a hadron dominated final state at late times, will require scrutiny.

Another mechanism that reduces the shoving is when the endpoints have limited momenta, k_x in the x-direction in the parallel frame. A parton loses momentum to the string at a rate $t\kappa$, and a gluon being connected to two string pieces loses momentum at twice that rate. After a time $t = |k_x|/2\kappa$ a gluon will therefore have lost all its momentum to the string and turn back, gaining momentum from the string in the opposite direction. As explained in section 3 (figure 3), this means that a new string region opens up which is then not in the same parallel $x - y$ plane.

In this article we do not treat this new string region, but will comment on them in the following sections.

4.3 Generating the shoving

We now want to take the force between two string pieces in eq. (11) and apply it in the parallel frame. In ref. [36] everything was done in the laboratory frame and all strings were assumed to be parallel to the beam, and there generation of the shove was done by discretizing time and rapidity, calculating a tiny transverse momentum exchange in each such point. Here we instead use the parallel frame and discretize the transverse momentum into tiny fixed-size *nudges*.

Going back to the case where we have two completely parallel strings we have from the expression for the force from eq. (11) as

$$\frac{dp_\perp}{dtdx} = f(d_\perp(t)) \tag{20}$$

and we get the total transverse momentum push on the strings as

$$\Delta p_\perp = \int dt \int dx f(d_\perp(t)), \tag{21}$$

where we note that the integration limits in x are time-dependent. Now we will instead nudge several times with a fixed (small) transverse momentum, $\delta p_\perp$ according to some (un-normalized) probability distribution $P(t)$, which would give us the total push

$$\Delta p_\perp = \int dt P(t) \delta p_\perp, \tag{22}$$

and for small enough $\delta p_\perp$ we can make the trivial identification

$$P(t) = \frac{1}{\delta p_\perp} \int dx f(d_\perp). \tag{23}$$

In any string scenario we can now order the nudges in time (in the parallel frame), and we can ask the question which of the pairs of string pieces will generate a transverse nudge of size $\delta p_\perp$ first. This gives us a situation that looks much like the one in parton showers where the question is which parton radiates first. And just as in a parton shower we will use the so-called Sudakov-veto algorithm [2, 78]. The main observation here is that the probability of nothing to happen before some

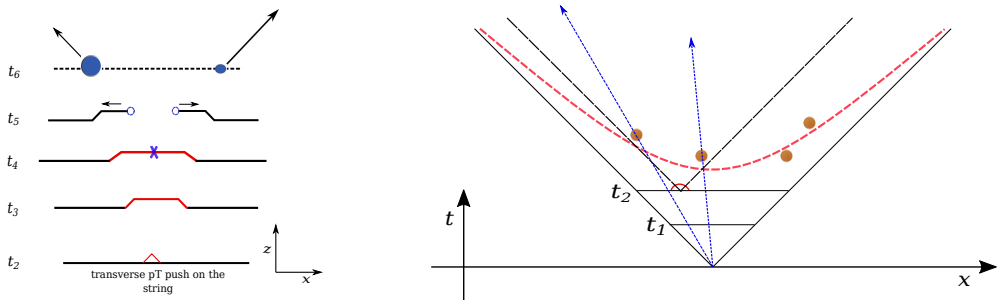

Figure 6: The left figure illustrates how a nudge deforms the geometry of a string piece from the time it is applied until the string breaks. The right figure illustrates how the final state hadrons that are will share the transverse momentum of a nudge are chosen.

time t exponentiates, so that the (now normalized) probability for the first thing to happen at time t is given by

$$P(t)e^{-\int_{t_{\text{min}}}^{t} dt' P(t')}. \tag{24}$$

In the Sudakov-veto algorithm, one can then generate the next thing to happen in all pairs of strings individually, and then pick the pair where something happens first. In addition, since $P(t)$ may be a complicated function, one may chose to generate according to an simplified overestimate, $\hat{P}(t) \geq P(t)$, for which generating according to eq. (24) is easier. In this way we get a trial time, t_t, for the first thing to happen and then for that particular time calculate the true value of $P(t_t)$, and accept the chosen time with a probability $P(t_t)/\hat{P}(t_t)$. If we reject, we then know we have *under*estimated the probability of nothing haven happened before t_t, which means we can generate the next trial time from $t_{\text{min}} = t_t$ (in eq. (24)).

In our case we will make the overestimate by treating the strings as being completely parallel, only separated in z and overestimating the limits in the x-integration. We then generate a time and a point along the x axis, calculate the actual repulsion force there, to get the true probability for accepting the generated time.

The whole procedure can be seen as discretizing in time with a dynamically sized time step with larger time steps where the force is small, and vise versa. This is a very efficient way of evolving in time, and efficiency is important since we will calculate several nudges in each pair of string pieces in an event, and in the case of AA, there may be up to $\mathcal{O}(10^4)$ string pieces per event at the LHC.

4.4 Transferring the nudges to the hadons

Each time a nudge has been included somewhere along a string piece, the string is deformed slightly. It will correspond to a gluon kink on the string, however, since the transverse momentum of this kink is small, the $\delta p_\perp$ will soon start propagating along the string as indicated in figure 6 (left). A hadron that is produced along the string where there happens to be such a kink will absorb the corresponding nudge in transverse momentum. In practice this is done by finding the point where the proper time of the kink is τ_H, the averaged hadronization time, and finding the primary hadron with the corresponding pseudorapidity (which is strongly correlated to the hyperbolic angle of the creation point, *c.f.* section 2.1) in the parallel frame, as sketched out in figure 6 (right). In this way each nudge is added to two hadrons from each of the two interacting string pieces. It should be noted that the fact that the two hadrons receive an extra transverse momentum in the same direction, will also mean that they come closer together in pseudorapidity. In addition, energy and momentum conservation is achieved by the adjusting the longitudinal momentum of the two hadrons separately in the two string pieces will also (on average) pull the hadrons closer together in rapidity. In the results below in section 6.2 this becomes visible in the overall multiplicity distribution.

It should be noted that the deformation of the string must be taken into account, not only in the pair of string pieces where the nudge was generated, but in all pairs involving one of the string pieces, triggering a recalculation of the next nudge in all these pairs. To do this in detail turns out to be forbiddingly time consuming, so instead we estimate an average shift of a string piece only after a certain number of nudges (typically $\mathcal{O}(10)$) and distribute it evenly along the string. [5]

5 Results for simple initial state geometries

The most widely employed models for describing the space–time evolution of a final state interactions of heavy ion collisions as a QGP (after the decay of a CGC as discussed in the introduction), are based on relativistic dissipative fluid dynamics (see *e.g.* ref. [79] for a review). A key feature of such models, is that the observed momentum-space anisotropy of the final state, originates from the azimuthal spatial anisotropy of the initial state density profile. The final state anisotropy is quantified

[5] The total number of nudges is proportional to the square of number of string pieces, N_S^2. Requiring recalculation for all affected pairs after each nudge increases the complexity to $\mathcal{O}(N_S^3)$. If we in addition would take into account the detailed geometry change for every previous nudge, would make the complexity $\mathcal{O}(N_S^5)$, which would be forbiddingly inefficient.

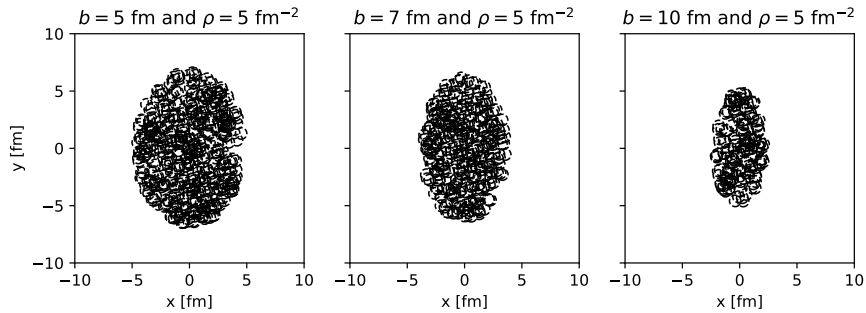

Figure 7: Examples of a sampled ellipse configuration in the Pb-Pb toy model, at three different impact parameters, with $\rho = 5$ fm^{-2}.

in flow coefficients (v_n's), which are coefficients of the Fourier expansion of the single particle azimuthal particle yield, with respect to the event plane (Ψ_n) [80, 81]:

$$E\frac{d^3N}{d^3p} = \frac{1}{2\pi}\frac{d^2N}{p_\perp dp_\perp dy}\left(1 + 2\sum_{n=1}^{\infty} v_n \cos(n(\phi - \Psi_n))\right). \tag{25}$$

Here E is the particle energy, $p_\perp$ the transverse momentum, ϕ the azimuthal angle and y the rapidity. In this section, we will explore the models' response to initial state geometry in a toy setup without non-flow contributions from jets, *i.e.* not real events.

"Toy" systems with known, simple input geometries can be better suited for exploring the basic model dynamics. In section 5.1 we set up a toy model for high energy nuclear–nuclear collisions in which the shoving model can be applied, and in section 5.2 we use the toy model to study the high-density behaviour of the shoving model. The parameters of the shoving model are not tuned, but set at reasonable values of $g = 0.5$, $R_S = \tau_S = 1$ fm amd $\tau_H = 2$ fm.

5.1 Isolating flow effects to v_2 in a toy model

In this and the following section, we restrict our study to systems with constrained straight strings. The strings are drawn between u$\bar{\text{u}}$ pairs, with cms energy of 15 GeV, a small Gaussian kick in p_x, p_y, and p_z fixed by energy-momentum conservation. This ensures that all strings will be stretched far enough in rapidity, that a study of final state hadrons with $|\eta| < 1$ will not be perturbed by any edge effects. Final

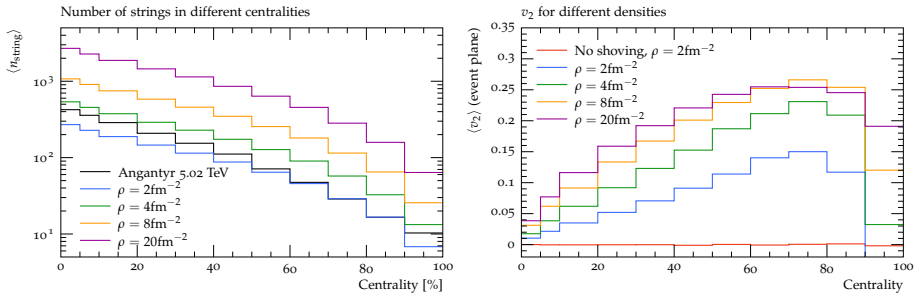

Figure 8: The number of string pieces (left) and v_2 (right) as function of centrality in the Pb-Pb toy model, for different values of ρ. In (right) compared to the number of strings generated by Angantyr around mid-rapidity for Pb-Pb collisions at $\sqrt{s_{\text{NN}}} = 5.02$ TeV.

state hadrons studied in the figures, are all hadrons emerging from strings breakings (*i.e.* no decays enabled)[6].

To study the model response in a heavy-ion like geometry, we set up a toy geometry in the shape of an ellipse, drawn between two overlapping nuclei of $r_{\text{Pb}} = 7.1$ fm. The ellipse has a minor axis (β) given by $2\beta = 2r_{\text{Pb}} - b$, and a major axis ($\alpha$) given by $2\alpha = \sqrt{4r_{\text{Pb}}^2 - b^2}$, where b is the impact parameter. The elliptic overlap region is filled randomly with strings, given a certain density (ρ). Example events for $\rho = 5$ fm^{-2} are shown in figure 7. We note that this configuration is deliberately chosen to maximize v_2 (elliptical flow) at the expense of v_3 and v_4, though with a fluctuating initial state geometry, some v_3 and v_4 will always be present.

We quantify the initial anisotropy by the participant eccentricity [84], here employed on the strings:

$$\epsilon_2 = \frac{\sqrt{\langle r^2 \cos(2\phi)\rangle^2 + \langle r^2 \sin(2\phi)\rangle^2}}{\langle r^2 \rangle}, \tag{26}$$

where r and ϕ are the usual polar coordinates of the string centers, but with the origin shifted to the center of the distribution.

For the calculation of flow coefficients v_2, we use as Ψ_n the event plane angle of the initial state, again calculated from string centers, with the origin shifted to the center. Thus:

$$\Psi_n = \frac{1}{n} \arctan\left(\frac{\langle r^2 \sin(n\phi)\rangle}{\langle r^2 \cos(n\phi)\rangle}\right) + \frac{\pi}{n}. \tag{27}$$

[6]We note that even a single string configuration can give rise to shoving effects, if the string overlaps with itself. Such configurations could possibly arise to the necessary degree in e^+e^- collisions, though experimental results so far have not shown any indication of flow [82, 83].

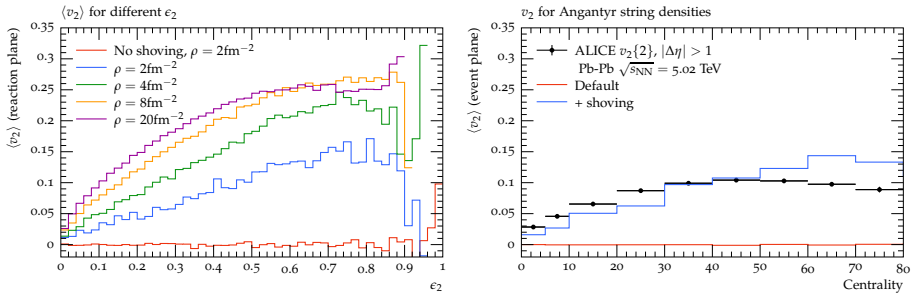

Figure 9: The average v_2 flow coefficient for for different constant densities as function of ϵ_2 (left), and v_2 as function of centrality with string densities from Angantyr (right). Data from ALICE [86] added to guide the eye.

We note that Ψ_n with this definition will in general be different from 0 (which is the event plane angle of the initial overlapping ellipses by construction), due to fluctuations. Flow coefficients can then be calculated as:

$$v_n = \langle \cos(n(\phi - \Psi_n)) \rangle. \tag{28}$$

We begin by studying average quantities as a function of collision centrality, here defined by the impact parameter of the two colliding nuclei, for exemplary values of string density $\rho = \{2, 4, 8, 20\}$ fm^{-2}. In figure 8 (left) we show the average number of strings in bins of centrality[7]. The numbers are compared to the number of string dipoles between $\eta = -1$ and $\eta = 1$ with a total $p_\perp < 3$ GeV, generated by the Angantyr model [40] in Pb-Pb collisions at $\sqrt{s_{\mathrm{NN}}} = 5.02$ TeV. The Angantyr model has been shown to give a good description of charged multiplicity at mid-rapidity in AA collisions [85], and this comparison is therefore useful to provide a comparison to realistic string densities at current LHC energies.

In figure 8 (right), the average v_2 as a function of centrality is shown for the same densities as figure 8 (left), as well as for a reference without shoving, with $\rho = 2$ fm^{-2}. Again, several observations can be made. First of all, for a fixed centrality v_2 will increase with increasing density. Due to the definition of v_2 made in this section, there are no non-flow contributions.

It should be noted that the density intervals are not evenly spaced. It is seen directly from figure 8, that v_2 saturates with increasing density. The point is made more clear in figure 9 (left), where $\langle v_2 \rangle$ (again for different densities) is shown for all centralities, as function of ϵ_2. Here it can furthermore be seen that v_2 to a good

[7]The centrality is here defined by the impact parameter between two colliding disks needed to give a certain elliptic geometry.

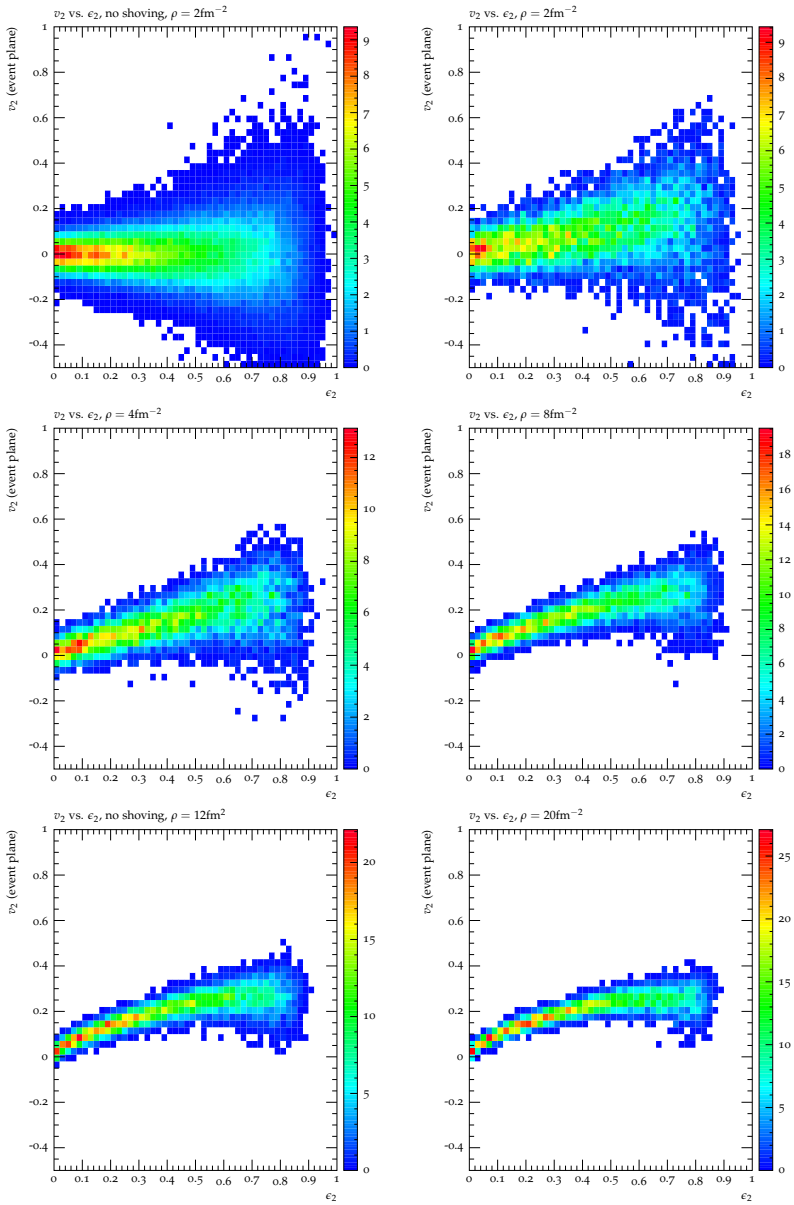

Figure 10: The correlation between ϵ_2 and v_2 for no shoving, $\rho = 2$ fm^{-2} (upper left) and with shoving for five different densities: $\rho = 2$ fm^{-2} (upper right), $\rho = 4$ fm^{-2} (middle left), $\rho = 8$ fm^{-2} (middle right), $\rho = 12$ fm^{-2} (lower left) and $\rho = 20$ fm^{-2} (lower right).

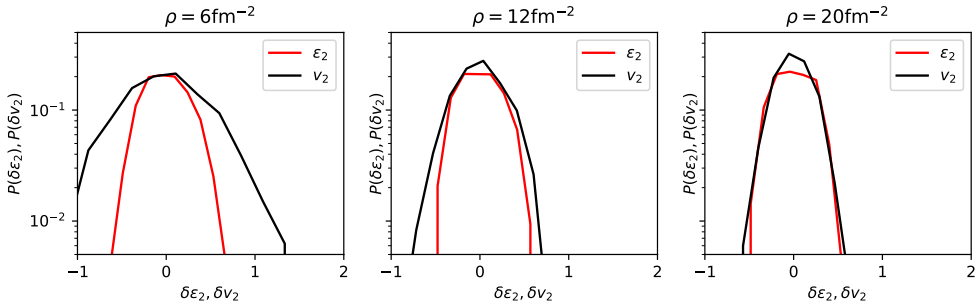

Figure 11: Probability distributions of ϵ_2 and v_2 in the 20-30% centrality bin, for three different values of ρ.

approximation rises linearly with eccentricity at densities comparable to current experiments, whereas at higher densities, the response has an additional component. This point will be explored further in section 5.2. Finally, in figure 9 (right), we show v_2 from the toy model in a way which is more comparable to experiment. In this figure, string multiplicity for each toy-event are generated with Angantyr, and an elliptic initial condition of the *same* impact parameter is constructed. This provides more realistic string densities at different centralities, and as it can be seen, this construction does a reasonable job at describing v_2 as a function of centrality. A no-shoving reference is also added to this figure, and as expected, it is consistent with zero. Finally it can be added that v_3 and v_4 are, as could be expected from the engineered initial conditions, both compatible with zero. (Not shown in any figure here.)

5.2 Towards the hydrodynamical limit at high string density

As mentioned earlier, hydrodynamic calculations are often employed for heavy ion phenomenology, when it concerns interactions of the final state, leading to collective flow. Whether or not the shoving model will, in the end, describe heavy ion data to a satisfactory degree, it is interesting to ask to what kind of hydrodynamics the shoving model will become in the large density limit. While analytic exploration of this question will be left to future studies, it is possible at this point to study similarities in the phenomenology of the two approaches. Similarities were already indicated in figure 9 (left), where the same type of almost linear response as seen in hydrodynamics [87] and in multiphase transport [88] is seen at string densities comparable to experimental ones. It is interesting here to first of all note the

difference between the shoving response at high densities, and the aforementioned hydrodynamic response. Fitting to a linear plus a cubic term, both hydrodynamics and transport yields a positive coefficient for the cubic term, where shoving in the high density limit yields a negative one. It is furthermore seen directly from the figure that, in the high-ϵ_2 limit, $\rho = 8$ fm^{-2} yields a higher v_2 than $\rho = 20$ fm^{-2}. While systems of this density are not yet experimentally realized, the results here points to prospects for higher energy future experiments, as well as higher luminosity at current experiments, allowing extraction of data at higher densities.

It is interesting to also study flow fluctuations. An obvious route is to follow the paper by Niemi *et al.*[89], which studied the correlation between flow coefficients and eccentricities, and noted that v_2 and v_3 have a strong linear correlation with ϵ_2 and ϵ_3. In figure 10, we show the correlation between ϵ_2 (from eq. (26)) and v_2, for five values of ρ, as well as for a no-shoving reference. No centrality selection is performed, as the toy geometry of the system impose a strict relationship between eccentricity and centrality defined by impact parameter, and binning in centrality would thus not add any information. With no shoving figure 10 (upper left), the average value is, as shown before, consistent with zero, while fluctuations are large. The shoving effect is now added, starting at small density ($\rho = 2$ fm^{-2}), figure 10 (upper right). It is readily seen that a linear response is obtained, and the distribution of v_2 is rather wide. At higher (intermediate) densities $\rho = 4$ and 8 fm^{-2}, in figure 10 (middle left) and (middle right), a stronger correlation appears, though not as narrow as in ref. [89]. For $\rho = 8$ fm^{-2} the linear response is broken. Finally for the densest considered states, $\rho = 12$ and 20 fm^{-2} in figure 10 (lower left) and (lower right) both the average value and the fluctuations starts to saturate, and at higher densities than the ones shown here, neither changes considerably.

To further study the scaling of v_2 with ϵ_2, we study the scaled event-by-event variables:

$$\delta\epsilon_2 = \frac{\epsilon_2 - \langle\epsilon_2\rangle}{\langle\epsilon_2\rangle}, \quad \text{and} \quad \delta v_2 = \frac{v_2 - \langle v_2\rangle}{\langle v_2\rangle}. \tag{29}$$

In figure 11 the distributions of $\delta\epsilon_2$ and δv_2, are shown for the densities $\rho = \{6, 12, 20\}$ fm^{-2}, in the 20-30% centrality bin. It should be noted that, due to the purely elliptical sampling region, the shape of the distribution cannot be compared directly to those of ref. [89]. The main conclusion is, however, clear. In the dense limit, in the rightmost panel, the two distributions are almost identical. This means that the shoving model, in this limit, reproduces a key global feature of hydrodynamics, namely full scaling of final state (purely momentum space) quantities with the global initial state geometry. We note, however, that, in contrast to the plasma, the string system expands only in the two transverse dimensions, as there

is no expansion in the longitudinal direction.

A notable discussion pertains to the issue whether or not heavy ion collisions at RHIC and LHC energies, reach a high enough string density for the shoving model to behave like hydrodynamics, as indicated above. In figure 8 (left), it was shown that Pb-Pb collisions at LHC energies produce an amount of strings corresponding to toy model densities of little less than 4 fm^{-2} for very central events, 2-3 fm^{-2} for mid-central events and less than 2 fm^{-2} for the most peripheral events. Even though the toy model predicts linear scaling of $\langle v_2 \rangle$ with $\langle \epsilon_2 \rangle$ for experimentally reachable densities, the fluctuations in string shoving and hydrodynamics do not exhibit the same scaling. A further direct study of flow fluctuations in non-central heavy ion collisions would thus be of interest both on the phenomenological and experimental side.

6 Results with Angantyr initial states

In the previous section, we have shown that given a simple initial state of long, straight strings without any soft gluons, the shoving mechanism can produce a response which (a) scales with initial state geometry in the same way as a hydrodynamic response, and (b) can produce flow coefficients in momentum space at the same level as measured in experiments. In this section we go a step further, and present the response of the model given a more realistic initial string configuration, as produced by the Angantyr model, which can be compared to data. In section 4 we described several of the challenges faced when interfacing the shoving model to an initial state containing many soft gluons, which in particular is the case in AA collisions. Throughout this section we use the same canonical values of shoving model parameters as in the previous section.

6.1 Results in pp collisions

Already the original implementation of the shoving model was shown in ref. [36] to give a satisfactory description of the pp "ridge". We will in this section focus on flow observables as calculated at high energy heavy ion experiments, *i.e.* flow coefficients calculated using the generic framework formalism [90, 91], in the implementation in the Rivet program [92].

It is in principle possible to generate pp events using the normal PYTHIA MPI model [93, 94, 95]. It would, however, be computationally inefficient, since emphasis should be given to high multiplicity results. The results presented here therefore use the modifications of the MPI framework presented as part of the Angantyr

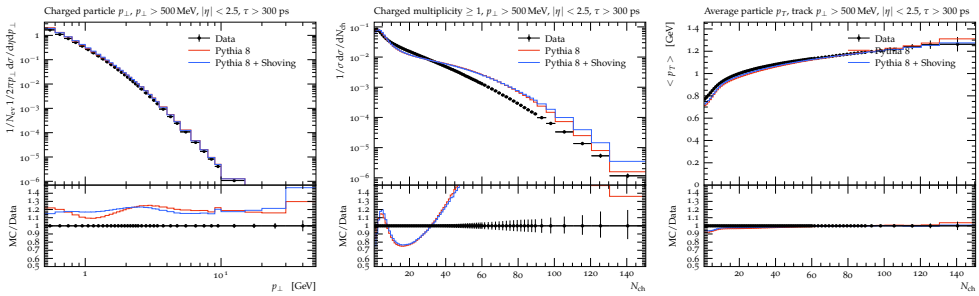

Figure 12: Comparison of PYTHIA (non-diffractive) to PYTHIA + shoving to basic $p_\perp$ (left), multiplicity (middle) and $\langle p_\perp \rangle$ distributions in pp collisions at $\sqrt{s} = 13$ TeV to data by ATLAS.

heavy ion model [40], notably the ability to bias the impact parameter selection towards very central pp collisions, and re-weighting back to the normal distribution.

We first note, that while the shoving mechanism does not change the total multiplicity of an event, it will change the multiplicity in fiducial region measured by an experiment, because it will push particles from the unmeasured low-$p_\perp$ region to (measured) higher $p_\perp$. It is therefore necessary to slightly re-tune the model parameters, to obtain a correct description of basic observables such as $p_\perp$ distributions and total multiplicity. In practise, the parameter $p_{\perp,0}$, which regulates[8] the $2 \to 2$ parton cross section is increased from the default value of 2.28 to 2.4. In figure 12 we show a comparison between PYTHIA (with the above mentioned impact parameter sampling) and PYTHIA + shoving, for a few standard minimum-bias observables, compared the charged $p_\perp$ distribution (left), the distribution of number of charged particles (middle) and $\langle p_\perp \rangle (N_{ch})$ (right), all at $\sqrt{s} = 13$ TeV. Data by ATLAS [96], the analysis implemented in the Rivet framework [97].

The agreement between simulation and data for the multiplicity distribution, is not as good as normally expected from PYTHIA . This is expected, as only non-diffractive collisions were simulated. More interesting is the slight difference between the two simulations, where it is clearly visible that in spite of the re-tuning, shoving still produce more particles in the high-N_{ch} limit. In the $p_\perp$ distribution, it is seen that shoving has the effect of increasing the spectrum around around $p_\perp = 1$ GeV. While the normalization is off (due to the exclusion of diffractive events in the simulation), shoving brings the shape of the low-$p_\perp$ part of the spec-

[8] The divergence of the partonic $2 \to 2$ cross section is regularized for $p_\perp \to 0$ by a factor $p_\perp^4/(p_{\perp 0}^2 + p_\perp^2)^2$, and by using an $\alpha_s(p_{\perp 0}^2 + p_\perp^2)$. Tuning is done by `MultipartonInteractions:pT0Ref` which is the p_{T0} value for the reference CM energy (where `pT0Ref` = `pT0(ecmRef)`).

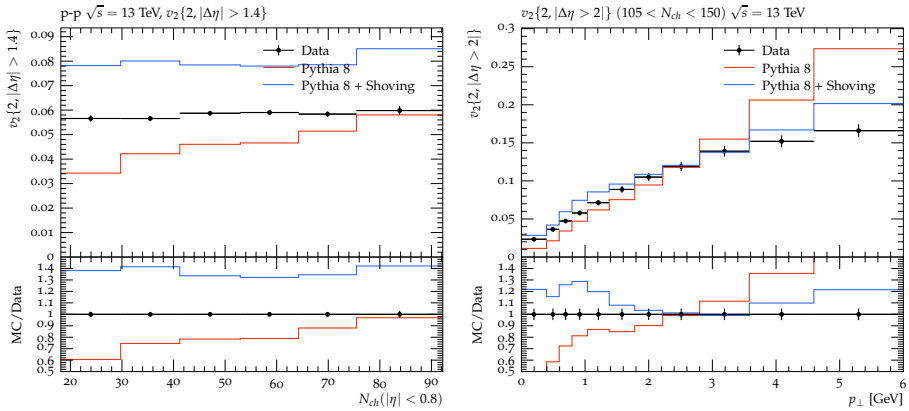

Figure 13: Comparison to $v_2\{2\}$ as function of multiplicity with ALICE high multiplicity trigger (left), and versus $p_\perp$ in high multiplicity events (right). Data from pp collisions at $\sqrt{s} = 13$ TeV by ALICE [98] and CMS [99].

trum closer to data. Finally the $\langle p_\perp \rangle (N_{ch})$ is almost unchanged.

We now turn our attention to flow coefficients, and show v_2 calculated by two-particle correlations in figure 13. In figure 13 (left) the multiplicity dependence of $v_2\{2\}$ with $|\Delta\eta| > 1.4$ is shown, and in figure 13 (right) the $p_\perp$-dependence of $v_2\{2\}$ ($|\Delta\eta| > 2$) in high multiplicity events is shown. Several conclusions can be drawn from the two figures.

First of all, it is seen that v_2 as a function of multiplicity (in figure 13 (left)) is too high with shoving enabled. We emphasize that the model parameters have not been tuned to reproduce this data, and in particular that successful description of this data will also require a good model for the spatial distribution of strings in a pp collision – a point we will return to in a moment. We do, however, note that the additional v_2 added by the shoving model, persists even with an η separation of correlated particles (as $|\Delta\eta|$ cuts are applied), a feature which separates the shoving model from *e.g.* colour reconnection approaches, which have been pointed out to produce flow-like effects in pp collisions [100, 101, 102]. We also note that the $p_\perp$-dependence of v_2 is drastically improved, as seen in figure 13 (right). In particular the high-$p_\perp$ behaviour of this quantity is interesting, as it decreases wrt. the baseline when shoving is enabled.

In figure 14 comparisons to $v_3\{2\}$ (left) and $v_4\{2\}$ (right) are performed. While it is clear that shoving adds a sizeable contribution to both, it is equally clear that data is not very well reproduced. We remind the reader that any v_n produced by the shoving model comes about as a response to the initial geometry, and the initial geometry used by default in PYTHIA , consists of two overlapping 2D Gaussian

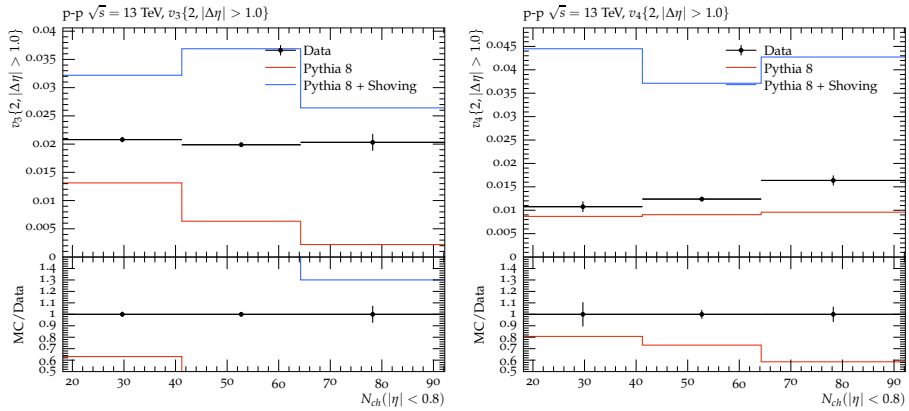

Figure 14: Comparison to $v_3\{2\}$ (left) and $v_4\{2\}$ (right) as function of multiplicity with ALICE high multiplicity trigger. Data from pp collisions at $\sqrt{s} = 13$ TeV by ALICE [98].

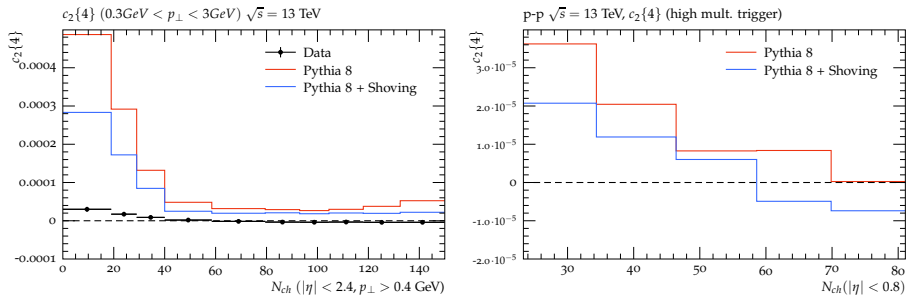

Figure 15: The four-particle cumulant $c_2\{4\}$, compared to data from CMS [99] (left), and with the ALICE high multiplicity trigger (no data, right).

distributions. It was shown in ref. [34], that applying more realistic initial conditions, can drastically change the eccentricities of the initial state in pp collisions. So while the description at this point is not perfect, the observations that a clear effect is present, bears promise for future studies. Further on, correlations between flow coefficients, the so-called symmetric cumulants [91, 103], will be an obvious step. But at this point, without satisfactory description of the v_n's themselves, it is not fruitful to go on to even more advanced observables.

Finally, in figure 15, we show results for the four-particle cumulant $c_2\{4\}$. We briefly remind the reader about some definitions. The 2- and 4-particle correlations

in a single event are given by the moments [90]:

$$\begin{aligned}\langle 2\rangle &= \langle \sum_{i,j} \exp[in(\phi_i - \phi_j)]\rangle \\ \langle 4\rangle &= \langle \sum_{i,j,k,l} \exp[in(\phi_i + \phi_j - \phi_k - \phi_l)]\rangle. \end{aligned} \tag{30}$$

The averages are here taken over all combinations of 2 or 4 non-equal particles in one event. The four particle cumulant is the all-event averaged 4-particle azimuthal correlations, with the 2-particle contribution subtracted:

$$c_n\{4\} = \langle\langle 4\rangle\rangle - 2\langle\langle 2\rangle\rangle^2. \tag{31}$$

The double average here means first an average over particles in one event, and then average over all events.

As discussed in ref. [104], when the correlation is dominated by flow and the multiplicity is high, then the flow coefficient $v_2\{4\}$ is given by $\sqrt[4]{-c_2\{4\}}$. Clearly $c_2\{4\}$ must be *negative* for this to be realized. This, in turn, means that the relative difference between the 2 -and 4-particle azimuthal correlations, must be right from eq. (31). As it was also pointed out in ref. [104], the non-flow contribution to four-particle correlations is much smaller than for two-particle correlations, as the cumulant becomes flow-dominated when $v_n \gg 1/M^{3/4}$ (M is the multiplicity) in the former case, but only when $v_n \gg 1/\sqrt{M}$ in the latter. In a pp collision M is small compared to a heavy ion collision, and it can therefore be reasonably expected that the four particle correlations will only be flow dominated at sufficiently high multiplicity. Since data show a real $v_2\{4\}$, the importance of the sign of $c_2\{4\}$ in model calculations for pp, have recently been highlighted [105, 106]. Importantly, standard hydrodynamic treatments do not obtain a negative sign of $c_2\{4\}$ in pp collisions, even with specifically engineered initial conditions [107].

In the results from the shoving model in figure 15, we note that while a negative $c_2\{4\}$ is not produced when comparing to CMS results, it is produced in high multiplicity events in the ALICE acceptance, using the high multiplicity trigger. There are several possible reasons for this apparent discrepancy. The acceptances are quite different, and since the sign of $c_2\{4\}$ is an observed characteristic, rather than a fundamental feature of the model, it is difficult to point out why a given model should produce different results in different acceptances – though it is possible. More interesting, is the possible effect of the high multiplicity trigger. In figure 15 (left), it is seen that both default PYTHIA , as well as PYTHIA with the shoving model, over-predicts $c_2\{4\}$ at low-multiplicity by a large margin. As noted in the original

paper, this is also the case for the 2-particle cumulant. A reasonable explanation for this over-prediction could be, that PYTHIA collects too many particles in mini-jets in general. With a high multiplicity forward trigger, a strong bias against this effect is put in place, and the underlying model behaves more reasonable. In any case, the finding of a negative $c_2\{4\}$ in high-multiplicity events with the shoving model is an interesting and non-trivial result, which will be followed up in a future study.

6.2 Results in Pb-Pb collisions

We now turn to Pb-Pb collisions, where we use the Angantyr model in PYTHIA keeping the same settings as in section 6.1. The results for Pb-Pb collision events at 5.02 TeV has been compared to ALICE data points via Rivet routines [9]. The anisotropic flow coefficients plotted here have been calculated, as in the previous section, using multi-particle cumulant methods as done in the ALICE experiment.

Centrality measures used in these analyses are of two kinds: for the plot in figure 16 we use the centrality binning of the generated impact parameter by Angantyr, and for the plots in figure 17, we use Angantyr generated centrality binning which mimics the experimental centrality definition where in ALICE the binning is in the integrated signal in their forward and backward scintillators. However, the difference between the two centrality measures is small in Pb-Pb collisions [92].

In figure 16, we plot the charged particle multiplicity for seven centrality classes (0-5%, 5-10%, 10-20%, 20-30%, 30-40%, 40-50%, 50-60%) as a function of pseudorapidity in the range $-3.5 < \eta < 5$ for $\sqrt{s_{NN}} = 5.02$ TeV in Pb-Pb collisions comparing it to the study performed by ALICE[108]. We use this figure as our control plot to check that when we turn shoving on, the description of other observables are not destroyed.

We observe that this implementation fairly well preserves the Angantyr description of the multiplicity distributions. The overall multiplicity of the shoving curve is however a bit lower when compared to default Angantyr, which is because of the increased `pT0Ref` as mentioned in 6.1. Also, as discussed in section 4.3, when strings are shoved and the particles on average get a larger $p_\perp$ which also means that they come closer together in pseudorapidity. The overall effect is that particles are generally *dragged* closer towards mid-rapidity, reducing the two-humped structure seen for plain Angantyr.

We will look into further improvement of the multiplicity description by shoving through tuning, normalization of the distribution functions and accurate description of centrality as in experiments in the future.

[9] The Rivet routines are not yet validated by the experimental community.

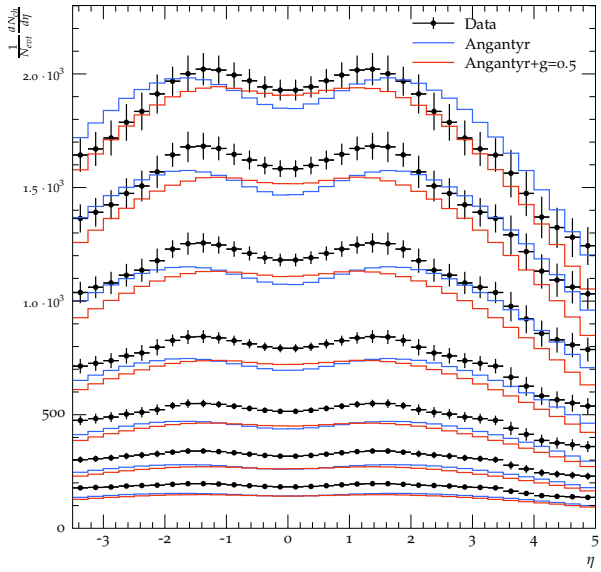

Figure 16: Charged particle multiplicity over a wide range of η in Pb-Pb collisions at $\sqrt{s_{NN}} = 5.02$ TeV for centralities 0-5%, 5-10%, 10-20%, ..., 50-60% [108].

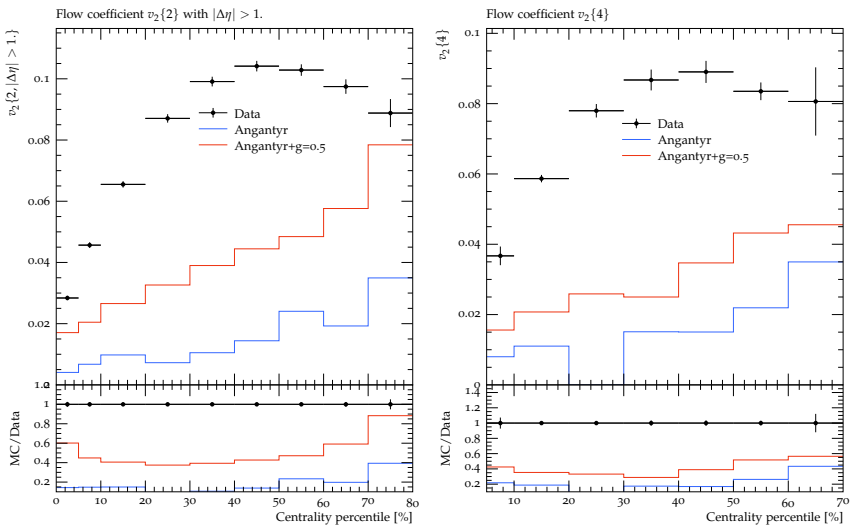

Figure 17: The flow coefficient $v_2\{2\}$ (left) with $|\Delta\eta| > 1$ and $v_2\{4\}$ (right) for $0.2 < p_\perp < 5.0$ GeV in Pb-Pb collisions at $\sqrt{s_{\mathrm{NN}}} = 5.02$ TeV [86].

Figure 17 presents the centrality dependence of the harmonic flow coefficient v_2 from two-particle cumulant on the left with $|\Delta\eta| > 1$ and four-particle cumulants on the right, integrated over the $p_\perp$ range $0.2 < p_\perp < 5.0$ GeV for 5.02 TeV Pb-Pb collisions [86] for generated centrality. We note that Angantyr with shoving results in an increased v_2 in the right direction with respect to data. We see in data that $v_2\{2\}$ increases from central to peripheral collisions, reaching a maximum of around 0.10 between $40 - 50\%$ centrality. $v_2\{4\}$ also shows a similar behaviour with a maximum around 0.09 between $40 - 50\%$ centrality.[10] String shoving result clearly lacks the curvature of the data points, but doubles the contribution in $v_2\{2\}$ as compared to Angantyr. The underlying cause for this behaviour is that the current implementation of shoving alone is not sufficient to generate the large overall response to the anisotropy in the initial collision geometry of the nuclei. An increased g factor or delayed hadronization time or an early onset of shoving, and a combination of these factors, do not give rise to enough v_2 either.

In section 5.1, we showed that shoving can generate sufficient v_2 as seen in data with completely straight strings without any gluon kinks. With Angantyr, we have more realistic final states with many and often soft gluon emissions from the multi-parton interactions and the initial- and final-state evolution models, which hinder the process of strings shoving each other by cutting short their interaction time, hence resulting in the overall observation of the lack of enough transverse nudges generated via this mechanism.

7 Conclusions and outlook

In this paper we have argued that a hot thermalized plasma is not necessarily formed even in central AA collisions, not even in Pb–Pb collisions at the highest attainable energies at the LHC. Instead we note that the string-based approach to simulating hadronic final states in the Angantyr model in PYTHIA8 gives a very reasonable description of the number and general distribution of particles in AA events, and take this as an incentive to study string hadronization in dense collision systems more carefully.

Our string picture is qualitatively different from the more conventional picture, where the colliding nuclei are described in terms of a CGC, that in the moment of collision turns into a so-called *glasma*, which very soon decays into a thermalized QGP. Similar to the string picture, the glasma has longitudinal fields stretched between the nucleus remnants, and these fields are kept together in flux tubes as the

[10] In the plot for $v_2\{4\}$, there is lack of statistics in the centrality bin 20-30% for Angantyr without shoving.

remnants move apart. There are, however, also essential differences. The glasma turns rapidly into a thermalized plasma. Such a plasma expands longitudinally in a boost invariant way, with decreasing energy density as a result. The initial density must therefore be quite high to give the observed particle density after freezeout. In contrast the energy density in the strings is constant up to the time for hadronization. When the strings become longer, the energy in the new string pieces is taken from the removing nucleus remnants, and not from depleting the energy in the strings already formed. In the string scenario we estimate the energy density at mid-rapidity to around 5 GeV/fm^3 (in PbPb at the LHC), while in the glasma we find that it ought to be one or two orders of magnitude higher.

The low energy density in the string scenario implies that the vacuum condensate is very important to form the strings. The break-down of the glasma is often motivated by the so-called "Nielsen–Olesen instabilities". These authors showed that a longitudinal chromo-electric field added to the QCD Fock vacuum is unstable, and transverse fields grow exponentially. This growth does not go on forever. Instead higher order corrections will lead to a Higgs potential analogous to the potential describing the condensate of Cooper-pairs in a superconductor or the vacuum condensate in the EW Higgs model. Adding a (not too strong) linear field to this non-trivial ground state will then give flux tubes, similar to the vortex lines in a superconductor. We take this as an indication that it may indeed be possible that strings can be formed and actually survive the initial phase of the collision, without a thermalized plasma being formed. (The energy density needed in the glasma may, however, be strong enough to destroy the "superconducting" phase.)

Another important difference between the two scenarios is that the glasma contains both chromo-electric and chromo-magnetic fields, not only chromo-electric fields as in the string picture. This implies CP-violating effects in the glasma, but this feature is not discussed in this paper.

In an earlier paper we argued that in a dense environment where the strings overlap in space–time, they should repel each other and we showed with a very simple model that this could induce flow in pp. Here we have motivated the model further, and compared to lattice calculations to estimate the transverse shape and energy distribution of the string-like field. We have also improved the implementation of the model, where the strings no longer have to be completely parallel in order to calculate the force between them. Instead we show that for a pair of arbitrary string pieces, we can always find a Lorentz frame where they will be stretched out in parallel planes, allowing us to easily calculate the force there. We have further improved the time discretization, and instead of processing string interactions in fixed time intervals, the shoving model is implemented as a parton shower with dynam-

ical time steps, greatly improving the computational performance of the model. Finally we have improved the procedure for transferring the nudges from string interactions to final state hadrons.

The implementation used for obtaining the results presented here is not yet quite complete. Although it circumvents the production of huge amounts of soft gluons in the shoving, which was a major problem for our previous implementation, it still has a problem with dealing with the soft gluons that are already there from the initial- and final-state parton showers. Gluon kinks lose energy with twice the force compared to a quark. A soft gluon therefore will soon loose all its energy, and new straight sections of the string will be formed, which in the current implementation are not taken into account.

In addition the implementation only allows shoving at points in space–time after the strings have expanded to the equilibrium size, $R_S \sim \tau_S$, and before they start to break up in hadrons at proper times around τ_H. Clearly shoving should be present also at times before τ_S, and the force between very close strings should then be higher, but our implementation currently cannot handle situations with varying string radii. Also, at times later than τ_H, after the string break-up, one could expect some shoving between the hadrons being formed, and after they are formed one needs to consider final state re-scattering.

In light of these shortcomings of the current implementation, it is not surprising that when we apply the model to complete partonic final states generated by Angantyr, we cannot quantitatively reproduce the amount of v_2 measured in experiments. But we do see that the shoving actually does give rise to flow effects. We also see that in pp we currently get a bit too large v_2, but we would like to emphasise that we have here not tried to do any tuning of the model parameters. Instead these are kept at canonical values,

To investigate the model further and to make it plausible that the shoving model, when implemented in full, actually may be able to reproduce also quantitatively the flow effects measured in AA collisions, we looked at what happens when applying it to a toy model of the initial state. To account for the missing string pieces due to soft gluons, we here used parallel strings without gluon kinks. The strings are randomly distributed with variable density in an ellipsoid shape in impact parameter space. In this way the shoving was unhampered by soft gluons, and we found that the model is able to get the azimuthal anisotropies in momentum space as expected from the eccentricity of the shape in impact parameter. By then matching the string density to the one we have in Angantyr for different centralities, we could also see that the resulting v_2 was much closer to measured data.

Showing that we can get reasonable azimuthal anisotropies in AA collisions

using a purely string-based scenario is, of course, not enough to prove that a thermalized QGP is *not* formed in such collisions. To do this we need to also be able to describe other measurements, such as strangeness enhancement and jet quenching and, more importantly find new observables where a string based scenario predicts results that cannot be reconciled with the QGP picture. And for this we not only need to improve the implementation of the shoving model, but also revisit our rope model and also our "swing" model for colour reconnections. The rope model has been shown to give reasonable descriptions of strangeness enhancement in high multiplicity pp, and using the parallel frame presented here, we should be able to get a better handle on the space–time picture of the string overlaps needed to be able to apply it in AA. Also for the swing model we can take advantage of the parallel frame to properly understand which partons may reconnect and when and where they may do so. And since in the parallel frame hard and soft partons are treated on an equal footing this could also have interesting effect on jets.

In the end we hope that these models will be implemented in PYTHIA8 together with the Angantyr model, so that we get a complete platform for generating fully hadronic final states that can be compared to any type of measurement in any kind of collision (AA, pA, pp, …). This would then give us a perfect laboratory to investigate a purely string-based picture as an alternative to the conventional QGP approach.

Acknowledgments

This work was funded in part by the Knut and Alice Wallenberg foundation, contract number 2017.0036, Swedish Research Council, contracts number 2016-03291, 2016-05996 and 2017-0034, in part by the European Research Council (ERC) under the European Union's Horizon 2020 research and innovation programme, grant agreement No 668679, and in part by the MCnetITN3 H2020 Marie Curie Initial Training Network, contract 722104.

A Vortex lines in a superconductor

The microscopic properties in a superconductor, the magnetic field, H, and the condensate wavefunction (order parameter), ψ, can be determined by the LG equations (see *e.g.* ref. [66]). The theory contains two characteristic lengths, the penetration depth λ for the magnetic field and the coherence length ξ for the condensate. In its generalization to a relativistic theory, the Lagrangian contains a Higgs potential for the condensate. Here the lengths λ and ξ correspond to the (inverse) masses of the gauge boson and the Higgs particle respectively.

For a flux tube the wavefunction ψ is undetermined along a "vortex line", and has a phase changing by $2\pi n$ when going around the vortex line, with n an integer. The total flux in the flux tube is then quantized to n times a flux quantum $\Phi_0 = 2\pi/q$, where for a normal superconductor $q = 2e$ is the charge of a Cooper pair. This quantum would also correspond to the charge of a magnetic monopole. The change in phase is related to a vortex-like current in the condensate, which keeps the flux confined within the flux tube.

At the boundary between a normal and a superconducting phase, the pressure from the condensate and the magnetic field balance each other. The condensate goes to zero over a distance ξ in the superconductor, and the magnetic field is suppressed over a distance λ. As a result, when ξ is larger than λ (or more exactly $\xi > \sqrt{2}\,\lambda$), both the condensate and the field are suppressed over a range $\xi - \lambda$. This is a *type I* superconductor, and it implies that the surface provides a positive contribution to the energy. In equilibrium the surface then tends to be as small as possible. If in contrast λ is larger than ξ (*type II* superconductor), the condensate and the field can coexist over a range $\sim \lambda - \xi$, and the surface provides a negative contribution to the energy, favouring a large surface. If the flux tube has more than one flux quantum, there is then a tendency to split it into a number of vortices, each with one unit of flux. In case of a large total flux, there is a repulsive force between nearby flux tubes. The system will then tend to expand, forming an "Abrikosov lattice".

The interaction between the condensate and the electromagnetic field in a superconductor is described by the LG equations, which in its relativistic generalization corresponds to the Abelian Higgs model relevant for the Abelian projection of the QCD field. The Lagrange density is here given by

$$\mathcal{L} = -\frac{1}{4}F_{\mu\nu}F^{\mu\nu} + [(\partial_\mu + ieA_\mu)\psi^*][(\partial_\mu - ieA_\mu)\psi] - \alpha|\psi|^2 - \frac{\beta}{2}|\psi|^4. \quad (32)$$

When the parameter α is smaller than zero, the scalar field ψ forms a condensate $\psi = \psi_0 = \sqrt{-\alpha/\beta}$. The mass of the Higgs particle and the massive gauge boson,

given by $\sqrt{-2\alpha}$ and $e\sqrt{-2\alpha/\beta}$ respectively, correspond to (the inverse of) the coherence length ξ and the penetration depth λ. The LG equations are obtained from Euler-Lagrange's equations varying ψ (or ψ^*) and A_μ.

In an extreme type II superconductor with $\xi \ll \lambda$, the LG equations have a solution $\psi = const.\ e^{-i\phi}$ (for $\rho > \xi$), for a vortex line which carries one unit of flux. The corresponding magnetic field is here given by

$$H(\rho) = C \cdot K_0(\rho/\lambda), \tag{33}$$

where $C = \Phi/(2\pi\lambda^2)$ is a constant, Φ is the total flux, and K_0 is a modified Bessel function. The Bessel function has a logarithmic dependence on ρ for $\rho < \lambda$, but falls exponentially for $\rho > \lambda$. The field is confined within this range by an electric current $j = \lambda\,|\mathrm{curl}\,\mathbf{H}| = (C/\lambda)\,K_1(\rho/\lambda)$ (also valid for $\rho > \xi$). In this extreme case, when ξ is very small, the contribution to the energy from destroying the condensate is also small, and the energy of the flux tube, the string tension κ, is given by the sum of the field energy and the energy in the current:

$$\kappa = \int_\xi d^2\rho\,\frac{1}{2}\left\{H(\rho)^2 + \lambda^2(\mathrm{curl}\,\mathbf{H}(\rho))^2\right\}. \tag{34}$$

We note that the energy is dominated by the contribution from the current, where $K_1(\rho/\lambda)$ is singular and $\sim \lambda/\rho$ for small ρ. Thus the total energy is proportional to $\ln(\lambda/\xi)$ for very small ξ.

When ξ is smaller than λ, but not close to zero, the following approximate solution is given by Clem [71]:

$$H(\rho) = C\,K_0(x_\perp/R), \quad \text{with}\ \ R = \sqrt{\rho^2 + \xi_v^2}\ \ \text{and}\ \ C = \Phi/(2\pi\lambda\,\xi_v\,K_1(\xi_v/\lambda)). \tag{35}$$

The new distance scale ξ_v depends on the ratio $\kappa_{LG} \equiv \lambda/\xi$, and is close to ξ for $\kappa_{LG} \approx 1/\sqrt{2}$, *i.e.* for a superconductor on the border between type I and type II. The expression in eq. (35) satisfies the one of the LG equations (obtained by varying the field A_μ) and Ampèr's equation $\mathbf{j} = \mathrm{curl}\,\mathbf{B} = \mathrm{curl}\,\mathrm{curl}\,\mathbf{A}$. It does, however, not satisfy the equation obtained by varying ψ, and for $\xi > \lambda$ this equation can be badly violated.

In a superconductor there are magnetic flux tubes, and magnetic monopoles would be confined. In QCD colour-electric flux tubes and colour-electric charges are confined. Thus for the Abelian projection the fields $F_{\mu\nu}$ will be replaced by the dual fields $\widetilde{F}_{\mu\nu}$, as discussed in section 2.2.

References

[1] T. Sjöstrand, S. Ask, J. R. Christiansen, R. Corke, N. Desai, P. Ilten, S. Mrenna, S. Prestel, C. O. Rasmussen, and P. Z. Skands, "An introduction to PYTHIA 8.2," *Comput. Phys. Commun.* **191** (2015) 159–177, 1410.3012.

[2] T. Sjöstrand, S. Mrenna, and P. Z. Skands, "PYTHIA 6.4 Physics and Manual," *JHEP* **05** (2006) 026, hep-ph/0603175.

[3] J. Bellm *et. al.*, "Herwig 7.0/Herwig++ 3.0 release note," *Eur. Phys. J.* **C76** (2016), no. 4 196, 1512.01178.

[4] M. Bähr *et. al.*, "Herwig++ Physics and Manual," *Eur. Phys. J. C* **58** (2008) 639–707, 0803.0883.

[5] **Sherpa** Collaboration, E. Bothmann *et. al.*, "Event Generation with Sherpa 2.2," *SciPost Phys.* 7 (2019), no. 3 034, 1905.09127.

[6] T. Gleisberg, S. Höche, F. Krauss, M. Schönherr, S. Schumann, F. Siegert, and J. Winter, "Event generation with SHERPA 1.1," *JHEP* **02** (2009) 007, 0811.4622.

[7] W. Broniowski, M. Chojnacki, W. Florkowski, and A. Kisiel, "Uniform Description of Soft Observables in Heavy-Ion Collisions at s(NN)**(1/2) = 200 GeV**2," *Phys. Rev. Lett.* **101** (2008) 022301, 0801.4361.

[8] B. Schenke, S. Jeon, and C. Gale, "Elliptic and triangular flow in event-by-event (3+1)D viscous hydrodynamics," *Phys. Rev. Lett.* **106** (2011) 042301, 1009.3244.

[9] H. Song, S. A. Bass, U. Heinz, T. Hirano, and C. Shen, "Hadron spectra and elliptic flow for 200 A GeV Au+Au collisions from viscous hydrodynamics coupled to a Boltzmann cascade," *Phys. Rev.* **C83** (2011) 054910, 1101.4638. [Erratum: Phys. Rev.C86,059903(2012)].

[10] F. G. Gardim, F. Grassi, M. Luzum, and J.-Y. Ollitrault, "Anisotropic flow in event-by-event ideal hydrodynamic simulations of $\sqrt{s_{NN}} = 200$ GeV Au+Au collisions," *Phys. Rev. Lett.* **109** (2012) 202302, 1203.2882.

[11] C. Gale, S. Jeon, B. Schenke, P. Tribedy, and R. Venugopalan, "Event-by-event anisotropic flow in heavy-ion collisions from combined Yang-Mills and viscous fluid dynamics," *Phys. Rev. Lett.* **110** (2013), no. 1 012302, 1209.6330.

[12] J. Noronha-Hostler, M. Luzum, and J.-Y. Ollitrault, "Hydrodynamic predictions for 5.02 TeV Pb-Pb collisions," *Phys. Rev.* **C93** (2016), no. 3 034912, 1511.06289.

[13] A. Andronic, P. Braun-Munzinger, K. Redlich, and J. Stachel, "Decoding the phase structure of QCD via particle production at high energy," *Nature* **561** (2018), no. 7723 321–330, 1710.09425.

[14] **CMS** Collaboration, V. Khachatryan *et. al.*, "Observation of Long-Range Near-Side Angular Correlations in Proton-Proton Collisions at the LHC," *JHEP* **09** (2010) 091, 1009.4122.

[15] **ALICE** Collaboration, J. Adam *et. al.*, "Enhanced production of multi-strange hadrons in high-multiplicity proton-proton collisions," *Nature Phys.* **13** (2017) 535–539, 1606.07424.

[16] E. Gotsman, E. Levin, and U. Maor, "A comprehensive model of soft interactions in the LHC era," *Int. J. Mod. Phys. A* **30** (2015), no. 08 1542005, 1403.4531.

[17] V. Khoze, A. Martin, and M. Ryskin, "Elastic scattering and Diffractive dissociation in the light of LHC data," *Int. J. Mod. Phys. A* **30** (2015), no. 08 1542004, 1402.2778.

[18] S. Ostapchenko, "Monte Carlo treatment of hadronic interactions in enhanced Pomeron scheme: I. QGSJET-II model," *Phys. Rev. D* **83** (2011) 014018, 1010.1869.

[19] A. Kovner, L. D. McLerran, and H. Weigert, "Gluon production from nonAbelian Weizsacker-Williams fields in nucleus-nucleus collisions," *Phys. Rev. D* **52** (1995) 6231–6237, hep-ph/9502289.

[20] A. Kovner, L. D. McLerran, and H. Weigert, "Gluon production at high transverse momentum in the McLerran-Venugopalan model of nuclear structure functions," *Phys. Rev. D* **52** (1995) 3809–3814, hep-ph/9505320.

[21] T. Lappi and L. McLerran, "Some features of the glasma," *Nucl. Phys.* **A772** (2006) 200–212, hep-ph/0602189.

[22] R. Venugopalan, "From Glasma to Quark Gluon Plasma in heavy ion collisions," *J. Phys.* **G35** (2008) 104003, 0806.1356.

[23] F. Gelis, "Color Glass Condensate and Glasma," *Int. J. Mod. Phys.* **A28** (2013) 1330001, 1211.3327.

[24] D. Kharzeev, R. Pisarski, and M. H. Tytgat, "Possibility of spontaneous parity violation in hot QCD," *Phys. Rev. Lett.* **81** (1998) 512–515, hep-ph/9804221.

[25] D. Kharzeev, A. Krasnitz, and R. Venugopalan, "Anomalous chirality fluctuations in the initial stage of heavy ion collisions and parity odd bubbles," *Phys. Lett. B* **545** (2002) 298–306, hep-ph/0109253.

[26] G. Chen, R. J. Fries, J. I. Kapusta, and Y. Li, "Early Time Dynamics of Gluon Fields in High Energy Nuclear Collisions," *Phys. Rev. C* **92** (2015), no. 6 064912, 1507.03524.

[27] N. Nielsen and P. Olesen, "An Unstable Yang-Mills Field Mode," *Nucl. Phys. B* **144** (1978) 376–396.

[28] N. Nielsen and P. Olesen, "Electric Vortex Lines From the Yang-Mills Theory," *Phys. Lett. B* **79** (1978) 304.

[29] E. S. Weibel, "Spontaneously Growing Transverse Waves in a Plasma Due to an Anisotropic Velocity Distribution," *Phys. Rev. Lett.* **2** (1959) 83–84.

[30] K. Dusling, M. Mace, and R. Venugopalan, "Multiparticle collectivity from initial state correlations in high energy proton-nucleus collisions," *Phys. Rev. Lett.* **120** (2018), no. 4 042002, 1705.00745.

[31] E. Avsar, G. Gustafson, and L. Lönnblad, "Energy conservation and saturation in small-x evolution," *JHEP* **07** (2005) 062, hep-ph/0503181.

[32] E. Avsar, G. Gustafson, and L. Lönnblad, "Small-x dipole evolution beyond the large-N(c) imit," *JHEP* **01** (2007) 012, hep-ph/0610157.

[33] E. Avsar, C. Flensburg, Y. Hatta, J.-Y. Ollitrault, and T. Ueda, "Eccentricity and elliptic flow in proton–proton collisions from parton evolution," *Phys. Lett. B* **702** (2011) 394–397, 1009.5643.

[34] C. Bierlich and C. O. Rasmussen, "Dipole evolution: perspectives for collectivity and γ^*A collisions," *JHEP* **10** (2019) 026, 1907.12871.

[35] H.-J. Drescher, A. Dumitru, C. Gombeaud, and J.-Y. Ollitrault, "The Centrality dependence of elliptic flow, the hydrodynamic limit, and the viscosity of hot QCD," *Phys. Rev. C* **76** (2007) 024905, 0704.3553.

[36] C. Bierlich, G. Gustafson, and L. Lönnblad, "Collectivity without plasma in hadronic collisions," *Phys. Lett. B* **779** (2018) 58–63, 1710.09725.

[37] C. Bierlich, G. Gustafson, L. Lönnblad, and A. Tarasov, "Effects of Overlapping Strings in pp Collisions," *JHEP* **03** (2015) 148, 1412.6259.

[38] B. Andersson, G. Gustafson, and B. Nilsson-Almqvist, "A Model for Low p(t) Hadronic Reactions, with Generalizations to Hadron - Nucleus and Nucleus-Nucleus Collisions," *Nucl. Phys. B* **281** (1987) 289–309.

[39] X.-N. Wang and M. Gyulassy, "HIJING: A Monte Carlo model for multiple jet production in p p, p A and A A collisions," *Phys. Rev.* **D44** (1991) 3501–3516.

[40] C. Bierlich, G. Gustafson, L. Lönnblad, and H. Shah, "The Angantyr model for Heavy-Ion Collisions in PYTHIA8," *JHEP* **10** (2018) 134, 1806.10820.

[41] J. Bjorken, "Highly Relativistic Nucleus-Nucleus Collisions: The Central Rapidity Region," *Phys. Rev. D* **27** (1983) 140–151.

[42] T. Sjöstrand and M. Utheim, "A Framework for Hadronic Rescattering in pp Collisions," 2005.05658.

[43] A. V. da Silva, W. M. Serenone, D. Dobrigkeit Chinellato, J. Takahashi, and C. Bierlich, "Improved heavy-ion collision baseline based on perturbative QCD and hadronic rescattering," 2002.10236.

[44] S. A. Bass *et. al.*, "Microscopic models for ultrarelativistic heavy ion collisions," *Prog. Part. Nucl. Phys.* **41** (1998) 255–369, nucl-th/9803035.

[45] K. Johnson, "The M.I.T. Bag Model," *Acta Phys. Polon. B* **6** (1975) 865.

[46] S. Nishino, K.-I. Kondo, A. Shibata, T. Sasago, and S. Kato, "Type of dual superconductivity for the $SU(2)$ Yang–Mills theory," *Eur. Phys. J.* **C79** (2019), no. 9 774, 1903.10488.

[47] A. Shibata, K.-I. Kondo, S. Nishino, T. Sasago, and S. Kato, "Type of dual superconductivity for $SU(2)$ and $SU(3)$ Yang–Mills theories," 1903.10487.

[48] M. Baker, P. Cea, V. Chelnokov, L. Cosmai, F. Cuteri, and A. Papa, "Isolating the confining color field in the SU(3) flux tube," *Eur. Phys. J.* **C79** (2019), no. 6 478, 1810.07133.

[49] A. Shibata, K.-I. Kondo, S. Kato, and T. Shinohara, "Non-Abelian dual superconductivity in SU(3) Yang-Mills theory: dual Meissner effect and type of the vacuum," *Phys. Rev.* **D87** (2013), no. 5 054011, 1212.6512.

[50] B. Andersson, G. Gustafson, J. Hakkinen, M. Ringner, and P. Sutton, "Is there screwiness at the end of the QCD cascades?," *JHEP* **09** (1998) 014, hep-ph/9807541.

[51] B. Schenke, P. Tribedy, and R. Venugopalan, "Event-by-event gluon multiplicity, energy density, and eccentricities in ultrarelativistic heavy-ion collisions," *Phys. Rev. C* **86** (2012) 034908, 1206.6805.

[52] B. Schenke, P. Tribedy, and R. Venugopalan, "Fluctuating Glasma initial conditions and flow in heavy ion collisions," *Phys. Rev. Lett.* **108** (2012) 252301, 1202.6646.

[53] **BRAHMS** Collaboration, I. G. Bearden *et. al.*, "Pseudorapidity distributions of charged particles from Au+Au collisions at the maximum RHIC energy," *Phys. Rev. Lett.* **88** (2002) 202301, nucl-ex/0112001.

[54] **BRAHMS** Collaboration, A. Jipa, "Overview of the results from the BRAHMS experiment," *Acta Phys. Hung.* **A22** (2005) 121–137, nucl-ex/0404011.

[55] S. McDonald, S. Jeon, and C. Gale, "IP-Glasma Phenomenology Beyond 2D," *Nucl. Phys. A* **982** (2019) 239–242, 1807.05409.

[56] H. B. Nielsen and P. Olesen, "A Quantum Liquid Model for the QCD Vacuum: Gauge and Rotational Invariance of Domained and Quantized Homogeneous Color Fields," *Nucl. Phys. B* **160** (1979) 380–396.

[57] J. Ambjørn, N. Nielsen, and P. Olesen, "A Hidden Higgs Lagrangian in QCD," *Nucl. Phys. B* **152** (1979) 75–96.

[58] P. Olesen, "On the QCD Vacuum," *Phys. Scripta* **23** (1981) 1000–1004.

[59] G. 't Hooft, "A Property of Electric and Magnetic Flux in Nonabelian Gauge Theories," *Nucl. Phys. B* **153** (1979) 141–160.

[60] M. Baker, J. S. Ball, and F. Zachariasen, "Dual QCD: A Review," *Phys. Rept.* **209** (1991) 73–127.

[61] G. 't Hooft, "Topology of the Gauge Condition and New Confinement Phases in Nonabelian Gauge Theories," *Nucl. Phys. B* **190** (1981) 455–478.

[62] J. Carmona, M. D'Elia, A. Di Giacomo, B. Lucini, and G. Paffuti, "Color confinement and dual superconductivity of the vacuum. 3.," *Phys. Rev. D* **64** (2001) 114507, hep-lat/0103005.

[63] P. Cea and L. Cosmai, "Abelian monopole and vortex condensation in lattice gauge theories," *JHEP* **11** (2001) 064, hep-lat/0103019.

[64] G. Ripka, *Dual superconductor models of color confinement*, vol. 639. 2004.

[65] A. Di Giacomo, "QCD monopoles, abelian projections and gauge invariance," 1707.07896.

[66] P. G. de Gennes, *Superconductivity in Metals and Alloys*. Addison–Wesley Publ. Co., 1966, 1989.

[67] K.-I. Kondo, S. Kato, A. Shibata, and T. Shinohara, "Quark confinement: Dual superconductor picture based on a non-Abelian Stokes theorem and reformulations of Yang–Mills theory," *Phys. Rept.* **579** (2015) 1–226, 1409.1599.

[68] P. Cea, L. Cosmai, F. Cuteri, and A. Papa, "Flux tubes in the SU(3) vacuum: London penetration depth and coherence length," *Phys. Rev.* **D89** (2014), no. 9 094505, 1404.1172.

[69] M. Baker, P. Cea, V. Chelnokov, L. Cosmai, F. Cuteri, and A. Papa, "The confining color field in SU(3) gauge theory," *Eur. Phys. J.* **C80** (2020), no. 6 514, 1912.04739.

[70] N. Battelli and C. Bonati, "Color flux tubes in $SU(3)$ Yang-Mills theory: an investigation with the connected correlator," *Phys. Rev.* **D99** (2019), no. 11 114501, 1903.10463.

[71] J. R. Clem , *J. Low Temp. Physics* **18** (1975) 427.

[72] R. Sommer, "Scale setting in lattice QCD," *PoS* **LATTICE2013** (2014) 015, 1401.3270.

[73] R. G. Edwards, U. M. Heller, and T. R. Klassen, "Accurate scale determinations for the Wilson gauge action," *Nucl. Phys.* **B517** (1998) 377–392, hep-lat/9711003.

[74] S. Necco and R. Sommer, "The N(f) = 0 heavy quark potential from short to intermediate distances," *Nucl. Phys.* **B622** (2002) 328–346, hep-lat/0108008.

[75] B. Andersson, G. Gustafson, G. Ingelman, and T. Sjöstrand, "Parton Fragmentation and String Dynamics," *Phys. Rept.* **97** (1983) 31–145.

[76] X. Artru, "Classical String Phenomenology. 1. How Strings Work," *Phys. Rept.* **97** (1983) 147.

[77] T. Sjöstrand, "Jet Fragmentation of Nearby Partons," *Nucl. Phys.* **B248** (1984) 469–502.

[78] L. Lönnblad, "Fooling Around with the Sudakov Veto Algorithm," *Eur. Phys. J.* **C73** (2013), no. 3 2350, 1211.7204.

[79] U. Heinz and R. Snellings, "Collective flow and viscosity in relativistic heavy-ion collisions," *Ann. Rev. Nucl. Part. Sci.* **63** (2013) 123–151, 1301.2826.

[80] S. Voloshin and Y. Zhang, "Flow study in relativistic nuclear collisions by Fourier expansion of Azimuthal particle distributions," *Z. Phys. C* **70** (1996) 665–672, hep-ph/9407282.

[81] A. M. Poskanzer and S. Voloshin, "Methods for analyzing anisotropic flow in relativistic nuclear collisions," *Phys. Rev. C* **58** (1998) 1671–1678, nucl-ex/9805001.

[82] A. Badea, A. Baty, P. Chang, G. M. Innocenti, M. Maggi, C. Mcginn, M. Peters, T.-A. Sheng, J. Thaler, and Y.-J. Lee, "Measurements of two-particle correlations in e^+e^- collisions at 91 GeV with ALEPH archived data," *Phys. Rev. Lett.* **123** (2019), no. 21 212002, 1906.00489.

[83] **Belle** Collaboration, A. Abdesselam *et. al.*, "Measurement of two-particle correlations in hadronic e^+e^- collisions at Belle," 8, 2020. 2008.04187.

[84] **PHOBOS** Collaboration, B. Alver *et. al.*, "System size, energy, pseudorapidity, and centrality dependence of elliptic flow," *Phys. Rev. Lett.* **98** (2007) 242302, nucl-ex/0610037.

[85] **ALICE** Collaboration, S. Acharya *et. al.*, "Centrality and pseudorapidity dependence of the charged-particle multiplicity density in XeXe collisions at $\sqrt{s_{\rm NN}}$ =5.44TeV," *Phys. Lett. B* **790** (2019) 35–48, 1805.04432.

[86] **ALICE** Collaboration, J. Adam *et. al.*, "Anisotropic flow of charged particles in Pb-Pb collisions at $\sqrt{s_{\rm NN}} = 5.02$ TeV," *Phys. Rev. Lett.* **116** (2016), no. 13 132302, 1602.01119.

[87] J. Noronha-Hostler, L. Yan, F. G. Gardim, and J.-Y. Ollitrault, "Linear and cubic response to the initial eccentricity in heavy-ion collisions," *Phys. Rev. C* **93** (2016), no. 1 014909, 1511.03896.

[88] D.-X. Wei, X.-G. Huang, and L. Yan, "Hydrodynamic response in simulations within a multiphase transport model," *Phys. Rev. C* **98** (2018), no. 4 044908, 1807.06299.

[89] H. Niemi, G. Denicol, H. Holopainen, and P. Huovinen, "Event-by-event distributions of azimuthal asymmetries in ultrarelativistic heavy-ion collisions," *Phys. Rev. C* **87** (2013), no. 5 054901, 1212.1008.

[90] A. Bilandzic, R. Snellings, and S. Voloshin, "Flow analysis with cumulants: Direct calculations," *Phys. Rev. C* **83** (2011) 044913, 1010.0233.

[91] A. Bilandzic, C. H. Christensen, K. Gulbrandsen, A. Hansen, and Y. Zhou, "Generic framework for anisotropic flow analyses with multiparticle azimuthal correlations," *Phys. Rev. C* **89** (2014), no. 6 064904, 1312.3572.

[92] C. Bierlich *et. al.*, "Confronting experimental data with heavy-ion models: RIVET for heavy ions," *Eur. Phys. J. C* **80** (2020), no. 5 485, 2001.10737.

[93] T. Sjöstrand and M. van Zijl, "A Multiple Interaction Model for the Event Structure in Hadron Collisions," *Phys. Rev.* **D36** (1987) 2019.

[94] T. Sjöstrand and P. Z. Skands, "Multiple interactions and the structure of beam remnants," *JHEP* **03** (2004) 053, hep-ph/0402078.

[95] R. Corke and T. Sjöstrand, "Interleaved Parton Showers and Tuning Prospects," *JHEP* **03** (2011) 032, 1011.1759.

[96] **ATLAS** Collaboration, G. Aad *et. al.*, "Charged-particle distributions in $\sqrt{s}$ = 13 TeV pp interactions measured with the ATLAS detector at the LHC," *Phys. Lett. B* **758** (2016) 67–88, 1602.01633.

[97] C. Bierlich *et. al.*, "Robust Independent Validation of Experiment and Theory: Rivet version 3," *SciPost Phys.* **8** (2020) 026, 1912.05451.

[98] **ALICE** Collaboration, S. Acharya *et. al.*, "Investigations of Anisotropic Flow Using Multiparticle Azimuthal Correlations in pp, p-Pb, Xe-Xe, and Pb-Pb Collisions at the LHC," *Phys. Rev. Lett.* **123** (2019), no. 14 142301, 1903.01790.

[99] **CMS** Collaboration, V. Khachatryan *et. al.*, "Evidence for collectivity in pp collisions at the LHC," *Phys. Lett. B* **765** (2017) 193–220, 1606.06198.

[100] A. Ortiz Velasquez, P. Christiansen, E. Cuautle Flores, I. Maldonado Cervantes, and G. Paić, "Color Reconnection and Flowlike Patterns in *pp* Collisions," *Phys. Rev. Lett.* **111** (2013), no. 4 042001, 1303.6326.

[101] C. Bierlich and J. R. Christiansen, "Effects of color reconnection on hadron flavor observables," *Phys. Rev.* **D92** (2015), no. 9 094010, 1507.02091.

[102] C. Bierlich, "Microscopic collectivity: The ridge and strangeness enhancement from string-string interactions," *Nucl. Phys. A* **982** (2019) 499–502, 1807.05271.

[103] J. L. Albacete, H. Petersen, and A. Soto-Ontoso, "Symmetric cumulants as a probe of the proton substructure at LHC energies," *Phys. Lett.* **B778** (2018) 128–136, 1707.05592.

[104] N. Borghini, P. M. Dinh, and J.-Y. Ollitrault, "Flow analysis from multiparticle azimuthal correlations," *Phys. Rev.* **C64** (2001) 054901, nucl-th/0105040.

[105] W. Zhao, Y. Zhou, H. Xu, W. Deng, and H. Song, "Hydrodynamic collectivity in proton-proton collisions at 13 TeV," *Phys. Lett. B* **780** (2018) 495–500, 1801.00271.

[106] J. Adolfsson *et. al.*, "QCD challenges from pp to A–A collisions," *Eur. Phys. J. A* **56** (2020), no. 11 288, 2003.10997.

[107] W. Zhao, Y. Zhou, K. Murase, and H. Song, "Searching for small droplets of hydrodynamic fluid in proton–proton collisions at the LHC," *Eur. Phys. J. C* **80** (2020), no. 9 846, 2001.06742.

[108] **ALICE** Collaboration, J. Adam *et. al.*, "Centrality dependence of the pseudorapidity density distribution for charged particles in Pb-Pb collisions at $\sqrt{s_{\mathrm{NN}}} = 5.02$ TeV," *Phys. Lett. B* **772** (2017) 567–577, 1612.08966.

Paper II

II

Jet modifications from colour rope formation in dense systems of non-parallel strings

Christian Bierlich, Smita Chakraborty, Gösta Gustafson, and Leif Lönnblad

To be published in *SciPost Physics*
e-Print: 2202.12783 [hep-ph]
MCnet-22–02, LU-TP-22–09

Abstract

We revisit our rope model for string fragmentation that has been shown to give a reasonable description of strangeness and baryon enhancement in high-multiplicity pp events at the LHC. A key feature of the model is that the enhancement is driven by the increased string tension due to strings overlapping in dense systems. By introducing an improved space–time picture for the overlap between fragmenting strings, where also non-parallel strings are properly taken into account, we are now able to investigate the enhancement both in jets and in the underlying event in a consistent way.

1 Introduction

One of the most characteristic features of Quark–Gluon Plasma (QGP) formation in heavy ion (AA) collisions, is that of so–called "jet quenching" [1]. In heavy ion collisions, jet quenching is mainly seen in energy loss or dispersion effects, manifest as, for example, suppression of high $p_\perp$ particle yields, with respect to scaled proton–proton (pp) case [2] or the suppression of away-side jets in central collisions [3]. With the higher energies available at LHC, the phenomenon has also been explored using Z bosons plus jets, where the Z decaying to leptons is used as an unaffected probe, to gauge the effect on the jet traversing the QGP [4].

Several experimental signatures for QGP production have, however, also been observed in high multiplicity pp collisions, including strangeness enhancement [5] and long-range multi-particle correlations [6], more commonly known as "collective flow". Jet quenching effects have so far not been observed in small systems (pp or proton–ion, pA), which begs the question if jet modification phenomena are completely absent in small systems, or if the correct way to look for it has just not been established [7]. One obvious reason for the difficulty, is that it is not possible, like in AA collisions, to look at differences when comparing to similar measurements for pp collisions. Comparisons with theoretical expectations are also difficult, as the expected effects from quenching in small systems are very small, and the signal is strongly affected by (uncertain) effects from initial state radiation. It should also be mentioned that most theoretical descriptions of jet quenching assumes that the jet is formed in a deconfined "bath" of free partons (*i.e.* the QGP), which may not be appropriate in small systems, where at most a few droplets would form. This includes approaches such as QGP-modified splitting kernels [8] at high virtualities, coupled with shower modifications by transport theory [9, 10] at lower ones, but also approaches like the one offered by JEWEL [11], where partonic rescattering off medium partons are combined with the Landau–Pomeranchuk–Migdal effect [12].

It should be noted that there are other mechanisms that may influence jet production. In particular, some generators include "colour reconnections", especially in combination with multi-parton interactions (see, *e.g.*, [13, 14]), but it has been shown (*e.g.*, in [15] and [16]), that colour reconnections may influence jet shapes even in e^+e^- annihilations. In addition it has been shown that the baryonic colour reconnection model in HERWIG [17] can give rise to strangeness enhancement in dense environments in pp collisions.

In a series of papers we have demonstrated, that collective flow and enhancement of strangeness and baryons, can be reproduced in high multiplicity pp events as a result of string-string interaction, when the infinitely thin string is generalized

to a confining colour fluxtube, similar to a vortex line in a superconductor [18]. As discussed in ref. [19], models of string interactions offers a novel and convenient framework for studying jet modifications in small systems, as they are implemented in the general purpose Monte Carlo event generator PYTHIA, which allows the user to generate realistic collision events, with the effects switched "on" or "off". The study of jet modification effects does therefore not need to rely on a (non-existing) reference system.

The aim of this paper is therefore to look at possible effects of jet modification via increased strangeness and baryon numbers in jets. A very important tool is here the method developed in ref. [20], to account for the interaction between strings which are not parallel to each other. This was not possible in earlier versions of string-string interaction, but is naturally very important for handling the interaction between string pieces connected to a jet and strings in the underlying event.

The remainder of this paper is organised as follows. In section 2, we recap the Lund string hadronization framework, taking into account the transverse extension of strings, and discuss how the string tension increase when such strings overlap, leading to strangeness and baryon enhancement. Then we present the parallel frame and our updated rope model in section 3. In section 4 we investigate how the average string tension varies as a function of multiplicity and transverse momentum, and then investigate the observable modifications the updated rope model predicts for jets and the underlying event in pp collisions at the LHC, before we present our conclusions in section 5.

2 String hadronization and colour fluxtubes

In this section we will briefly introduce relevant parts of the Lund string hadronization model, building up to the rope hadronization model used for the model results. For more detailed reviews on Lund strings, we refer the reader to the large body of existing literature. The original papers deal mainly with hadronization of a single straight string [21, 22]. Gluons were introduced as 'kinks' on a string in refs. [23, 24]. Somewhat dated reviews are presented in refs. [25, 26], and a number of recent papers on Lund strings present the model in a more modern context [27, 28, 20, 29], including our original paper on rope hadronization [30].

The Lund string is a "massless relativistic string" (or a "Nambu-Goto string"). Such a string has no transverse extension, and it also has no longitudinal momen-

tum, which implies that it is boost invariant. [1] This may be a good approximation for a linear colour fluxtube, where the width is not important. In section 2.2 we will discuss going beyond this approximation.

2.1 Lund string hadronization

Hadronization of a straight string

We first look at a single, straight string stretched between a quark and an anti-quark. The string can break via $q\bar{q}$ pair creation, in a process which can be regarded as a tunneling process as discussed in ref. [32]. For a single quark species the production probability is given by

$$\frac{\mathrm{d}\mathcal{P}}{\mathrm{d}^2 p_\perp} \propto \kappa \exp\left(-\frac{\pi \mu_\perp^2}{\kappa}\right). \tag{1}$$

Here $\mu_\perp^2 = \mu^2 + p_\perp^2$ is the *quark* squared transverse mass. The exponential conveniently factorizes, leaving separate expressions for selection of mass and $p_\perp$ to be used in the Monte Carlo event generator. With $\kappa \approx 1$ GeV/fm, this result implies that strange quarks are suppressed by roughly a factor 0.3 relative to a u- or a d-quark (and that the probability to produce a c-quark with this mechanism is $\sim 10^{-11}$). It also means that the quarks are produced with an average $p_\perp \sim 250$ MeV, independent of its flavour.

When the quarks and antiquarks from neighbouring breakups combine to mesons, their momenta can be calculated as an iterative process. The hadrons are here "peeled off" one at a time, each taking a fraction (z) of the *remaining* light-cone momentum ($p^\pm = E \pm p_z$) along the positive or negative light-cone respectively. The probability for a given z-value is here given by

$$f(z) \propto \frac{(1-z)^a}{z} \exp(-b m_\perp^2 / z). \tag{2}$$

Here $m_\perp$ is the transverse mass of the *meson*, and the two parameters a and b are to be determined by tuning to data from $\mathrm{e^+e^-}$ collisions. In principle the a–parameter could depend on the quark species, but in default PYTHIA (the Monash tune) it is the same for strange and non-strange quarks. Baryon–antibaryon pairs can be produced via production of a diquark–antidiquark pair, and in this case the a-parameter has to be modified. The parameter b must, however, be universal.

An important consequence of eq. (2) is the probability distribution in proper time (τ) for string breakup vertices. Expressed in terms of the quantity $\Gamma = (\kappa\tau)^2$, the distribution is given by:

[1] For the kinematics of such a string see ref. [31].

$$\mathcal{P}(\Gamma)\mathrm{d}\Gamma \propto \Gamma^a \exp(-b\Gamma)\mathrm{d}\Gamma. \quad (3)$$

The breakup-time is an important ingredient for string interactions, as the hadronization time sets an upper limit on the available time for strings to push each other and form ropes. As such, hadronization of a system of interacting strings will *not* happen when the system has reached equilibrium, but will be cut off when the string hadronizes. For strings hadronizing early, one can then imagine a mixed phase of strings and hadrons, before the transition to a pure hadron cascade. In this paper we consider only the effect of string interactions, and leave the interplay with the hadronic cascade for a future paper. We note, however, that a full hadronic cascade has recently been implemented in PYTHIA [33, 34], revealing only minor effects in proton collisions. Typical values for a, b and κ give an average breakup time of around 1.5 fm. This can not be identified as the hadronization time (or freeze-out time). This could equally well be interpreted as the time when the quark and the antiquark meet for the first time. In addition the breakup times fluctuate, and each string will hadronize at different times.

Gluons and non-straight strings

An essential component in the Lund hadronization model is that a gluon is treated as a point-like "kink" on the string, carrying energy and momentum. A gluon carries both colour and anti-colour, and the string can be stretched from a quark, via a set of colour-ordered gluons, to an anti-quark (or alternatively in a closed loop of colour-ordered gluons).

When a gluon has lost its energy, the momentum-carrying kink is split in two corners, moving with the speed of light but carrying no momentum, stretching a new straight string piece between them. When two such corners meet, they can "bounce off"; the string connecting them then disappears, but a new one is "born". In a pp collision a typical string will contain several gluons, connected by string pieces which are stretched out, may disappear and then be replaced by new string pieces. All these string pieces move transversely in different directions, but at any time the string consists of a set of straight pieces. For a description of how such a string hadronizes, we refer to refs. [35, 20]. The interaction between strings with several non-parallel pieces is discussed in section 3.

2.2 Strings as colour fluxtubes

The description of a confining colour field by an infinitely thin string is necessarily an approximation, relevant only when the result is insensitive to the width. In high multiplicity events this is no longer the case, and the strings have to be treated as colour fluxtubes, with a non-zero width. We here first discuss the properties of a single fluxtube, and then the interaction between two or more parallel fluxtubes. The generalization to non-parallel fluxtubes is presented in section 3.

2.2.1 A single fluxtube

The simplest model for a QCD fluxtube is the MIT bag model [36]. Here a homogenous longitudinal colour-electric field is kept inside a tube by the pressure from the vacuum condensate. An improved description is obtained in lattice calculations. A common method is here to use the method of Abelian projections, proposed by 't Hooft [37], which is based on partial gauge fixing. The result of these calculations show that the field is dominated by a longitudinal colour-electric field, surrounded by a transverse colour-magnetic current in the confining vacuum condensate [38, 39]. This picture is very similar to the confinement of the magnetic field in a vortex line in a superconductor (with electric and magnetic fields interchanged, see *e.g.* ref. [40]).

As observed in ref. [20] the measured shape of the colour electric field obtained in ref. [41] is well approximated by a Gaussian distribution:

$$E(\rho) = E_0 \exp\left(-\rho^2/2R^2\right), \tag{4}$$

where ρ is the transverse distance in cylinder coordinates. The width of a fluxtube is difficult to estimate in lattice calculations, as it is naturally given in lattice units, see *e.g.* ref. [42]. In the bag model, the width is roughly given by $\sqrt{\langle\rho^2\rangle} \approx 1$ fm (where ρ is the radial coordinate), while lattice calculations give radii of ~ 0.5 fm or even less [43, 44, 38].

The field density in eq. (4) is related to the string tension through

$$\int d^2\rho E^2(\rho)/2 = \pi E_0^2 R^2 = g\kappa, \tag{5}$$

where g is the fraction of the total energy of the string associated with the colour electric field. We expect g to be of the order 1/2, which is the value obtained in the bag model, where the energy in the field and the expelled condensate are of equal size. For a further discussion of the vacuum condensate and colour fluxtubes we refer to ref. [45] and references therein.

2.2.2 Interacting parallel fluxtubes

High multiplicity collisions will give a high density of fluxtubes, with a corresponding high energy density. In ref. [20] we discussed the collective effects expected from the initial expansion, and in this paper we will concentrate on the effects of rope hadronization, and in particular study the production of strange hadrons. Here we first restate our treatment of interaction between parallel fluxtubes, presented in ref. [30]. How this can be generalized to a general situation with non-parallel fluxtubes will be discussed in section 3 below.

Rope formation

For two overlapping parallel fluxtubes, separated by a transverse distance δ, we get from eq. (4) the interaction energy of the field

$$\begin{aligned} &\int d^2\rho(\mathbf{E}_1(\rho)+\mathbf{E}_2(\rho))^2/2 - 2\int d^2\rho E^2(\rho)/2 \\ &\quad = \int d^2\rho \mathbf{E}_1(\rho)\cdot\mathbf{E}_2(\rho) = 2\pi E_0^2 R^2 e^{-\delta^2/4R^2}. \end{aligned} \tag{6}$$

Such a system will expand transversely, and if it does not hadronize before, it will reach equilibrium, where the energy density corresponds to the free energy density in the vacuum condensate.

The expression in eq. (6) does not include the surface energy for the combined flux tube. In the bag model this is zero, and in equilibrium the transverse area will be doubled, and the interaction energy will be zero. For a vortex line in a dual QCD superconductor, it depends on the properties of the superconductor, but also here the interaction energy will be much reduced at the time of hadronization. It will then be necessary to go beyond the Abelian approximation. For two fluxtubes stretched by quarks, the two quarks can either form a colour sextet or an anti-triplet, and with more fluxtubes also higher multiplets are possible. Here lattice calculations show that a set of overlapping strings form a "rope", with a tension proportional to the second Casimir operator for the colour multiplet at the end of the rope [46].

Biro, Nielsen, and Knoll pointed out [47] that if a rope is formed by a number of strings with random charges, they add up as a random walk in colour space. This implies that the net colour grows as the square root of the number of strings. A rope stretched by m colour charges and n anti-charges can then form a colour multiplet characterised by two numbers p and q, such that an arbitrary state, by a

rotation in colour space, can be transformed into a state with p coherent colours (*e.g.* red) and q coherent anti-colours (*e.g.* anti-blue), such that the colour and the anti-colour do not form a colour singlet. Such a multiplet is denoted $\{p, q\}$, and we always have $p \leq m$ and $q \leq n$.

For any such multiplet we can write down the number of states, *i.e.* the multiplicity[2] of the multiplet:

$$N = \frac{1}{2}(p+1)(q+1)(p+q+2). \tag{7}$$

As mentioned above, the total tension of such a rope is proportional to the second Casimir operator for the multiplet, which gives

$$\kappa^{\{p,q\}} = \frac{C_2(p,q)}{C_2(1,0)}\kappa^{\{1,0\}} = \frac{1}{4}\left(p^2 + pq + q^2 + 3p + 3q\right)\kappa^{\{1,0\}}, \tag{8}$$

where $\kappa^{\{1,0\}} \equiv \kappa$ is the tension in a single string.

In the PYTHIA treatment used here, there are, however, other effects also addressing string coherence effects. Importantly, parts of this colour summation is in an approximate way treated by "colour reconnection". As a simple example we can look at two anti-parallel strings with triplet–anti-triplet pairs in each end. These can either form an octet or a singlet, with probabilities 8/9 and 1/9 respectively. Here the octet (denoted $\{1, 1\}$) gives

$$\kappa^{\{1,1\}} = \kappa \cdot C_2^{\{1,1\}}/C_2^{\{1,0\}} = 9\kappa/4. \tag{9}$$

The singlet ($\{0, 0\}$), with no string at all, gives $\kappa^{\{0,0\}} = 0$.

The colour reconnection process in a situation with several strings can be related to an expansion in powers of $1/N_c$, as discussed in refs. [48, 49].

For the special case of $N_c = 3$ there is also a different kind of reconnection. For a rope formed by two parallel strings, the two triplets in one end can give either a sextet or an anti-triplet (and a corresponding anti-sextet or triplet in the other end) with probabilities 2/3 and 1/3 respectively. For the latter we simply have just a single string.

The two original colour triplets are connected in a "junction", and such a reconnection can be particularly important for baryon production. This possibility is

[2]The multiplicity provides the standard nomenclature for multiplets, where $N = 1$ is called "singlet", $N = 3$ is called "triplet", $N = 6$ is called "sextet" etc. We will here, when necessary, use the slightly more verbose notation $\{p, q\}$, which allows one to distinguish between *e.g.* a triplet and an anti-triplet.

not implemented in the present version of our Monte Carlo, but will be included in future work. We note that for an arbitrary number of colours, the corresponding situation is only obtained when $N_c - 1$ colour charges combine to one anti-colour charge. The junction formation with three strings does therefore, for $N_c \neq 3$, correspond to a configuration where N_c strings are connected, which cannot be directly interpreted as a $1/N_c$ correction.

We will in the following adopt a picture where the process of string (rope) fragmentation follows after a process of colour reconnections, and that this will leave the system in a state with p parallel and q anti-parallel strings forming a coherent multiplet $\{p, q\}$.

Rope hadronization

A rope specified by the multiplet $\{p, q\}$, can break via a succession of single $q\bar{q}$ productions, through the tunnelling mechanism in eq. (1). In each step a multiplet $\{p, q\}$ is changed to either $\{p-1, q\}$ or $\{p, q-1\}$. It is here important to note that *the tunneling is not determined by the total tension in the rope, but by the energy released, determined by the reduction in the tension* caused by the production of the new $q\bar{q}$ pair. Hence, we get from eq. (8) an effective string tension, when the field goes from $\{p+1, q\}$ to $\{p, q\}$, given by

$$\kappa_{\text{eff}} = \kappa^{\{p+1,q\}} - \kappa^{\{p,q\}} = \frac{2p + q + 4}{4}\kappa. \tag{10}$$

The consequence of this picture is that we can treat the rope fragmentation as the sequential decay of the individual strings forming the rope, much in the same way as an everyday rope would break thread by thread. Technically it means that we can use the normal string fragmentation procedure in PYTHIA8, with the modification that we in each break-up change the fragmentation parameters according to the effective string tension calculated from the overlap of neighbouring strings. The changes to these parameter explained in detail in ref. [30], and are for reference also listed in appendix A. The changes are somewhat convoluted, since most of the parameters only indirectly depend on the string tension, but the main effect easily seen in eq. (1), namely that an increased string tension will increase the probability of strange quarks and diquarks relative to light quarks in the string breakup.

3 Rope hadronization with non-parallel strings

Our previous work on rope formation [30] relied on the assumption that strings in high energy hadron collisions can be assumed to be approximately parallel to each other and to the beam axes. This prevented a detailed investigation of possible effects in hard jets, especially those traversing the dense environment of an AA collision. In our recent work on the shoving model [20] we found a remedy where the interaction between any pair of strings can be studied in a special Lorentz frame, even if they are not parallel to each other or to the beam. We call it "the parallel frame", and it can be shown that any pair of straight string pieces can be transformed into such a frame, where they will always lie in parallel planes.

Below we will use this parallel frame to calculate the increased string tension in the rope formation of arbitrarily complex string configurations.

3.1 The parallel frame formalism

In the previous rope implementation [30], the way to determine if any two string pieces are overlapping was to boost them to their common centre-of-mass frame and here measure the distance between them at a given space-time point of break-up. This was done in a fairly crude way, not really taking into account that the two string pieces typically cannot be considered to be parallel in this frame. In general there is no frame where two arbitrary string pieces can be considered to be exactly parallel, but in the *parallel frame* introduced in ref. [20] it can be shown that any two string pieces will always be stretched out in parallel planes in a symmetric way. This works for all pairs of string pieces, even if one piece is in a high transverse momentum jet and the other is in the underlying event.

In figure 1 we show a space–time picture of two string pieces stretched between two pairs of partons in this parallel frame. Since massless partons are propagating at the speed of light irrespective of the magnitude of their momenta, only the angles between them are important for the following. In the parallel frame the two string pieces have the same opening angle θ, and the partons of one piece propagate with an angle $\theta/2$ w.r.t. the z-axis. The partons of the other propagate in the opposite direction, with an angle $\pi - \theta/2$. At any given time, both string pieces will lie in planes parallel to the xy-plane and to each other. Looking at the projections of the string pieces on the xy-plane, we denote the angle between them by ϕ, and the frame is chosen such that all partons form an angle $\phi/2$ with the x-axis.

To simplify the calculations we write the momenta of the partons using their transverse momentum, $p_\perp$, and pseudo-rapidity difference, η, with respect to the z-axis, rather than the energy and opening polar angle (where $p_z = e\cos\frac{\theta}{2} =$

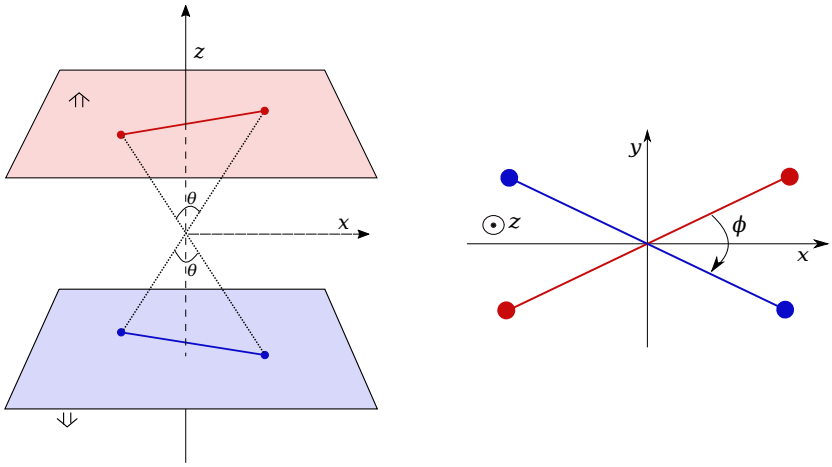

Figure 1: The parallel frame showing the parallel planes of two strings and the opening angle θ and skewness angle ϕ.

$p_\perp \sinh\frac{\eta}{2}$), and get, using the notation $p = (e; p_x, p_y, p_z)$,

$$\begin{aligned}
p_1 &= p_{\perp 1}\left(\cosh\frac{\eta}{2};\quad \cos\frac{\phi}{2},\quad \sin\frac{\phi}{2},\quad \sinh\frac{\eta}{2}\right),\\
p_2 &= p_{\perp 2}\left(\cosh\frac{\eta}{2};-\cos\frac{\phi}{2},-\sin\frac{\phi}{2},\quad \sinh\frac{\eta}{2}\right),\\
p_3 &= p_{\perp 3}\left(\cosh\frac{\eta}{2};\quad \cos\frac{\phi}{2},-\sin\frac{\phi}{2},-\sinh\frac{\eta}{2}\right),\\
p_4 &= p_{\perp 4}\left(\cosh\frac{\eta}{2};-\cos\frac{\phi}{2},\quad \sin\frac{\phi}{2},-\sinh\frac{\eta}{2}\right).
\end{aligned} \tag{11}$$

Clearly we have six degrees of freedom, and we can construct six independent squared invariant masses, $s_{ij} = (p_i + p_j)^2$. This means that for any set of four *massless* partons we can (as long as no two momenta are completely parallel) solve for $p_{\perp i}$, which will give us:

$$\begin{aligned}
p_{\perp 1}^2 &= \frac{s_{12}}{4}\sqrt{\frac{s_{13}s_{14}}{s_{23}s_{24}}},\quad p_{\perp 2}^2 = \frac{s_{12}}{4}\sqrt{\frac{s_{23}s_{24}}{s_{13}s_{14}}},\\
p_{\perp 3}^2 &= \frac{s_{34}}{4}\sqrt{\frac{s_{13}s_{23}}{s_{14}s_{24}}},\quad p_{\perp 4}^2 = \frac{s_{34}}{4}\sqrt{\frac{s_{14}s_{24}}{s_{13}s_{23}}},
\end{aligned} \tag{12}$$

and furthermore solve for the angles ϕ and η:

$$\cosh\eta = \frac{s_{14}}{4p_{\perp 1}p_{\perp 4}} + \frac{s_{13}}{4p_{\perp 1}p_{\perp 3}} \quad \text{and} \quad \cos\phi = \frac{s_{14}}{4p_{\perp 1}p_{\perp 4}} - \frac{s_{13}}{4p_{\perp 1}p_{\perp 3}}. \tag{13}$$

To further specify the frame we renumber the particles so that $\phi < \pi/2$ to have the strings more parallel to the x-axis and not to the y-axis, and we define the x-axis to be their combined *rope* axis. The result is that for a breakup at a given space–time point in one string piece, we can in the parallel frame have a reasonable handle on the overlap with any other string piece.

3.2 Overlap in the parallel frame

In eq. (6) we wrote down the interaction energy of two completely parallel strings separated by a small distance. We now want to use this to estimate the effective overlap of two strings that are not completely parallel, but lie in parallel planes.

At a specific point along the x-axis in the parallel frame we denote the separation between the strings in the yz-plane by (δ_y, δ_z) and integrate the interaction of the field given the skewness angle ϕ to obtain

$$\begin{aligned}
\mathcal{I}(\delta_y, \delta_z, \phi) &= \int d^2\rho \mathbf{E}_1(\rho)\cdot\mathbf{E}_2(\rho) \\
&= E_0^2\cos\phi \int dy\, dz \exp\left(-\frac{y^2\cos\frac{\phi}{2} + z^2}{2R^2}\right)\exp\left(-\frac{(y-\delta_y)^2\cos\frac{\phi}{2} + (z-\delta_z)^2}{2R^2}\right) \\
&= 2\pi E_0^2 R^2 \frac{\cos\phi}{\cos\frac{\phi}{2}}\exp\left(-\frac{\delta_y^2\cos\frac{\phi}{2} + \delta_z^2}{4R^2}\right).
\end{aligned} \tag{14}$$

Here we note that the skewness angle enters both in the scalar product and in the strength of the field along the y-axis, and that the overlap vanishes for orthogonal strings.

We can now define the relative overlap as $\mathcal{I}(\delta_y, \delta_z, \phi)/\mathcal{I}(0,0,0)$ and use it as a probability (assuming that $\mathbf{E}_1\cdot\mathbf{E}_2 > 0$) that a breakup in one string is affected by an increased string tension due to the overlap with the other. This would then correspond to a $\{2,0\} \to \{1,0\}$ transition giving an effective string tension $\kappa_{\text{eff}} = 3\kappa/2$ in eq. (10). If the strings instead points in the opposite directions along the x-axis ($\mathbf{E}_1\cdot\mathbf{E}_2 < 0$) this would correspond to a $\{1,1\} \to \{0,1\}$ breakup with $\kappa_{\text{eff}} = 5\kappa/4$.

In this way we can for each breakup in one string piece, take all other string pieces in an event, and for each go to the parallel frame to determine if it will

contribute to p or q. In our implementation described below, we sum the relative overlaps in p and q respectively and round them off to integers, rather than treating them as individual probabilities for each pair of string pieces, which on average gives the same result.

It should be pointed out that in the parallel frame we also have a handle on which string breaks up first. If we assume that the string breaks at a common average proper time along the string, τ_H, we can in the parallel frame calculate the proper time of the other string in space–time point where we calculate the overlap. If the latter is at larger τ_H, we conclude that the other string has already broken up, and can no longer contribute to an increased string tension in the break-up being considered.

3.3 Monte Carlo implementation

The main technical problem with implementing the rope model in PYTHIA8, is the order in which the string fragmentation proceeds. First, the flavour and transverse momentum of the break-up is chosen (eq. (1)) together with the type of the chopped-off hadron. Only then is the momentum fraction, z, chosen according to eq. (2), and only then do we know exactly where the string breaks and can calculate the κ_{eff} in that point. But we need to know κ_{eff} to be able to calculate a break-up, so we have a kind of *Catch-22* situation.

The way we solve this is to perform a trial break-up to pre-sample the overlap of a given string, and use the overlap there to get an approximate κ_{eff}. Then we discard the sample break-up and produce a new one using this κ_{eff}. On the average we will then get a reasonable estimate of the overlap around a break-up. For a general break-up in the underlying event this should be good enough, but if we are interested in details of the hadron production in, *e.g.*, the tip of a jet, this procedure may be inappropriate (see further discussion below in section 4.3).

The procedure to calculate κ_{eff} looks as follows:

1. Produce a trial break-up in the string being fragmented, and deduce from which string piece it comes.
2. Pair this piece with every other string piece in the event, make a Lorentz transformation to the parallel frame of each pair.
3. Using the pseudo-rapidity of the produced hadron in each such frame, and assuming the break-up occurred at the proper time, τ_H, find the space-time point of the break-up of the first string piece.

4. In the corresponding yz-plane determine the proper time of the other string piece and if that is less than τ_H, calculate the overlap according to eq. (14), and determine if this overlap should contribute to p or q in the breakup.
5. With the summed p and q (rounded off to integer values), we now calculate κ_{eff} according to eq. (10).
6. Throw away the trial break-up with its produced hadron and change the PYTHIA8 fragmentation parameters according to the obtained κ_{eff} and generate the final break-up.

As mentioned in section 2.1, some care has to be taken when it comes to soft gluons. Normally, all string pieces can be said to be *dipoles* between colour-connected partons, and in any parallel frame this string piece is parallel to the xy-plane. But a soft gluon may have lost all its momentum before the string breaks, and the break-up can then occur in a piece of the string that is not parallel to the string pieces of the connected dipoles. To include this possibility we introduce *secondary* dipoles, so that if we have two dipoles connected to a soft gluon, *e.g.* $q_i - g_j$ and $g_j - \bar{q}_k$, then a secondary string will be included spanned between the momenta of q_i and $\bar{q}_k$, but using the space-time point where the gluon has lost all its momentum to the connected string pieces, as a point of origin.

The problem with soft gluons is present also for our shoving model in [20], and the solution with secondary dipoles is now also used there. This will be described in more detail in a future publication, where we also describe the procedure for including these *higher order* dipoles in cases where we have several consecutive soft gluons along a string.

3.4 Interplay with the Shoving model

Clearly our rope model is very tightly connected with our shoving model. They both rely on the parallel frame and technically they both use the same infrastructure for looking at overlaps between string pieces. However, here there is again a kind of *Catch-22*.

Physically the shoving precedes the hadronization, and pushes the strings apart before they hadronize. As this affects the value of κ_{eff}, the shoving should be executed first. However, for technical reasons the pushes are applied directly to the produced hadrons rather than to the individual string pieces. Therefore we must calculate the hadronization before we can execute the pushes.

We are currently working on a solution to this problem, and plan to present it in a future publication. The main effect of the shoving is expected to be a dilution of the strings resulting in a lowered κ_{eff}. As discussed in [20] the precise value

of the string radius is not known, and in that paper we simply used a canonical value of 1 fm. Also the string radius will affect the values of κ_{eff}, and preliminary studies show that the effects of string dilution from shoving are of the same order as moderate decrease of the string radius of around 10%.

4 Results in pp collisions

In this section, features of the rope hadronization model with the parallel frame-formalism are investigated in pp collisions. Since the main feature of this new formalism is the much improved handling of string pieces which are not parallel to the beam axis (*i.e.* jets), we will mostly concentrate on observables in events containing a process with high momentum transfer, but in section 4.1 we first show the behaviour in minimum bias collisions. Here the most fundamental check of the dependence of κ_{eff} with final state multiplicity, but more relevant for the parallel frame formalism, is the dependence of κ_{eff} on particle $p_\perp$. In section 4.2 we compare to existing experimental results in the underlying event (UE) for Z-triggered events. This is to ensure that the existing description of such observables is not altered by our model. Finally in section 4.3, we present predictions for the jet observables that are affected by rope formation in pp.

4.1 Model behaviour

In this section, we explore the variation of the effective string tension κ_{eff} with rope hadronization, for minimum bias pp events. The κ_{eff} is shown for primary hadrons, *i.e.* the effective string tension used to form a given hadron, produced directly in the hadronization process. Results are shown for two collision energies, $\sqrt{s} = 7$ and 13 TeV, and two values of string radius, $R = 0.5$ and 1 fm.

In figure 2, the dependence of $\langle \kappa_{\text{eff}}/\kappa \rangle$ with respect to $N_{\text{ch.}}$ in $|\eta| < 0.5$ is shown on the left, and $p_{\perp,\text{prim.}}$ on the right. On the right, only events with $\mathrm{d}N_{\text{ch.}}/\mathrm{d}\eta > 10$ are shown, to focus on events with several parton interactions. (At 13 TeV this corresponds to keeping roughly the 30% of events with the highest multiplicity [50].)

On the left plot of figure 2, it is seen that $\langle \kappa_{\text{eff}}/\kappa \rangle$ rises with around 30% for $R = 1$ fm and 10% for $R = 0.5$ fm, almost irrespective of $\sqrt{s}$, with the rise at 13 TeV being only slightly higher. The two main points to take away from this figure, is a) that $\mathrm{d}N_{\text{ch.}}/\mathrm{d}\eta$ is a good proxy for string density irrespective of collision energy, and thus works as a good scaling variable, and b) that any result will be very sensitive to the choice of R.

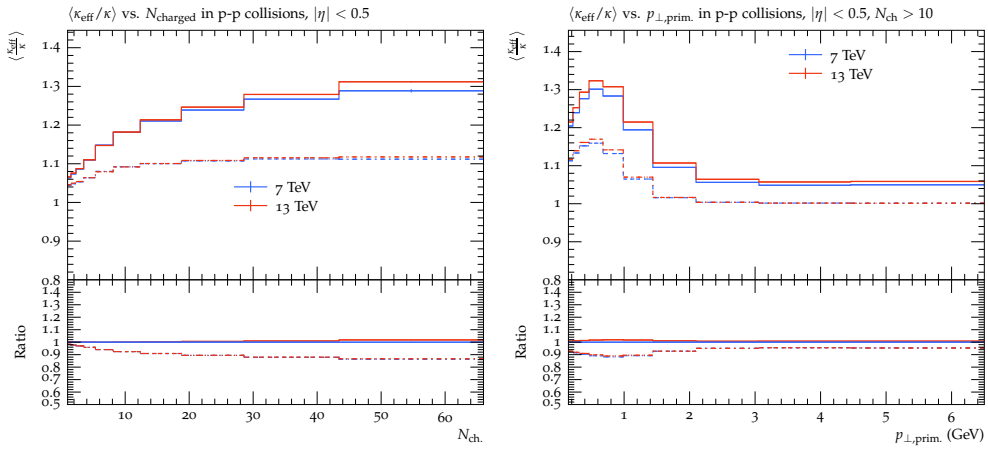

Figure 2: $\langle \kappa_{\text{eff}}/\kappa \rangle$ vs. $N_{\text{ch.}}$ (left) and vs. $p_{\perp,\text{prim.}}$ for $N_{\text{ch.}} > 10$ (right). Solid lines have string radius $R = 1$ fm and dot-dashed lines have $R = 0.5$ fm. Blue and red lines are for minimum-bias event at 7 and 13 TeV respectively.

On the right plot of figure 2, we observe that the increase in κ_{eff} is larger for primary hadrons in the lower $p_\perp$ bins for both values of R. This means that the lower $p_\perp$ primary hadrons are formed from regions with high density of strings with more overlaps with adjacent strings. However, the higher $p_\perp$ partons correspond to "mini-jet" situations and are more separated in space-time from the bulk of strings. Such strings have less overlaps resulting in a lower κ_{eff}. Hence the high $p_\perp$ primary hadrons formed from such string break-ups show this effect.

In the lowest $p_\perp$ bins of $\langle \kappa_{\text{eff}}/\kappa \rangle$ vs $p_{\perp,\text{prim.}}$ plot, it is seen that κ_{eff} drops to lower values. This behaviour arises from the fact that low $p_\perp$ particles are biased towards low κ_{eff} values due to the $p_\perp$-dependence on κ in the tunneling probability in eq. (1).

Overall we observe that rope hadronization significantly increases the string tension at high-multiplicities and for low $p_\perp$ final-state particles. For higher $p_\perp$ the effect is smaller, but does not disappear completely.

4.2 Underlying event observables in reconstructed Z events

Before moving on to study rope effects on jets, it is important to assess whether rope formation drastically changes existing observables, currently well described by the existing model. In events with a Z-boson present, the most likely place for such a change to occur, is in the UE. To this end, we use a standard UE analyses implemented in the Rivet program [53].

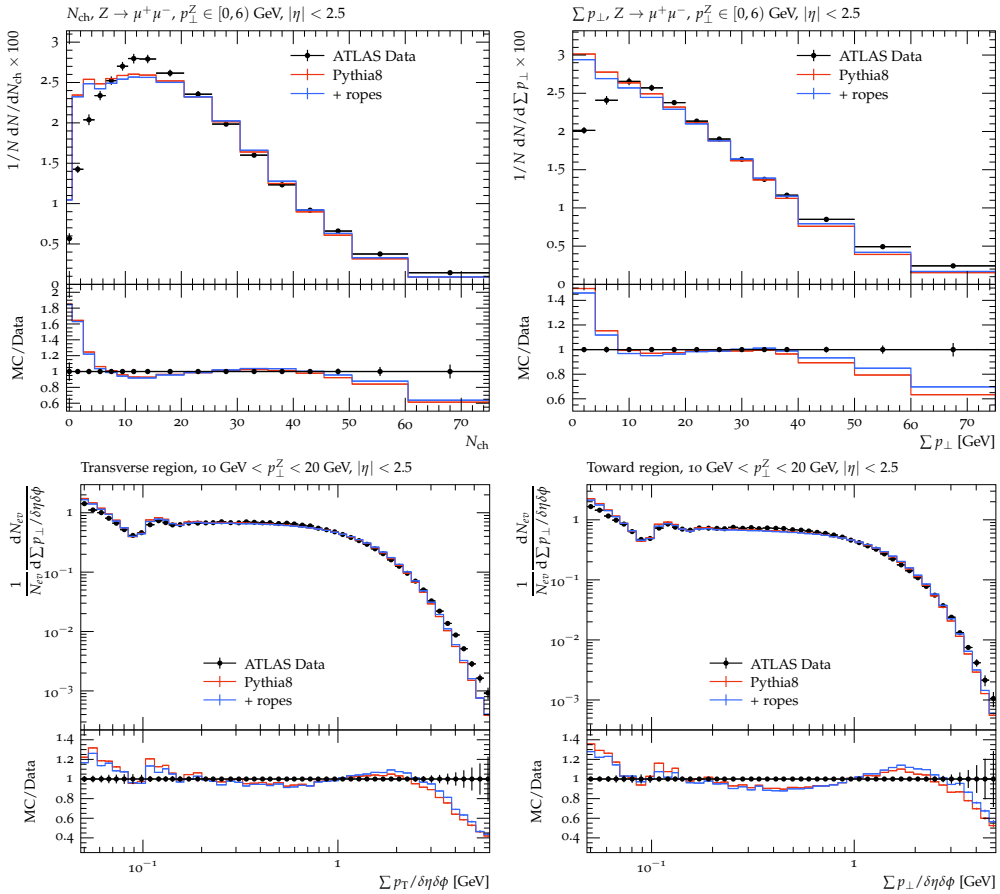

Figure 3: Associated particle production in Z$\to \ell^-\ell^+$ events at $\sqrt{s} = 7$ TeV compared to the default PYTHIA tune and with rope hadronization. **Top row:** Distribution of charged particle multiplicity, N_{ch}, (top left) and summed scalar transverse momenta, $\Sigma p_\perp$ (top right) measured for events with $p_\perp^Z$ range 0-6 GeV[51]. **Bottom row:** $\Sigma p_\perp$ distributions in different azimuthal regions, in events with $p_\perp^Z$ range 10-20 GeV [52]. Left: *transverse* region, $\pi/3 < |\Delta\phi_Z| < 2\pi/3$, right: *towards* region $|\Delta\phi_Z| < \pi/3$.

In figure 3, $N_{\text{ch.}}$ and $\Sigma p_\perp$ for Z$\to \ell^-\ell^+$ events in pp collisions at 7 TeV are compared to ATLAS data[51, 52]. The Z-boson is reconstructed from the electron or muon channel with invariant mass $66 < m_{\ell^-\ell^+} < 166$ GeV in $|\eta| < 2.5$.

The charged particle multiplicity and summed scalar $p_\perp$ distributions for Z$\to \mu^-\mu^+$ channel with $0 < p_\perp^Z < 6$ GeV, are shown in top row of figure 3. It is seen that adding rope hadronization, overall preserves the distributions as produced by

default PYTHIA8. We note that rope hadronization has a slight effect of pushing particles from lower to higher $\Sigma p_\perp$ regions, which follows from the $p_\perp$-dependence of the tunnelling probability in eq. (1).

The particle $p_\perp$ in the away region (opposite azimuthal region to that of the Z boson), balances the $p_\perp^Z$. Hence the towards and transverse regions with respect to the Z boson are much less affected by a recoiling jet and therefore have cleaner UE activity.[3] These regions are sensitive to the hadronization mechanism, rope hadronization effects will be apparent here. So we look at the UE-sensitive observables such as scalar summed $p_\perp/\delta\eta\delta\phi$ distributions for charged particles in events with $p_\perp^Z$ in the range 10-20 GeV in the bottom row of figure 3. These plots show the $\Sigma p_\perp$ distributions in the transverse ($\pi/3 < |\Delta\phi_Z| < 2\pi/3$) and towards ($|\Delta\phi_Z| < \pi/3$) regions[52]. We see that the rope hadronization curve follows the default PYTHIA8 curve, again preserving the overall physics behaviour of PYTHIA8, except for a slight shift in $\Sigma p_\perp$, as in the top right plot.

We conclude that UE measurements are equally well described with rope hadronization as without, and it is therefore not necessary to re-tune fragmentation parameters before proceeding to give predictions for jet observables.

4.3 Strangeness yields in Z+jet events

To investigate experimentally observable consequences of our rope model in terms of the yield of different hadron species inside jets, we have chosen to study its effects in Z+jets events at LHC energies. It has been shown in, *e.g.*, ref. [54], that such events are very useful for separating regions of phase space dominated by the UE from the regions dominated by jets. By selecting events where the Z boson is well balanced by a hard jet in the opposite azimuthal region, we can study the UE in a cone around the Z, where there should be very little activity related to the jet, and thus we can get a good estimate of the UE activity on an event-by-event basis. In this way we can get a reliable way of correcting jet observables for UE effects, not only for the transverse momentum of the jet but also for the flavour content.

4.3.1 Overall jet features

To observe the modification in the flavour production in the jet, we want to look at the yield ratios of different hadron species. Hence we have written a Rivet analysis where we first locate a reconstructed Z boson for $m_{\mu^-\mu^+}$ in the range 80-100 GeV and $|\eta| < 2.5$ and search for the hardest associated jet in the opposite azimuthal

[3] It should here be noted that the charged particle activity in events with a hard interaction such as Z-production is generally higher than in minimum bias events.

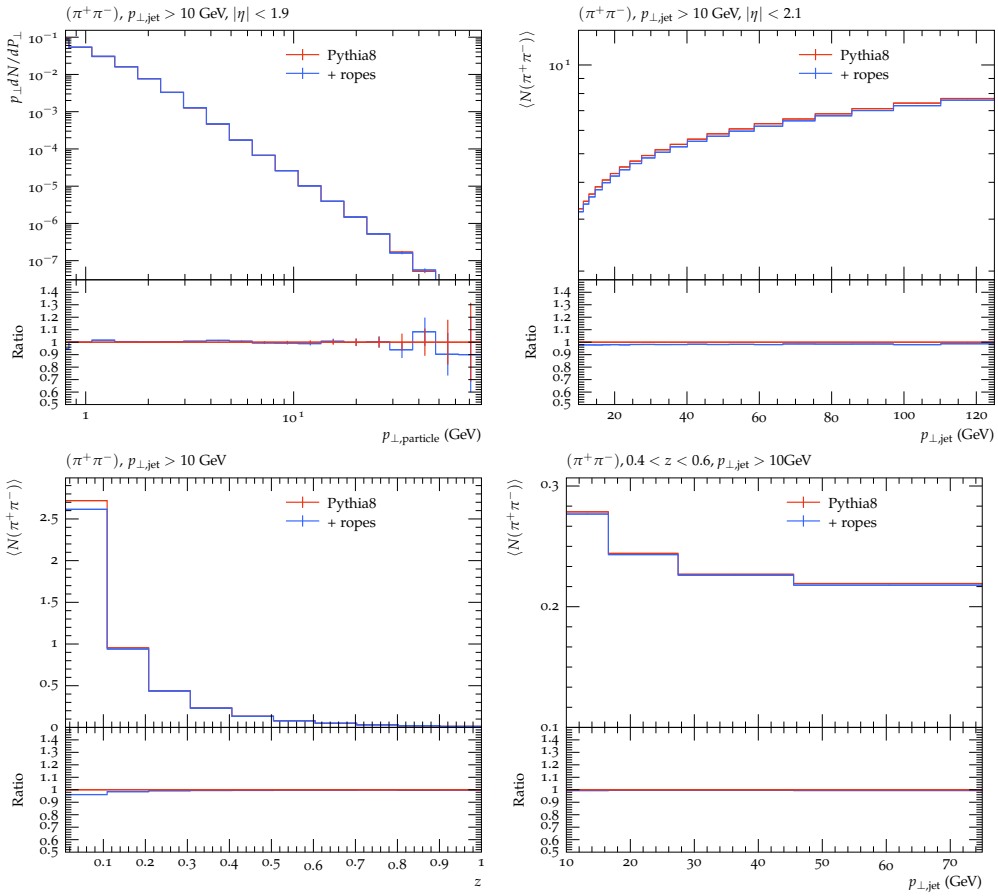

Figure 4: Pion yields in Z+jet events in 13 TeV pp collisions vs. $p_{\perp,\text{particle}}$ in the UE (top left), vs. $p_{\perp,\text{jet}}$ in the jet cone (top right), as a function of $z = p_{\perp,\text{particle}}/p_{\perp,\text{jet}}$ (bottom left), and vs. $p_{\perp,\text{jet}}$ for $0.4 < z < 0.6$ (bottom right).

hemisphere. We further restrict the Z boson by requiring it to be within $|\eta| < 1.9$ and $p_\perp^Z > 8$ GeV using the standard Z-finding projection in Rivet. Once we find such a Z boson in the event, we search for the associated hardest (charged particle) jet using the anti-k$_T$ [55] algorithm with a radius $R_j = 0.4$ in $|\eta| < 2.1$ with the azimuthal separation $\Delta\phi_{\text{jet},Z} \geq 2\pi/3$.

To subtract UE contributions from the jet $p_\perp$, we calculate a characteristic $\Sigma p_{\perp,\text{UE}}$, by summing up the $p_\perp$ of the charged final state particles (not including muons from the Z decay) that lie within a cone of radius $\sqrt{2}R_j$ around the Z boson. Therefore, for a given event, the yields of the particles is calculated twice: once within the jet cone, then within a cone of radius $\sqrt{2}R_j$ with respect to the

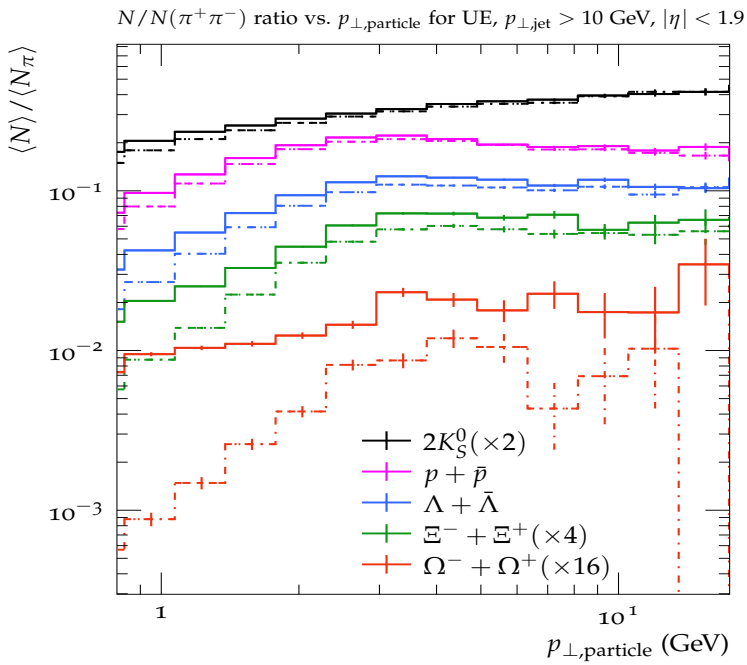

Figure 5: Yield ratio of different strange hadron species and protons to pions in the UE cone vs. $p_{\perp,\text{particle}}$, scaled by factors to show them clearly. Solid lines are with rope hadronization and dot-dashed lines are for default PYTHIA8.

Z boson. The latter serves as our underlying event reference and we subtract half of this yield from the yield inside the jet cone to get the final yield of the hadrons in that event associated with the jet. Denoting the initial jet-$p_\perp$ as $p_{\perp,\text{pseudojet}}$, the corrected $p_{\perp,\text{jet}}$ becomes:

$$p_{\perp,\text{jet}} = p_{\perp,\text{pseudojet}} - 0.5 \times \Sigma p_{\perp,\text{UE}} \tag{15}$$

and the corresponding yields:

$$\text{yield}_{\text{jet}} = \text{yield}_{\text{pseudojet}} - 0.5 \times \text{yield}_{\text{UE}} \tag{16}$$

This method of UE subtraction can easily be extended to pA and AA collisions to give a comparable result among the three systems. Similar methods have previously been used in heavy ion collisions [56]. We do this analysis for pp collisions at $\sqrt{s} = 13$ TeV with $p_{\perp,\text{jet}} \geq 10$ GeV for string radius $R = 1$ fm.

To examine the model performance in reproducing general features of the jets, such as particle multiplicity as a function of their transverse momentum and of the

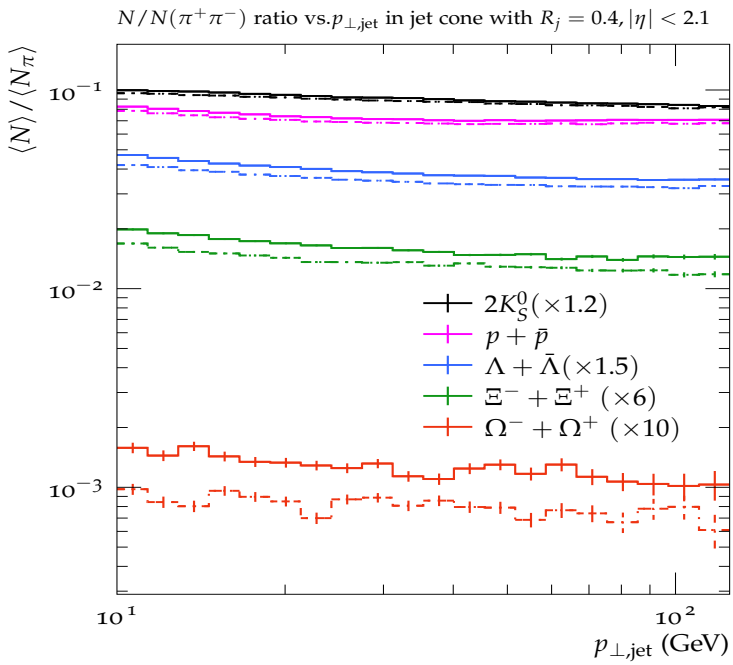

Figure 6: Yield ratio of different strange hadrons and protons to pions in the jet cone, for $R_j = 0.4$ vs. $p_{\perp,\text{jet}}$, scaled by factors to show them clearly. Solid lines are with rope hadronization and dot-dashed lines are for default PYTHIA8.

transverse momentum of the jets, we look at the pions. Our rope model is known to have very small effects on the overall multiplicity [30], and we know that pions in general are dominating the particle production, even though we expect a slight drop in pions, since high κ_{eff} will favour strange hadrons and baryons over pions. In figure 4 we show the pion yield as a function of particle $p_\perp$ in the UE cone, and the UE-subtracted yield as a function of $p_{\perp,\text{jet}}$ in the jet cone in figure 4. We also show the pion yield with respect to $z = p_{\perp,\text{particle}}/p_{\perp,\text{jet}}$ and in the mid-z region as a function of $p_{\perp,\text{jet}}$. Indeed we find that the rope effects are very small for pion production, both in the UE and in the jet, with the possible exception of the lowest bin in the z distribution. We will revisit the bottom row plots in connection with strangeness yields in the jet cone in section 4.3.2.

In the UE region, the density of strings is high resulting in a higher number of overlaps among them. As a result, we would expect large effects due to rope hadronization in the UE. In order to observe this effect, we look at the yield ratio of the strange hadrons to pions in the UE cone. In figure 5, we show the yield ratio to pions for strange mesons (K^0_S) and baryons (Λ, Ξ and Ω) and protons

with respect to $p_{\perp,\text{particle}}$. Yields of Ξ and Ω baryons have been scaled by a multiplicative factor to show them in comparison to the other species. As expected, the different yields are higher with rope hadronization turned on as compared to default PYTHIA8. The highest enhancement for each species is observed for the lowest $p_{\perp,\text{particle}}$ ranges which subsequently decreases for higher particle $p_\perp$ (which follows figure 2 in section 4.1). Therefore, this plot show us that with rope hadronization, we get increased yields of baryons and strangeness. This plot also shows us the UE contribution to strangeness yields to that of within the jet.

Turning to flavour production *inside* the jet cone in figure 6, we show the UE-subtracted yield ratio to pions for the same set of hadron species as before, now with respect to $p_{\perp,\text{jet}}$. As rope hadronization will increase both strangeness and baryon production, the largest enhancement is expected for multistrange baryons. For K^0_S, only a slight increase is observed, while the increase for protons is higher. The Λ yield due to rope hadronization is even higher due to combined baryon and strangeness enhancement. The yield of Ξ is $\sim$ 20% higher due to rope hadronization, than default PYTHIA8 and the Ω yield with rope hadronization is more than 50% higher. This shows that both baryon and strangeness yields are enhanced by rope hadronization. We note that the increase in the yield ratio due to rope hadronization is rather constant over all $p_{\perp,\text{jet}}$. Hence if we look at the enhancement as a function of the transverse momentum ratio of the particle species to that of the jet, that would help us identify the $p_\perp$ ranges where rope effects are higher.

4.3.2 Jet substructure observables

Now we take a closer look at the particle to pion yield ratios as a function of z and $p_{\perp,\text{jet}}$. Studies have been performed where the ratio of $p_\perp$ of the individual sub-jets to that of the leading jet serves as a distinguishing observable for jet modification[57]. Since we want to look at the strange flavour yields in the jet cone, we take a simpler approach. We only plot the yield ratios in bins of z, which is the ratio of the particle $p_\perp$ to the jet $p_\perp$.

In figure 7, we show the yield ratio of strange hadrons to pions *vs.* z. We observe that the particle yields are increased at low (close to the UE) to intermediate z values. Furthermore, this enhancement is smaller for K^0_S and larger for the strange baryon Λ, and for multistrange baryons Ξ and Ω as expected. However, strangeness and baryon enhancement drops at higher z. This highlights the behaviour that rope hadronization effects decrease with higher $p_\perp$, as we noted in figure 2 in section 4.1.

We note that, even though the parallel frame formalism allows the calculation of κ_{eff} in events with jets, the current implementation is lacking in the region $z \approx 1$,

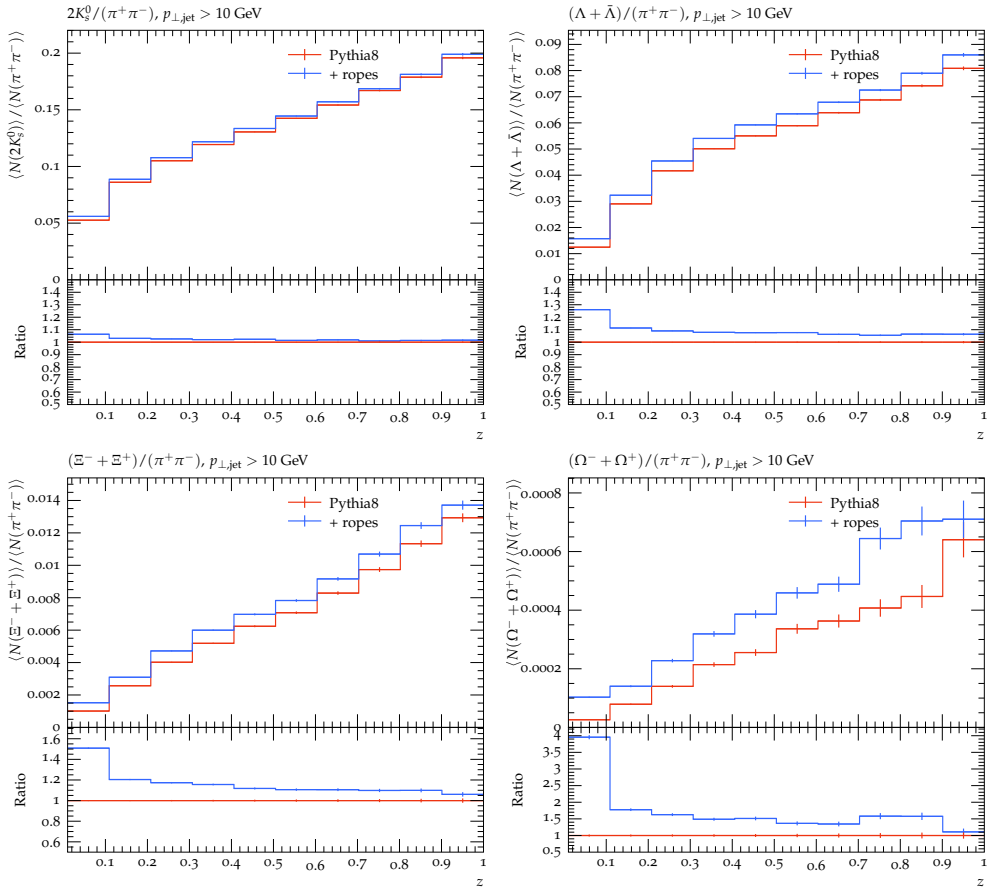

Figure 7: Yield ratios as a function of $z = p_{\perp,\text{particle}}/p_{\perp,\text{jet}}$ for pp collisions at $\sqrt{s}$=13 TeV: $2K^0_S/(\pi^+\pi^-)$ (top left) $(\Lambda+\bar{\Lambda})/(\pi^+\pi^-)$ (top right), $(\Omega^- + \Omega^+)/(\pi^+\pi^-)$ and $(\Xi^- + \Xi^+)/(\pi^+\pi^-)$ (bottom left).

as already mentioned in section 3.3. The previously mentioned *Catch-22* situation, is purely related to the implementation, and can be further understood by considering the shape of the Lund symmetric fragmentation function in eq. (2), which is vanishing near $z = 1$. For a particle with z close to one, the pre-sampled overlap is therefore likely to have been calculated with a too-small z, which in turn means that it is calculated for the wrong part of the string. In pp collisions this effect is small but non-negligible, which we have confirmed by an *a posteriori* check (as the correct overlaps can be calculated after the fact, but too late to be used in event generation). Another issue, which would be present even in a perfect implementation, and therefore potentially more severe, is the absence of interactions

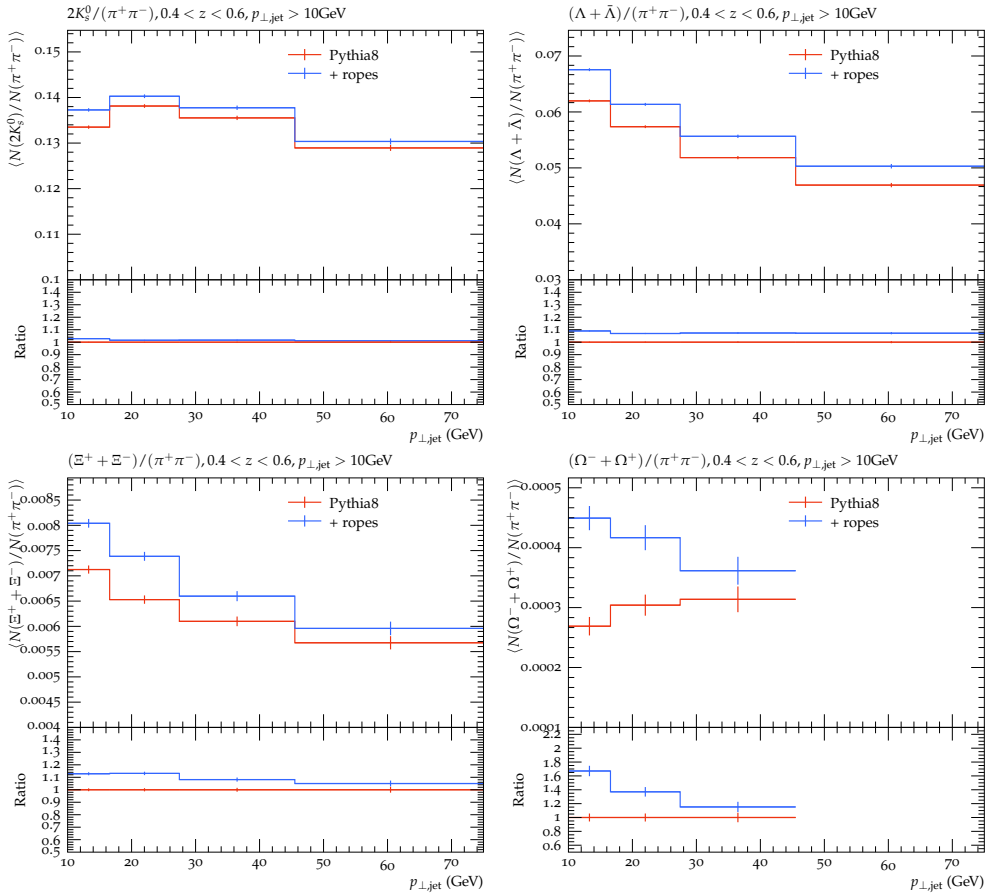

Figure 8: Yield ratios of particles with $0.4 < z < 0.6$, as a function of $p_{\perp,\text{jet}}$ for pp collisions at $\sqrt{s}$=13 TeV: $2K^0_s/(\pi^+\pi^-)$ (top left), $(\Lambda+\bar{\Lambda})/(\pi^+\pi^-)$ (top right), $(\Xi^- + \Xi^+)/(\pi^+\pi^-)$ (bottom left) and $(\Omega^- + \Omega^+)/(\pi^+\pi^-)$ (bottom right).

between hadrons formed early in time, and their surrounding environment. For most of the produced particles, and in particular in pp, this effect should also be small. But in the case of high z, the particle is always produced early, and the effect could be larger. We plan to develop the model further in this direction, but in the meantime we will in the following show results for particles at intermediate z values ($0.4 < z < 0.6$) where the effects arising from both these issues, should be negligible.

To test the modification in flavour yields at mid-z values, we look at particle yields as a function of $p_{\perp,\text{jet}}$. Since these particles are neither close to the tip of the jet, nor to the UE, it is more reasonable to the trial-hadron sampling of κ_{eff}

in these regions. Moreover, as the jet $p_\perp$ increases, the particles get further and further away from the UE. In figure 8, we show the yield ratio of strange hadrons to pions in the $0.4 < z < 0.6$ region vs. $p_{\perp,\text{jet}}$. We observe that the yields from the rope hadronization case are distinct compared to default PYTHIA8. The individual strange hadron yield to pion yield ratio increases as we go from the K^0_s meson to the Λ baryon (top row plots). For multistrange baryons, Ξ and Ω^- (bottom row plots), rope effects are amplified due to higher number of strange quarks, resulting in a 20% - 50% increase in their yields in low $p_{\perp,\text{jet}}$ ranges. However, as mentioned before, we would expect the enhancement in the yields to drop at higher $p_{\perp,\text{jet}}$ bins. This effect is rather small for Λ but prominent for Ξ and Ω. Ω (bottom right plot) is only shown up to 45 GeV due to statistics.

5 Conclusion

We have here presented a study on how an effect from a dense system of colour fluxtubes might be observed as strangeness enhancement in jets in high multiplicity pp events. In such events it is essential to properly estimate the interaction between non-parallel strings, including strings connected to a hard scattered parton and strings in the underlying event. This problem was solved in ref. [20], where the interaction of all string pairs can be calculated in a Lorentz frame, where two string pieces lie symmetrically in two parallel planes. We here show results for jet-triggered high-multiplicity pp collisions. The generalization to pA and AA collisions (using the Angantyr model [58]) will be presented in a future publication.

The interacting strings can form "colour ropes", which hadronize in a stepwise manner by $q\bar{q}$ pair creation. The increased energy in the rope gives a higher "effective string tension", κ_{eff}, which increases the number of strange quarks and diquarks in the breakups. In section 4.1 we found that this results in an increase of κ_{eff} with multiplicity in pp events at LHC energies. It is interesting to note that the increase for a given multiplicity is almost independent of the collision energy.

As expected we also found that the increase is quite dependent on the transverse momentum, since high-$p_\perp$ particles are typically produced in jets where the strings are not parallel with the bulk of the strings in the underlying event, thus reducing the effective overlap with these. The important question is then if the rope model, despite being reduced in jets, anyway will result in a modification of the hadron composition of jets.

To study the effects on jets we focused our investigation on Z+jet events, with the Z decaying to lepton pairs. As pointed out in *e.g.* ref. [54], it is possible, in such events, to get a relatively clean separation between the jets and the particle produc-

tion in the underlying event. In particular the hadrons produced in a cone around the direction of the Z particle should have very little to do with the recoiling jet, and can therefore be used to correct any observable in the jet cone for underlying-event contributions on an event-by-event basis.

The modified κ_{eff} also affects the fragmentation parameters. In section 4.2 results for multiplicity and the transverse momentum distribution in the underlying event in pp Z+jet events, were compared with results from default PYTHIA8 and with data from ATLAS. After confirming that the rope hadronization gives negligible effects on these general features of the underlying event, we feel comfortable that we can study strangeness and baryon enhancement in the jets in a way, which is not biased by the underlying-event corrections.

In section 4.3 our main results for strangeness and baryon number enhancement in jets were presented, with the underlying event subtracted. We note that the effect is most important for strange baryons, and growing with the number of strange quarks. Thus it is largest for Ω baryons, and from the plots showing the Ω/π ratio as a function of the jet transverse momentum, we note that rope effects are very small for large jet $p_\perp$ as expected, but quite noticeable for low jet $p_\perp$.

From this we conclude that it may indeed be possible to find jet modifications due to collective effects, in our rope model, in small collision systems. The size of the effect is, however, a bit uncertain. In part this is due the uncertainty in the transverse size of the string, and our canonical choice of $R = 1$ fm may be a bit large. Although it should be possible to tune this parameter to fit the overall strangeness and baryon enhancement, it is then also important to also take into account the effects of repulsion between the strings. Both of these effects will be addressed in future publications.

Looking ahead, it is also interesting to investigate the effects of colour reconnection, in particular models that include junction formations, which will also influence the baryon production. In the end we hope to develop a picture where most collective effects can be interpreted as interactions among strings, not only in pp collisions but also in pA and AA.

Acknowledgements

This work was funded in part by the Knut and Alice Wallenberg foundation, contract number 2017.0036, Swedish Research Council, contracts number 2016-03291, 2016-05996 and 2017-0034, in part by the European Research Council (ERC) under the European Union's Horizon 2020 research and innovation programme, grant agreement No 668679, and in part by the MCnetITN3 H2020 Marie Curie Initial Training Network, contract 722104.

A Dependence of fragmentation parameters on κ_{eff}

There are several hadronization parameters in PYTHIA8, and even if they are in principle independent, several of them has an implicit dependence on the string tension. In our implementation of the rope hadronization, we take the parameters as tuned to e^+e^- data, where we expect no rope effects, and for each breakup in the string fragmentation we rescale the parameters according to the estimated change in string tension at that point, due to the presence of overlapping string fields. The parameters under consideration is the same as in our previous implementation [30], and the dependence of the string tension is also the same. For completeness we list them here, but for further details we refer to [30].

In the following we will denote the change in string tension by h, according to $\kappa \mapsto \kappa_{\text{eff}} = h\kappa$. The following parameters is affected:

- ρ (`StringFlav:probStoUD`[4]): the suppression of s quark production relative to u or d type production. This parameter has a simple scaling

$$\rho \mapsto \tilde{\rho} = \rho^{1/h}. \tag{17}$$

- x (`StringFlav:probSQtoQQ`): the suppression of diquarks with strange quark content relative to diquarks without strange quarks (in addition to the factor ρ for each extra s-quark) also scales like

$$x \mapsto \tilde{x} = x^{1/h}. \tag{18}$$

- y (`StringFlav:probQQ1toQQ0`): the suppression of spin 1 diquarks relative to spin 0 diquarks (not counting a factor three due to the number of spin states of spin 1 diquarks) again scales like

$$y \mapsto \tilde{y} = y^{1/h}. \tag{19}$$

- σ (`StringPT:sigma`): the width of the transverse momentum distribution in string break-ups. This is directly proportional to $\sqrt{\kappa}$, giving

$$\sigma \mapsto \tilde{\sigma} = \sigma\sqrt{h}. \tag{20}$$

- ξ (`StringFlav:probQQtoQ`): the global probability of having a diquark break-up relative to a simple quark break-up. This has a somewhat more

[4] This is the parameter name in PYTHIA8.

complicated κ dependence and also has uncertainties related to the so-called popcorn model as described in [30]. We decompose it as three different parameters, $\xi = \alpha\beta\gamma$ with different κ-dependence, where β is related to the probability to have a $q\bar{q}$ fluctuation in general in the popcorn model which is independent of κ and is treated as an independent parameter, while γ is related to the masses and scales as

$$\gamma \mapsto \tilde{\gamma} = \gamma^{1/h}, \tag{21}$$

and α is related to the different di-quark states with an indirect dependence on ρ, x, and y

$$\alpha \mapsto \tilde{\alpha} = \frac{1 + 2\tilde{x}\tilde{\rho} + 9\tilde{y} + 6\tilde{x}\tilde{\rho}y + 3\tilde{y}\tilde{x}^2\tilde{\rho}^2}{2 + \tilde{\rho}}. \tag{22}$$

Taken together we get the following dependence:

$$\xi = \alpha\beta\gamma \mapsto \tilde{\xi} = \tilde{\alpha}\beta\left(\frac{\xi}{\alpha\beta}\right)^{1/h}. \tag{23}$$

- b (`StringZ:bLund`): the parameter in the symmetric fragmentation function eq. (2) scales with the ρ-parameter as follows

$$b \mapsto \tilde{b} = \frac{2 + \tilde{\rho}}{2 + \rho}\, b. \tag{24}$$

- a (`StringZ:aLund`): the other parameter in eq. (2) has an indirect dependence on b through the normalisation of the splitting function, $f(z)$. Keeping the normalisation unchanged does not give a simple analytic form for the scaling of $a \mapsto \tilde{a}$, and instead we use a numeric integration procedure.

References

[1] **PHENIX** Collaboration, K. Adcox *et. al.*, "Formation of dense partonic matter in relativistic nucleus-nucleus collisions at RHIC: Experimental evaluation by the PHENIX collaboration," *Nucl. Phys. A* **757** (2005) 184–283, nucl-ex/0410003.

[2] **STAR** Collaboration, J. Adams *et. al.*, "Evidence from d + Au measurements for final state suppression of high p(T) hadrons in Au+Au collisions at RHIC," *Phys. Rev. Lett.* **91** (2003) 072304, nucl-ex/0306024.

[3] **STAR** Collaboration, C. Adler *et. al.*, "Disappearance of back-to-back high p_T hadron correlations in central Au+Au collisions at $\sqrt{s_{NN}}$ = 200-GeV," *Phys. Rev. Lett.* **90** (2003) 082302, nucl-ex/0210033.

[4] **CMS** Collaboration, A. M. Sirunyan *et. al.*, "Study of Jet Quenching with Z + jet Correlations in Pb-Pb and pp Collisions at $\sqrt{s}_{NN} = 5.02$TeV," *Phys. Rev. Lett.* **119** (2017), no. 8 082301, 1702.01060.

[5] **ALICE** Collaboration, J. Adam *et. al.*, "Enhanced production of multi-strange hadrons in high-multiplicity proton-proton collisions," *Nature Phys.* **13** (2017) 535–539, 1606.07424.

[6] **CMS** Collaboration, V. Khachatryan *et. al.*, "Evidence for collectivity in pp collisions at the LHC," *Phys. Lett. B* **765** (2017) 193–220, 1606.06198.

[7] J. Adolfsson *et. al.*, "QCD challenges from pp to A–A collisions," *Eur. Phys. J. A* **56** (2020), no. 11 288, 2003.10997.

[8] A. Majumder, "The In-medium scale evolution in jet modification," 0901.4516.

[9] B. Schenke, C. Gale, and S. Jeon, "MARTINI: An Event generator for relativistic heavy-ion collisions," *Phys. Rev. C* **80** (2009) 054913, 0909.2037.

[10] Y. He, T. Luo, X.-N. Wang, and Y. Zhu, "Linear Boltzmann Transport for Jet Propagation in the Quark-Gluon Plasma: Elastic Processes and Medium Recoil," *Phys. Rev. C* **91** (2015) 054908, 1503.03313. [Erratum: Phys.Rev.C 97, 019902 (2018)].

[11] K. C. Zapp, "JEWEL 2.0.0: directions for use," *Eur. Phys. J. C* **74** (2014), no. 2 2762, 1311.0048.

[12] K. C. Zapp, F. Krauss, and U. A. Wiedemann, "A perturbative framework for jet quenching," *JHEP* **03** (2013) 080, 1212.1599.

[13] T. Sjöstrand and M. van Zijl, "A Multiple Interaction Model for the Event Structure in Hadron Collisions," *Phys. Rev. D* **36** (1987) 2019.

[14] S. Gieseke, C. Rohr, and A. Siodmok, "Colour reconnections in Herwig++," *Eur. Phys. J. C* **72** (2012) 2225, 1206.0041.

[15] P. Gras, S. Höche, D. Kar, A. Larkoski, L. Lönnblad, S. Plätzer, A. Siódmok, P. Skands, G. Soyez, and J. Thaler, "Systematics of quark/gluon tagging," *JHEP* **07** (2017) 091, 1704.03878.

[16] G. S. Chahal and F. Krauss, "Cluster Hadronisation in Sherpa," 2203.11385.

[17] S. Gieseke, P. Kirchgaeßer, and S. Plätzer, "Baryon production from cluster hadronisation," *Eur. Phys. J. C* **78** (2018), no. 2 99, 1710.10906.

[18] M. Baker, J. S. Ball, and F. Zachariasen, "Dual QCD: A Review," *Phys. Rept.* **209** (1991) 73–127.

[19] C. Bierlich, "Soft modifications to jet fragmentation in high energy proton–proton collisions," *Phys. Lett. B* **795** (2019) 194–199, 1901.07447.

[20] C. Bierlich, S. Chakraborty, G. Gustafson, and L. Lönnblad, "Setting the string shoving picture in a new frame," *JHEP* **03** (2021) 270, 2010.07595.

[21] B. Andersson, G. Gustafson, and C. Peterson, "A Semiclassical Model for Quark Jet Fragmentation," *Z. Phys. C* **1** (1979) 105.

[22] Andersson, B. and Gustafson, G. and Söderberg, B., "A General Model for Jet Fragmentation," *Z. Phys. C* **20** (1983) 317.

[23] B. Andersson and G. Gustafson, "Semiclassical Models for Gluon Jets and Leptoproduction Based on the Massless Relativistic String," *Z. Phys. C* **3** (1980) 223.

[24] B. Andersson, G. Gustafson, and T. Sjöstrand, "A Three-Dimensional Model for Quark and Gluon Jets," *Z. Phys. C* **6** (1980) 235.

[25] B. Andersson, G. Gustafson, G. Ingelman, and T. Sjöstrand, "Parton Fragmentation and String Dynamics," *Phys. Rept.* **97** (1983) 31–145.

[26] B. Andersson, *The Lund model*, vol. 7. Cambridge University Press, 7, 2005.

[27] S. Ferreres-Solé and T. Sjöstrand, "The space–time structure of hadronization in the Lund model," *Eur. Phys. J. C* **78** (2018), no. 11 983, 1808.04619.

[28] C. B. Duncan and P. Skands, "Fragmentation of Two Repelling Lund Strings," *SciPost Phys.* **8** (2020) 080, 1912.09639.

[29] C. Bierlich, S. Chakraborty, G. Gustafson, and L. Lönnblad, "Hyperfine splitting effects in string hadronization," 2201.06316.

[30] C. Bierlich, G. Gustafson, L. Lönnblad, and A. Tarasov, "Effects of Overlapping Strings in pp Collisions," *JHEP* **03** (2015) 148, 1412.6259.

[31] X. Artru, "Classical String Phenomenology. 1. How Strings Work," *Phys. Rept.* **97** (1983) 147.

[32] E. Brezin and C. Itzykson, "Pair production in vacuum by an alternating field," *Phys. Rev. D* **2** (1970) 1191–1199.

[33] T. Sjöstrand and M. Utheim, "A Framework for Hadronic Rescattering in pp Collisions," *Eur. Phys. J. C* **80** (2020), no. 10 907, 2005.05658.

[34] C. Bierlich, T. Sjöstrand, and M. Utheim, "Hadronic rescattering in pA and AA collisions," *Eur. Phys. J. A* **57** (2021), no. 7 227, 2103.09665.

[35] T. Sjöstrand, "Jet Fragmentation of Nearby Partons," *Nucl. Phys. B* **248** (1984) 469–502.

[36] K. Johnson, "The M.I.T. Bag Model," *Acta Phys. Polon. B* **6** (1975) 865.

[37] G. 't Hooft, "Topology of the Gauge Condition and New Confinement Phases in Nonabelian Gauge Theories," *Nucl. Phys. B* **190** (1981) 455–478.

[38] S. Nishino, K.-I. Kondo, A. Shibata, T. Sasago, and S. Kato, "Type of dual superconductivity for the $SU(2)$ Yang–Mills theory," *Eur. Phys. J. C* **79** (2019), no. 9 774, 1903.10488.

[39] A. Shibata, K.-I. Kondo, S. Nishino, T. Sasago, and S. Kato, "Type of dual superconductivity for $SU(2)$ and $SU(3)$ Yang–Mills theories," 1903.10487.

[40] K.-I. Kondo, S. Kato, A. Shibata, and T. Shinohara, "Quark confinement: Dual superconductor picture based on a non-Abelian Stokes theorem and reformulations of Yang–Mills theory," *Phys. Rept.* **579** (2015) 1–226, 1409.1599.

[41] P. Cea, L. Cosmai, F. Cuteri, and A. Papa, "Flux tubes at finite temperature," *JHEP* **06** (2016) 033, 1511.01783.

[42] R. Sommer, "Scale setting in lattice QCD," *PoS* **LATTICE2013** (2014) 015, 1401.3270.

[43] P. Cea, L. Cosmai, F. Cuteri, and A. Papa, "Flux tubes in the SU(3) vacuum: London penetration depth and coherence length," *Phys. Rev. D* **89** (2014), no. 9 094505, 1404.1172.

[44] M. Baker, P. Cea, V. Chelnokov, L. Cosmai, F. Cuteri, and A. Papa, "Isolating the confining color field in the SU(3) flux tube," *Eur. Phys. J. C* **79** (2019), no. 6 478, 1810.07133.

[45] C. Bierlich, G. Gustafson, and L. Lönnblad, "Collectivity without plasma in hadronic collisions," *Phys. Lett. B* **779** (2018) 58–63, 1710.09725.

[46] G. S. Bali, "Casimir scaling of SU(3) static potentials," *Phys. Rev. D* **62** (2000) 114503, hep-lat/0006022.

[47] T. S. Biro, H. B. Nielsen, and J. Knoll, "Color Rope Model for Extreme Relativistic Heavy Ion Collisions," *Nucl. Phys. B* **245** (1984) 449–468.

[48] L. Lönnblad, "Reconnecting colored dipoles," *Z. Phys. C* **70** (1996) 107–114.

[49] J. R. Christiansen and P. Z. Skands, "String Formation Beyond Leading Colour," *JHEP* **08** (2015) 003, 1505.01681.

[50] **ALICE** Collaboration, S. Acharya *et. al.*, "Charged-particle production as a function of multiplicity and transverse spherocity in pp collisions at $\sqrt{s} = 5.02$ and 13 TeV," *Eur. Phys. J. C* **79** (2019), no. 10 857, 1905.07208.

[51] **ATLAS** Collaboration, G. Aad *et. al.*, "Measurement of distributions sensitive to the underlying event in inclusive Z-boson production in pp collisions at $\sqrt{s} = 7$ TeV with the ATLAS detector," *Eur. Phys. J. C* **74** (2014), no. 12 3195, 1409.3433.

[52] **ATLAS** Collaboration, G. Aad *et. al.*, "Measurement of event-shape observables in $Z \to \ell^+\ell^-$ events in pp collisions at $\sqrt{s} = 7$ TeV with the ATLAS detector at the LHC," *Eur. Phys. J. C* **76** (2016), no. 7 375, 1602.08980.

[53] C. Bierlich *et. al.*, "Robust Independent Validation of Experiment and Theory: Rivet version 3," *SciPost Phys.* **8** (2020) 026, 1912.05451.

[54] **CMS** Collaboration, S. Chatrchyan *et. al.*, "Measurement of the Underlying Event Activity at the LHC with $\sqrt{s} = 7$ TeV and Comparison with $\sqrt{s} = 0.9$ TeV," *JHEP* **09** (2011) 109, 1107.0330.

[55] M. Cacciari, G. P. Salam, and G. Soyez, "The anti-k_t jet clustering algorithm," *JHEP* **04** (2008) 063, 0802.1189.

[56] R. B. Neufeld and I. Vitev, "The Z^0-tagged jet event asymmetry in heavy-ion collisions at the CERN Large Hadron Collider," *Phys. Rev. Lett.* **108** (2012) 242001, 1202.5556.

[57] L. Apolinário, J. G. Milhano, M. Płoskoń, and X. Zhang, "Novel subjet observables for jet quenching in heavy-ion collisions," *Eur. Phys. J. C* **78** (2018), no. 6 529, 1710.07607.

[58] C. Bierlich, G. Gustafson, L. Lönnblad, and H. Shah, "The Angantyr model for Heavy-Ion Collisions in PYTHIA8," *JHEP* **10** (2018) 134, 1806.10820.

Paper III

III

Strangeness enhancement across collision systems without a plasma

Christian Bierlich, Smita Chakraborty, Gösta Gustafson, and Leif Lönnblad

In review, *Physics Letters B*
e-Print: 2205.11170 [hep-ph]
MCnet-22–11, LU-TP-22–25

Abstract

We present novel *rope* hadronization results for strange hadron enhancement in pp, pPb, and PbPb collisions using PYTHIA/Angantyr at LHC energies. With the rope model for string fragmentation, we find that the strangeness and baryon enhancement has a coherent increase across all collision systems as a function of average charged central multiplicity, in qualitative agreement with LHC data. In AA collisions, we find that the baryonic yields overshoot data at high multiplicities, and we discuss how a combination of rope hadronization with other string interactions may tame this rise.

1 Introduction

Strangeness enhancement in both small and large systems is usually interpreted as a signal of a dense and hot Quark-Gluon Plasma (QGP) [1–3]. However, the Lund strings physically represent colour-electric flux tubes, and in a series of papers [4–7] we have demonstrated that interactions between overlapping flux tubes are able to reproduce not only enhanced rates for strangeness and baryons [4], but also collective flow [6] in pp collisions. The Angantyr model [8], which is a generalization of the Lund string model in PYTHIA to nucleus-nucleus (AA) collisions, is able to successfully reproduce many features of hadron production in these collisions. We note that in this picture the initial energy density and temperature do not have to be very high [6], and that the string degrees of freedom therefore survive the initial, mainly longitudinal expansion, until hadronization sets in. In a dense environment, the overlap among these transversely extended strings naturally causes interactions between overlapping flux tubes.

The string-string interaction can be a repulsive interaction between a pair of overlapping flux tubes, called string shoving [5, 6], giving rise to a transverse collective flow in high-density systems. The interaction can also give the formation of "colour ropes" as discussed in ref. [9]. The increased energy density in a rope implies that more energy is released when a new $q\bar{q}$ pair is produced (or a diquark-antidiquark pair in case of baryon production). This corresponds to a higher effective string tension κ (κ_{eff}) during the hadronization of a rope, which modifies the fragmentation parameters entering the Lund fragmentation function [4, 10, 11]. Quark-antiquark production in a colour-electric field can be regarded as a tunnelling process [12], which gives a production probability for different quark flavours proportional to $\exp(-\pi\mu^2/\kappa)$, where μ is the respective (di-)quark mass. An increased κ will here mainly reduce the suppression of strange quarks (and diquarks), while heavier quarks typically are too suppressed to be relevant for the hadronization process, and are only produced in hard scattering processes. Thus the higher κ_{eff} produces higher yields of both strange hadrons and baryons in pp collisions, as described in detail in ref. [4]. To use rope hadronization in Angantyr-generated pA and AA collisions, we require a common reference frame for every possible pair of strings. Such a reference frame would be a baseline for computing the interactions between every possible string pair. In this paper, we use a new implementation of the rope model, based on this so-called *parallel* frame [7], and show the resulting strangeness enhancement in pp, pPb, and PbPb systems. We conclude by examining our current approach and outlining possible improvements.

2 Strangeness enhancement due to rope hadronization

Our original rope hadronization model, and the recent re-implementation of it, are presented in detail in refs. [4] and [7] respectively. When we now apply the model to collisions involving heavy ions we use the Angantyr [8] model. Parton-level nucleon–nucleon collisions generated by PYTHIA are here stacked on top of each other, after having selected nucleon sub-collisions using a Glauber simulation. When hadronizing a given set of such sub-collisions, it is in principle straight forward to apply our rope model, but there are a few caveats, and the main one of these is related to *colour reconnections* (CR). To understand this issue we need go through some of the basics of the rope model.

Consider two simple strings, each stretched between a quark and an antiquark. If they are completely overlapping and anti-parallel, the colours of the quark and anti-quark in each end can either combine into a colour-octet or a colour-singlet. Lattice calculations show [13] that the tension in a *rope* between any multiplet and the corresponding anti-multiplet charge is proportional the second Casimir operator. Denoting a multiplet corresponding to p coherent triplet and q coherent anti-triplet colours by $\{p, q\}$, this gives

$$\kappa^{\{p,q\}}/\kappa^{\{1,0\}} = C_2^{\{p,q\}}/C_2^{\{1,0\}} = \frac{1}{4}\left(p^2 + pq + q^2 + 3p + 3q\right), \qquad (1)$$

where $\kappa^{\{1,0\}} \equiv \kappa$ is the tension in a single triplet string. Thus for an octet, we would have a string tension of $9\kappa/4$, while for a singlet, we would have no string at all. In pp collisions, all strings originate in a small region in coordinate space, and we have previously argued in ref. [7] that singlet case corresponds to the CR process in PYTHIA [14], where strings close in momentum space are allowed to reconnect, if the combined string length is thereby reduced. For high string densities we assumed that any combination of m triplets and n anti-triplets would then always combine into the highest possible multiplet [7].

For nuclear collisions, we must also account for the separation between vertices in coordinate space. In the Angantyr model, although there are CRs between strings formed in the same sub-collision, there are currently no reconnections between strings from different sub-collisions, since the current CR models in PYTHIA do not take into account the space-time separation.

To handle the space-time separation for rope formation, we here use the *parallel frame formalism* [7] to include separation between vertices in both coordinate and momentum space. It also accounts for strings with "kinks", coming from strings stretched between a quark-antiquak pair via a number of gluons. It constructs

a Lorentz transformation to a frame, where any two (straight) string pieces will always lie in parallel planes, moving away from each other with equal velocities.

To estimate the *formation of a rope* in the absence of CR, we now adopt a *random walk* in colour space combining elementary colour charges [9] where we add one overlapping string at the time. Adding a triplet to a $\{p, q\}$ multiplet can give three possibilities:

$$\{p,q\} \oplus \{1,0\} \;=\; \begin{cases} \{p+1,q\} \\ \{p,q-1\} \\ \{p-1,q+1\} \end{cases} \tag{2}$$

and similarly for adding an anti-triplet. For each added overlapping string, we choose randomly among these, according to the number of states in the corresponding multiplet, $N_{\{p,q\}} = (p+1)(q+1)(p+q+2)/2$. Since we always assume that we have a string being hadronized ($\{1,0\}$) to begin with, we never let p go to zero, but otherwise the random walk is unconstrained.

To estimate the *breakup of a rope* we note that the tension in a rope $\{p, q\}$ is given by the Casimir operator in eq. (1). In our model, the rope would break up one string at the time, and the tunnelling process implies that in each such a breakup, the effective string tension is given by the *reduction* of the rope tension due to the multiplet field being reduced from, *e.g.*, $\{p, q\} \mapsto \{p-1, q\}$:

$$\kappa_{\text{eff}} = \kappa^{\{p,q\}} - \kappa^{\{p-1,q\}} = \frac{2p+q+2}{4}\kappa. \tag{3}$$

In our new implementation, for any given breakup in a string being hadronized, we can consider each of the other string pieces in the event, and boost to the common parallel frame for this pair. Assuming that the dominant part of the string interaction is given by the colour-electric field, using an "Abelian projection" of the SU(3) field [9, 10], the total interaction is the sum of the interaction between all pairs ($\int d^3x\, \mathbf{E}^2_{\text{tot}} = \sum_{i,j} \int d^3x\, \mathbf{E}_i \mathbf{E}_j$). In the parallel frame, we can estimate the fractional overlap based on their space-time location, their relative angle, and assuming a Gaussian transverse shape as described in detail in ref. [7]. These fractional overlaps can then be added together to give the numbers of steps m and n in the random walk to obtain the multiplet $\{p, q\}$. (In contrast to the highest-multiplet procedure used in [7] and in figure 3 below, where we set $p = m$, $q = n$.)

In each of these breakups we can determine an effective string tension, κ_{eff}. This will influence the flavour of the $q\bar{q}$ pair responsible for the breakup via the tunnelling mechanism, notably increasing strange quark production. Also di-quarks

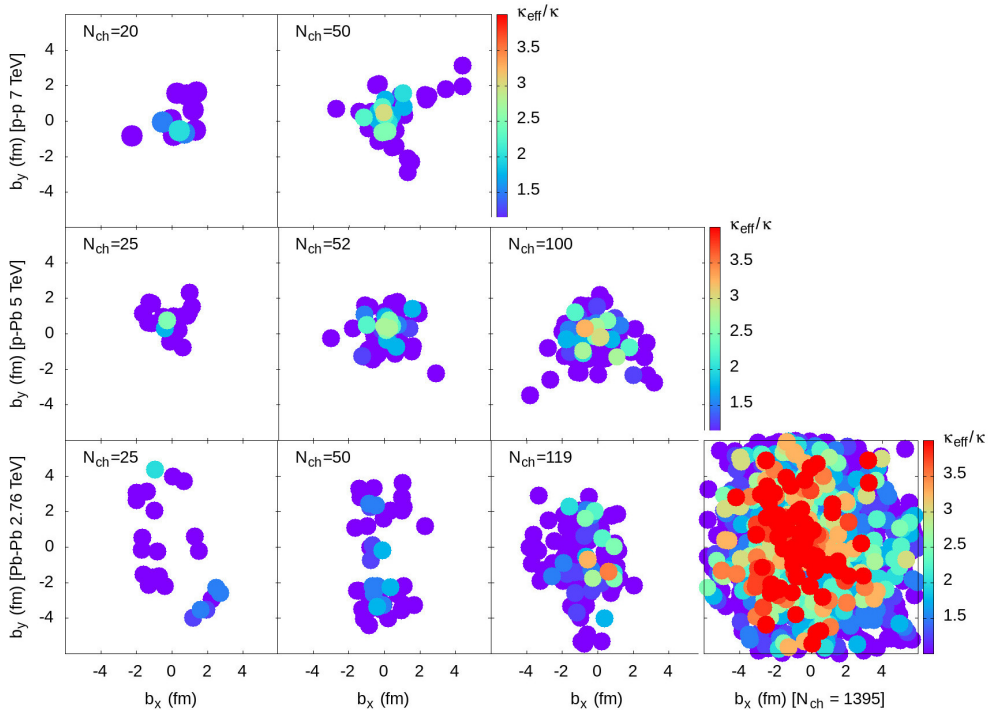

Figure 1: Production points of primary hadrons in impact parameter space produced in the central pseudo-rapidity bin in sample events from pp at 7 TeV (top row), pPb at 5.02 TeV (middle), and PbPb collisions at 2.76 TeV (bottom) for different intervals of central ($|\eta| < 0.5$) charged multiplicity: ~ 25 (first column), ~ 50 (second), ~ 100 (third) and >1000 (last column). The colour of the points indicates the $\kappa_{\text{eff}}/\kappa$ used in the string breakup where the primary hadrons were produced. The impact parameter vector is along the x-axis.

can be produced in the breakups, giving rise to baryon production, and especially strange baryons are enhanced by an increase in κ_{eff}. These effects are technically achieved by changing several parameters in PYTHIA8, as explained in ref. [4].

To illustrate the variations in κ_{eff}, we show in figure 1 sample events from pp, pPb, and PbPb collisions. Each point in each figure represents the production point in impact parameter space of a primary hadron (a hadron produced directly in the hadronization) produced in the central unit of pseudo-rapidity, and the colour indicates the $\kappa_{\text{eff}}/\kappa$ used to produce it. The size of the points correspond to the assumed width of the strings ($R \approx 0.5$ fm). Since the number of produced hadrons per unit rapidity is approximately the same in all vertical columns, the figure also gives an indication of the difference in (transverse) density of strings for different

systems.

We show events with a central charged multiplicity[1], $dN_{\text{ch}}/d\eta|_{\eta=0} \sim 25$ (left-most column), for pp, pPb, and PbPb, and we see that the PbPb event is much more spread out, as expected. We note that also the pp event is quite spread out. This is because (mini-)jets cause the hadron production to occur away from the centre of the collision. This is in line with the expectation that the increase in multiplicity in pp collisions is driven by additional jet production while in pA, and especially in AA, the increase is due to additional nucleon–nucleon sub-collisions. Although there is only one event from each collision system, we see that there is no dramatic difference in the average κ_{eff}. Also for $N_{\text{ch}} \sim 50$ (second column), we see no large difference in κ_{eff}, and while we see the expected almond-like shape for PbPb, the pp event is clearly more *jetty*. At $N_{\text{ch}} \sim 110$ (third column), there are fewer pp events, and we only show samples from pPb and PbPb. Here we see that the pPb has jets, but the difference between κ_{eff} in pPb and PbPb is still not large. To get higher κ_{eff}, we need extremely high multiplicities, available only in PbPb collisions, and we show such an event in the last column. The density of strings is here very large, but there are also large fluctuations in density, with *hotspots* spread out in the impact parameter plane.

3 Results

We now apply the rope hadronization mechanism to minimum bias events in the three systems with a canonical value of the string width $R = 0.5$ fm. The analysis for each system follows the procedure used by ALICE in ref. [3], where the event samples are divided in centrality bins, and the the ratio of each of the strange hadrons to the pion rate are presented as a function of the average central charged multiplicity, $\langle dN_{\text{ch}}/d\eta \rangle_{\eta=0}$, in each bin. We have used default PYTHIA/Angantyr, and the tuned hadronization parameters presented in ref. [10]. In figure 2 we show our result in all three systems, with and without rope hadronization compared to data [3].

We look at K^0_s, Λ, Ξ and Ω hadrons to π ratio for $|\eta| < 0.5$. Overall, the yields of strange mesons and baryons are significantly increased due to rope formation compared to the baseline prediction of Lund string hadronization without any rope effects, which is a major improvement. The magnitude of enhancement is directly related to string density before hadronization sets in, giving an increased κ_{eff}. The number of strings, in turn, is directly related to the average charge multiplicity at

[1]Note that N_{ch} is not the same as the number of primary hadrons.

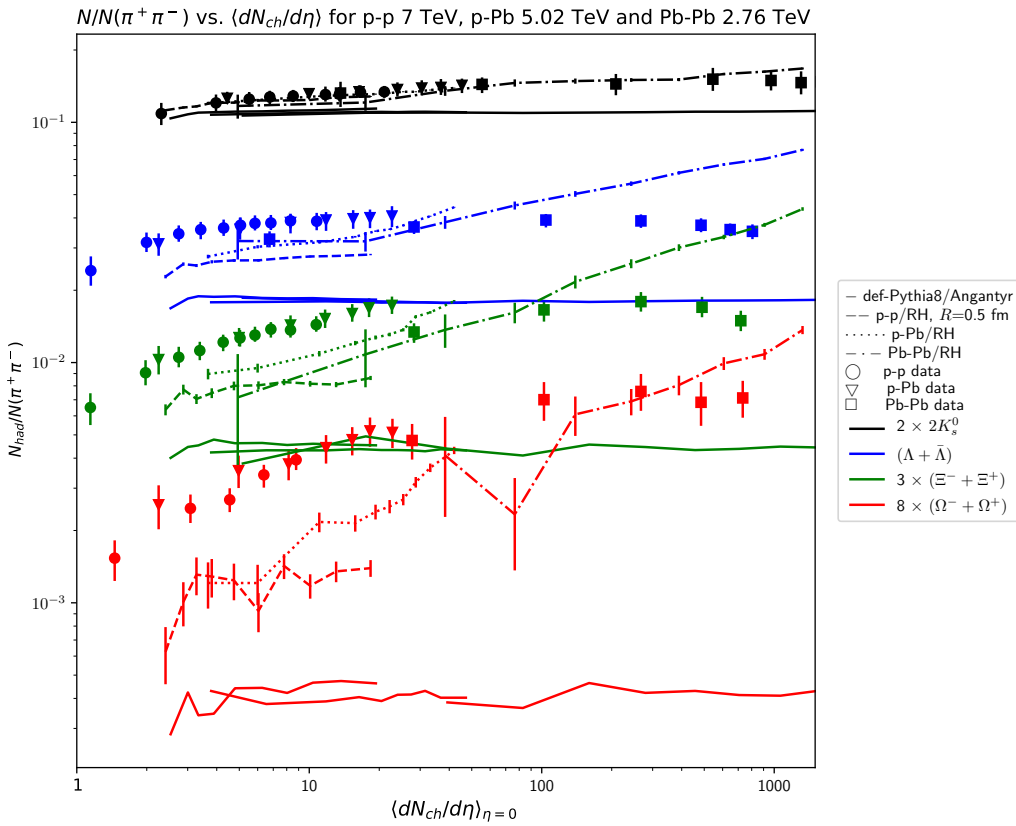

Figure 2: Strange hadron to pion yield ratios in pp at $\sqrt{s} = 7$ TeV, pPb at $\sqrt{s_{\rm NN}} = 5.02$ TeV, and PbPb at $\sqrt{s_{\rm NN}} = 2.76$ TeV, vs. $\langle dN_{\rm ch}/d\eta \rangle_{\eta=0}$. The data is taken from ALICE [3]. For clarity, error bars are only shown for the rope model results.

mid-rapidity,$\langle dN_{\rm ch}/d\eta \rangle_{\eta=0}$. Therefore, $dN_{\rm ch}/d\eta|_{\eta=0}$ is a perfect scaling variable to show the multiplicity dependence of $\kappa_{\rm eff}$, and hence also for strangeness and baryon enhancement. This scaling is in qualitative agreement with the data, and for K^0_s we also have quantitative agreement. However, we see that the increase with $\langle dN_{\rm ch}/d\eta \rangle_{\eta=0}$ is too steep, especially for the baryons, but also for K^0_s there is a tendency to overshoot the data at the highest multiplicity in PbPb. In our results for the rope model we have assumed $R = 0.5$ fm for the string radius, and increasing it to 1 fm would improve the comparison with data for low multiplicities (see figure 3), but would overshoot even more at the highest multiplicity PbPb bins.

We notice that the yield ratios in pPb and PbPb lack saturation at high $dN_{\rm ch}/d\eta|_{\eta=0}$, while pp is much flatter. As discussed above, this can be expected

since very high multiplicities in pp are, to a large extent, driven by increased (mini-)jets production, while the high multiplicities in AA are driven by an increase in soft nucleon sub-collisions. Since hadrons that are produced in jets come from strings that are not parallel to the bulk of the soft strings along the beam axis, and are produced further away from these, the effective number of overlaps is smaller.

From figure 2, it may seem that the steep rise in yield ratios is mainly a problem for the baryon production, but this is not necessarily the case. In figure 3, where we show the $(\Lambda + \bar{\Lambda})/2K^0_s$ ratio for pp at $\sqrt{s} = 7$ TeV, we observe that the increase in Λ/K follows the behaviour seen in data. There are, however, additional uncertainties in the string fragmentation for baryons. One such effect is the hyperfine correction [10] arising from spin-spin interactions between a quark and an antiquark or between two quarks. This especially affects the multi-strange particles, and there is room for further corrections to the baryon yields. However, this would mainly affect the overall yield of (multi) strange baryons, and would not affect the strong rise in figure 2, which is mainly driven by κ_{eff}.

Including colour reconnections between sub collisions, which are lacking in our current implementation will clearly affect the results. This would naively reduce the number of strings (n_s), but it would not necessarily reduce the rise of κ_{eff} since N_{ch} is approximately proportional to n_s. Hence, n_s would have to be increased again by modifying Angantyr parameters in order to fit data. Additionally, after that we would need to use the highest multiplet procedure which would increase κ_{eff}, although we see in figure 3 that this is not necessarily a large effect.

There is, however, one mechanism that can decrease the string density without decreasing n_s, and that is the repulsion between overlapping strings, which is addressed in the string shoving model [5, 6]. Owing to the technical difficulties outlined in ref. [7] string shoving is not included in our current results. However, shoving would spread out the strings more in dense environments, possibly taming the rise for high multiplicities in figure 2.

To look further into rope effects on the baryon yield, we show in figure 3 the rope model for two values of the string radius with the random walk (rw) formulation. We also show the yield ratio using highest multiplet (hm) formulation for $R = 0.5$ fm, which we use in ref. [7]. As discussed above, the highest multiplet is used together with CR in pp, assuming that the latter corresponds to the steps downward in eq. (2).

In figure 3, compared to default PYTHIA8, rope hadronization with random walk and $R = 0.5$ fm enhances the baryon vs. meson yields significantly in all multiplicity bins. However, following the highest multiplet procedure, the yield ratios are slightly higher, giving a better agreement with data. Here we note that

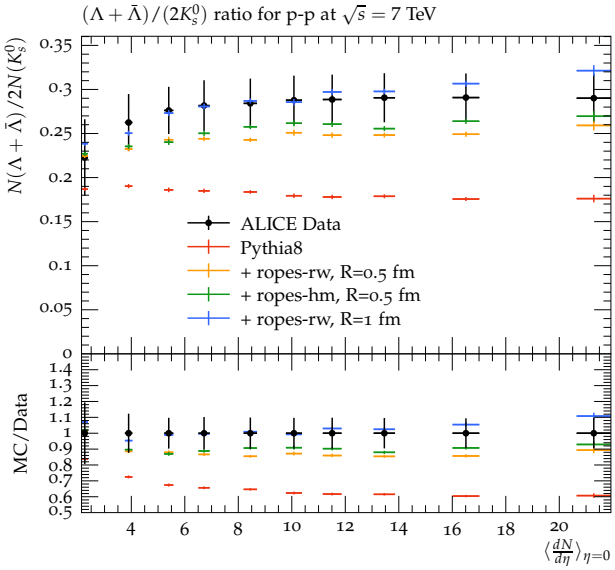

Figure 3: $(\Lambda+\bar{\Lambda})/2K^0_s$ yield ratio vs. $\langle dN_{\rm ch}/d\eta \rangle_{\eta=0}$, compared to pp minimum bias data at $\sqrt{s}=7$ TeV [3]. Effects of random walk with $R=0.5$ fm and 1 fm, and highest-multiplet with $R=0.5$ fm is shown.

with the random walk formulation, if R has a higher value such as 1 fm, the effect is in better agreement to data as shown in the figure. Therefore, we conclude that string shoving and CR would have non-trivial effects on strangeness and baryon yields, especially at high the highest string densities.

4 Conclusions

Based on the success of our previous rope model in explaining strangeness enhancement in small systems [3], we show here that our new implementation, based on the parallel frame, can model enhanced strange flavour production in *all* collision systems. The enhancement of strange hadrons shown here is due to modification of the string tension $\kappa_{\rm eff}$ in dense environments. The average $\kappa_{\rm eff}$ in string fragmentation, as shown in figure 1, combines the effects of local fluctuations in overlap among ropes during hadronization. Clearly the current rope model lacks the saturation at high multiplicities seen in data, but we believe that this is due to the lack of repulsion between overlapping strings, which we can achieve by combining the ropes with our shoving model. It should be noted that our rope model is very different from the conventional picture based on the formation of a QGP, so

even if the same strangeness enhancement can be achieved in both pictures, there are several other observables that would differ. In particular, it is central to the string model that there is a strong momentum correlation between strange and anti-strange hadrons, which should be completely lacking in a thermalized QGP.

String shoving would not only dilute a string system before hadronization via rope formation takes place, it can also give rise to final-state collective flow. Hence, in small systems, both string shoving and rope hadronization together give rise to two out of three typical QGP-like signals. On the other hand, hadronic rescattering [15, 16] also gives rise to final-state collectivity for central collisions in pA and AA. In addition, modification of jet energy and topology can arise due to CR. Therefore, to arrive to a complete string-based physical picture in AA collisions in PYTHIA/Angantyr, the combined effects of colour reconnections, string shoving, rope hadronization and hadron rescattering need to be included. Such a picture could then also be applied to other kinds of collision experiments, such as in cosmic ray showers, and not least at the future Electron–Ion collider.

5 Acknowledgements

This work was funded in part by the Knut and Alice Wallenberg foundation, contract number 2017.0036, Swedish Research Council, contracts number 2016-03291, 2016-05996 and 2017-0034, in part by the European Research Council (ERC) under the European Union's Horizon 2020 research and innovation programme, grant agreement No 668679, and in part by the MCnetITN3 H2020 Marie Curie Initial Training Network, contract 722104.

References

[1] J. Rafelski and B. Müller, "Strangeness Production in the Quark - Gluon Plasma," *Phys. Rev. Lett.* **48** (1982) 1066. [Erratum: Phys.Rev.Lett. 56, 2334 (1986)].

[2] **ALICE** Collaboration, B. B. Abelev *et. al.*, "Multi-strange baryon production at mid-rapidity in Pb-Pb collisions at $\sqrt{s_{NN}}$ = 2.76 TeV," *Phys. Lett. B* **728** (2014) 216–227, 1307.5543. [Erratum: Phys.Lett.B 734, 409–410 (2014)].

[3] **ALICE** Collaboration, J. Adam *et. al.*, "Enhanced production of multi-strange hadrons in high-multiplicity proton-proton collisions," *Nature Phys.* **13** (2017) 535–539, 1606.07424.

[4] C. Bierlich, G. Gustafson, L. Lönnblad, and A. Tarasov, "Effects of Overlapping Strings in pp Collisions," *JHEP* **03** (2015) 148, 1412.6259.

[5] C. Bierlich, G. Gustafson, and L. Lönnblad, "Collectivity without plasma in hadronic collisions," *Phys. Lett. B* **779** (2018) 58–63, 1710.09725.

[6] C. Bierlich, S. Chakraborty, G. Gustafson, and L. Lönnblad, "Setting the string shoving picture in a new frame," *JHEP* **03** (2021) 270, 2010.07595.

[7] C. Bierlich, S. Chakraborty, G. Gustafson, and L. Lönnblad, "Jet modifications from colour rope formation in dense systems of non-parallel strings," 2202.12783.

[8] C. Bierlich, G. Gustafson, L. Lönnblad, and H. Shah, "The Angantyr model for Heavy-Ion Collisions in PYTHIA8," *JHEP* **10** (2018) 134, 1806.10820.

[9] T. S. Biro, H. B. Nielsen, and J. Knoll, "Color Rope Model for Extreme Relativistic Heavy Ion Collisions," *Nucl. Phys. B* **245** (1984) 449–468.

[10] C. Bierlich, S. Chakraborty, G. Gustafson, and L. Lönnblad, "Hyperfine splitting effects in string hadronization," *Eur. Phys. J. C* **82** (2022), no. 3 228, 2201.06316.

[11] B. Andersson, G. Gustafson, G. Ingelman, and T. Sjöstrand, "Parton Fragmentation and String Dynamics," *Phys. Rept.* **97** (1983) 31–145.

[12] E. Brezin and C. Itzykson, "Pair production in vacuum by an alternating field," *Phys. Rev. D* **2** (1970) 1191–1199.

[13] G. S. Bali, "Casimir scaling of SU(3) static potentials," *Phys. Rev. D* **62** (2000) 114503, hep-lat/0006022.

[14] T. Sjöstrand and M. van Zijl, "A Multiple Interaction Model for the Event Structure in Hadron Collisions," *Phys. Rev. D* **36** (1987) 2019.

[15] T. Sjöstrand and M. Utheim, "A Framework for Hadronic Rescattering in pp Collisions," *Eur. Phys. J. C* **80** (2020), no. 10 907, 2005.05658.

[16] C. Bierlich, T. Sjöstrand, and M. Utheim, "Hadronic rescattering in pA and AA collisions," *Eur. Phys. J. A* **57** (2021), no. 7 227, 2103.09665.

Paper IV

IV

Impact of string interactions on the space-time evolution of hadronic vertices

Smita Chakraborty and Leif Lönnblad

To be submitted to *European Physical Journal C*
e-Print: 2207.14186 [hep-ph]
MCnet-22–12, LU-TP-22–50

Abstract

We investigate the space-time picture of string evolution and hadron production in a fully string-based model for high energy collisions involving heavy ions. We find that although the density of strings is quite large at the time of hadronization in a central heavy ion collision, the initial overlap between them right after the collisions is not necessarily large. We also find that when including string–string interactions using the so-called *shoving* model, the density of strings is decreased which should decrease the rapid increase in string tension in the rope hadronization with multiplicity that we found in a previous paper.

1 Introduction

The Angantyr [1] model for modelling heavy ion (HI) collisions in PYTHIA8 implements a fairly simple procedure for stacking nucleon–nucleon (NN) sub-collisions on top of each other, to build up full HI events. Each sub-collision is generated using the full power of the PYTHIA8 multi-parton interaction (MPI) framework together with initial- and final-state parton showers. The combined parton-level sub-events are then hadronized together with the Lund string fragmentation model [2]. Even though there are no collective effects in this model it is able to adequately describe multiplicities in both pPb and PbPb events at the LHC, and even predict multiplicities in XeXe [3]. This begs the question, if it is possible that the colour degrees of freedom generated in the initial stages on the perturbative level in terms of colour connections (dipoles) between produced partons, can survive the hot and dense environment of a HI collision in the form of strings that then fragment into hadrons.

In a series of articles [4–8] we have been investigating possible effects of interactions between strings in a dense environment, and have shown that such models may indeed give rise to collective effects such as anisotropic flow and strangeness enhancement, without the need of introducing a thermalised quark–gluon plasma (QGP). In this article we take a step back and investigate in more detail the space–time picture that arises from these models.

Among the string interactions, string shoving [6] and rope hadronization [7,8] would impact the final-state hadron yields the most in heavy-ion collisions. The novelty of these mechanisms is based on the equilibrium transverse extent of the colour-electric field (E) of each string. Once each string is formed, the colour-electric field spread transversely to reach an equilibrium width R, as established in ref. [6]. The electric field then is approximate by a Gaussian transverse shape,

$$E = N\exp\left(-\frac{\rho^2}{2R^2}\right), \tag{1}$$

where ρ is the transverse distance from a center of a string of radius R, in cylindrical coordinates. The effect of two strings' electric fields repelling each other, would give rise to a net 'shoving' effect, which would push either string pieces away. In our implementation, this effect is modelled by looking at the strings after the final radius has been reached, and then transferring the push to primary hadrons by shifting their $p_\perp$ after hadronization.

Also the hadronization process is affected by the interaction between colour-electric fields of the strings. We have suggested that the stings would form wider

'colour-ropes' with larger effective string tension κ_{eff}, than just the sum of the tension of the individual strings. When such ropes hadronize, the higher κ_{eff} is released, which is available for tunnelling mechanism [2], and therefore producing more strange quarks. Thus, rope hadronization influences the strangeness yields in collision systems.

In a recent work [8], where we apply our rope hadronization to AA collisions, we find that rope hadronization by itself enhances strangeness yields too much in central PbPb events as compared to data. We believe that this occurs due to an overestimation of the string density at the time of hadronization in case of heavy-ion collisions. As we noted in that publication, inclusion of string shoving mechanism would produce a more accurate impact-parameter distribution of strings at the time of hadronization. The $p_\perp$ pushes generated due to shoving would dilute the system due to the dense initial state generating larger shoving force.

In the current implementation, rope hadronization and string shoving mechanisms are not completely compatible. In the perfect case, rope formation would require the precise locations of the string pieces in impact parameter. That would require pushing the string pieces with the $p_\perp$ generated due to string shoving at each time step during string evolution, but as mentioned above, in our implementation in ref. [6], the $p_\perp$ is only transferred to the primary hadrons, formed from hadronization. Therefore, the rope effects are somewhat approximate in all systems, and this mostly affects the yields in AA collisions, giving an overestimate of the string density.

Further work on reproducing signals such as final-state collective effects in AA in PYTHIA would require hadronic rescattering [9, 10] and string interactions to work together. The effectiveness of the implementation will depend on how accurately the string interactions are able to produce the primary hadronic vertices as initial conditions to the hadronic rescattering. In this publication, we investigate the impact of string shoving and rope hadronization on primary hadron vertices.

The manuscript is organised as follows. In section 2, we describe the space-time evolution of strings and their transverse overlaps in pp and AA collisions. In section 3, we present how the primary hadron vertices are determined in PYTHIA, and discuss how these are affected by the shoving and rope models. Lastly, we present our conclusions and further comments in section 4.

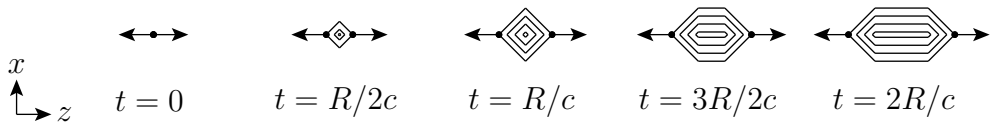

Figure 1: Illustration on the time-evolution of the force field between a colour and an anti-colour charge produced in the same point and flying apart from each other along the x axis with the speed of light. R is the string radius.

2 Space-time evolution of strings

The Angantyr model [1] can be said to be a straight forward extention of the multi-parton interaction model for pp in PYTHIA to HI collisions. The model is based on an advanced Glauber [11, 12] calculation, which includes so-called Glauber–Gribov [13] corrections. The obtained nucleon–nucleon (NN) sub-collisions, are produced with the full PYTHIA8 MPI machinery, and are basically stacked together and hadronized. Some modifications are needed when one nucleon in one nuclei interacts with several nucleons in the other. In this case only one such sub-collision is treaded as *primary* and is modelled as a full pp collision in PYTHIA, while the others are treated as diffractive excitations similar to the wounded nuclei model [14] as described in detail in [1].

As in PYTHIA, the final-state hadron multiplicity in Angantyr is driven by multiple (semi–hard) scatterings among the partons of the colliding nucleons. These are treated perturbatively, even if they can be rather soft, which means that the scatterings are well localised. In this picture, the partons are then connected by colour lines, or *dipoles*, and the colour field between the partons in such a dipole is initially also well localised, but will spread out with the speed of light (c) both longitudinally and transversely as the partons fly apart. While the longitudinal extension will continue to grow, the transverse extension will stop due to confinement, and we get a string-like field with a constant string tension, $\kappa \approx 1$ GeV/fm, that will eventually break and form hadrons.

A simplified picture of the time-evolution of a single string piece between a coloured and an anti-coloured parton flying apart with the speed of light is given in figure 1. Parameterising a point along the string by the proper time, τ, and hyperbolic angle, we get in each time step, that the points where the radius reaches the confinement value, (R), will have $\tau c = R$.

To illustrate the density of strings in a HI collision we have generated a sample central PbPb event at $\sqrt{s_{NN}} = 2.76$ TeV, shown in figure 2. The impact parameter is ≈ 0.2 fm, resulting in a charged multiplicity in the central pseudorapidity bin of $dN_{\text{ch}}/d\eta|_{\eta=0} \approx 1750$. We then look at the strings that span $z = 0$ in the laboratory

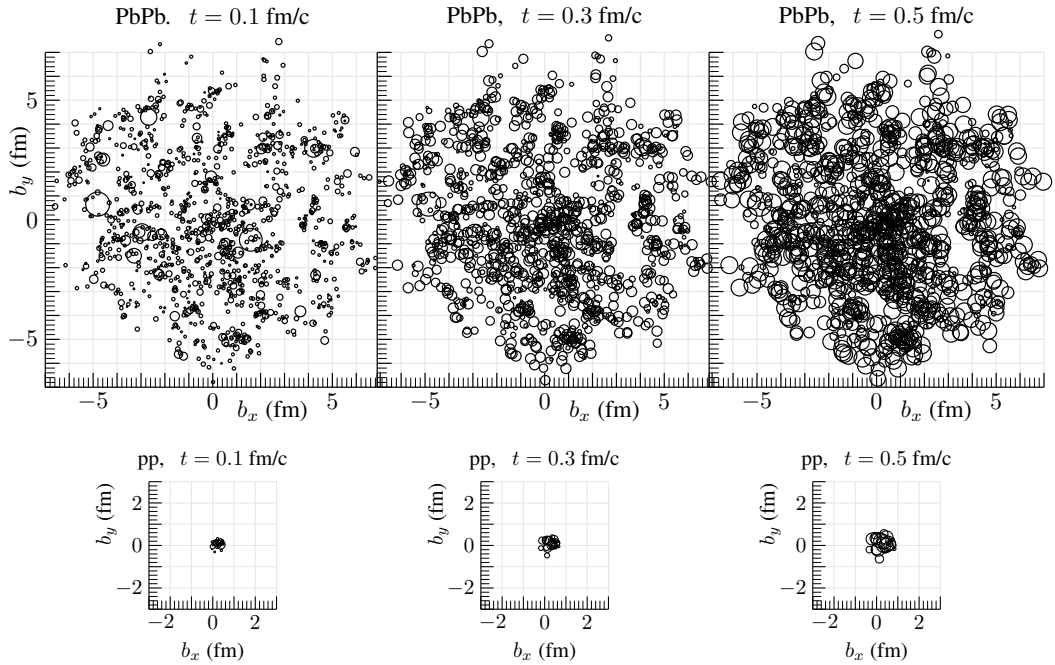

Figure 2: The evolution of the colour fields between partons in a sample PbPb event (top) and a sample pp event (bottom), both generated at $\sqrt{s_{NN}} = 2.76$ TeV. Each circle represents the position in impact parameter space of a colour dipole field that stretches across $z_{\text{lab}} = 0$ at different times after the collision, $t_{\text{lab}} = 0.1$ fm/c (left), 0.3 fm/c (middle), and 0.5 fm/c (right). The radius of each circles corresponds to the transverse extent of the colour field of the dipole as given by the proper time of the string field at that point.

frame, and for each such string we look at its size in different time steps (also in the laboratory frame). For each of these we position in figure 2 a correspondingly sized circle in the impact parameter plane. To be more precise, the radius of each circle is given by the proper time (multiplied by c) at the position along the string piece given $z = 0$ and time in the laboratory frame, limited from above by $R = 0.5$ fm. In addition, to take into account of how well localised the field were from the beginning, the diameter of each circle is limited from below by $\hbar c/p_{\perp\text{max}}$, where $p_{\perp\text{max}}$ is the largest transverse momentum of the two partons spanning the field.

In the top left plot in figure 2, we see that initially, the collision region is only sparsely populated by the colour fields. Comparing to the lower left panel, where

we show a high multiplicity ($dN_{\rm ch}/d\eta|_{\eta=0} \approx 50$) pp event at the same collision energy ($\sqrt{s} = 2.76$ TeV), there are very few regions in the PbPb event where the colour fields are more densely packed. At later times ($t = 0.3$ fm/c in the middle panels), more of the collision area is filled up by colour fields, and at $t = 0.5$ fm/c (right panels), almost the whole area is filled, and this is also when the colour fields start to be confined to their maximum radius (0.5 fm in this simulation). Most dipoles, however, have a tranverse momentum, and due to the time-dilation, only some of them has reach their final radius at $t = 0.5$ fm/c.

Clearly the overlap between the colour fields in the PbPb event becomes quite large, which raises the question if the string picture is really appropriate for heavy ion collisions. On the other hand, the overlap is also quite high in the pp collision, and we know that PYTHIA is able to describe a vast range of hadronic final-state observables in pp. We want to see how far we can go with the string picture and, rather than resorting to a hydro-dynamical approach with a quark–gluon plasma, we assume that the string degrees of freedom are still relevant for hadronization.

Due to the large overlap among the strings, we need to worry about possible string–string interactions, and in the following sections we will discuss the space-time picture in our models for string shoving and rope hadronization.

There is also a third effect that we will not discuss here, namely colour reconnections. The assignment of colour connections between partons in PYTHIA8 is essential, not only for the string fragmentation but also for the parton shower, which is based on the dipole picture. The assignment of colours are, however, made on the perturbative level in the $N_C \to \infty$ limit, and in a dense system, there must be corrections to this. Indeed, already in the first multi-parton interaction implementation in PYTHIA [15] the concept of colour reconnections was introduced where the colour connections between partons were allowed to change before hadronization, in a way that favoured shorter strings.

However, the colour reconnection models in PYTHIA8 are based on a pure momentum picture and does not take into account the space–time separation between partons, so they are not suitable for heavy ion collisions. And in the Angantyr model, there are therefore only reconnections within each NN collision, while reconnections between them are not possible. We are currently working on a new reconnection model that takes space–time constraints into account, but it is not yet fully implemented.

3 Corrections to hadronic vertices from string interactions

In this section, we present the shoving and rope models and how they affect the primary hadronic vertices. In both of these models, the cumulated effect of interactions between many stings are calculated by summing up pair-wise interactions between string pieces. To calculate the interaction between two string pieces, we use a special Lorentz frame, which we call the parallel frame. Here, any two string pieces spanned between two pairs of (massless) partons in any string system, will at any given time be straight lines lying in parallel planes.[1] This greatly facilitates the calculation of the transverse shoving force, as well as the increased string tension in the rope hadronization.

3.1 String shoving

In our previous implementation of the shoving model [6] we did not treat soft gluons properly. Gluons act like transverse excitations or *kinks* on a string. Since each gluon is connected to two string pieces, it will lose energy to the strings twice as fast as a quark. In any given reference frame, a gluon with energy e will therefore have lost all its energy after a time $t = e/2\kappa$. What happens then is that a new string region is formed and will give a straight string piece starting from the point where the gluon stops, expanding as if dragged out by the momenta of the partons to which the stopped gluon is colour connected. In general, a string spanned between a quark to an anti-quark via series of gluons $(q_0, g_1, g_2, \ldots, g_{n-1}, \bar{q}_n)$ can be treated as a series of string regions, or *plaquettes*. In these regions, we have the primary plaquettes spanned between the momenta (p_i, p_{i+1}) (where the momenta of the gluons is divided by two), corresponding to the original dipoles, but also secondary ones spanned between (p_i, p_{i+2}) with space–time vertices shifted by p_{i+1}/κ. Similarly we get higher order plaquettes, spanned by (p_i, p_{i+n}) with vertices offset by $\sum_{j=i+1}^{i+n-1} p_j/\kappa$. This is explained in detail in refs. [16] and [17].

In our updated shoving implementation, we now allow for all such plaquettes. Just as for the primary dipoles, we can for each plaquette look at any other plaquette in another string, go to the corresponding parallel frame, and calculate the transverse force between them there.

The shoving is implemented as discretised pushes with a small ($\sim$ 20 MeV) transverse momentum, $\delta p_\perp$. In principle, this would correspond to adding a small

[1] The full construction of the parallel frame is given in ref. [6, 7].

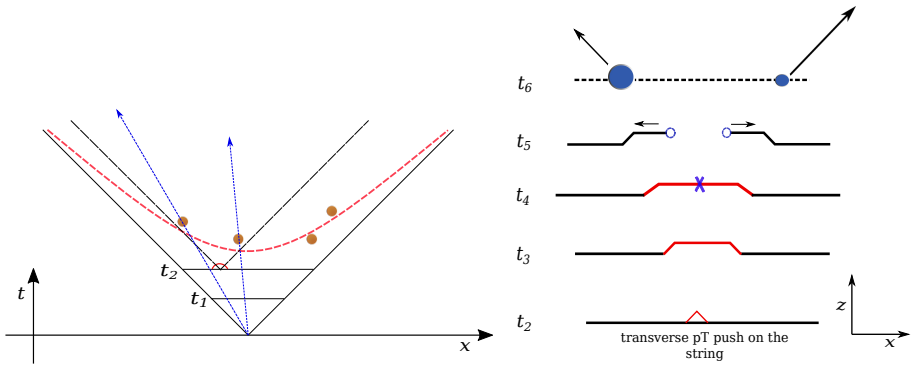

Figure 3: Figures showing propagation of a localised push on a string moving along the z-axis. The left figure shows the space–time picture, and the right figure shows the deformation in of the string in the z direction in different time steps.

gluon to a string, but as its energy would be very small it would stop almost immediately (after a time, $\delta t = \delta p_\perp / 2\kappa$). This would form a new plaquette which will start to spread out with the speed of light in both directions of the string, resulting in a shift of the string in the z direction[2] with $\delta_z = c\delta t$. This is illustrated in figure 3 for one of the string pieces (the other string will get a push in the opposite z direction in a similar way).

Implementing each new push with a new plaquette would give forbiddingly complicated string configurations,[3] and instead the transverse momentum of each push, which is localised in the edges of the expanding region (with $\delta p_\perp / 2$ on each side), is transferred directly to the closest primary hadrons after the hadronization.

Note that, when introducing secondary plaquettes, a push propagating along the straight string piece may encounter a *corner* between two plaquettes and continue propagating in another plaquette. Currently, such situations are only treated approximately, assuming that the push will continue with in the same directions as in the parallel frame where it is produced and the transverse momentum to the primary hadron closest to that direction.

Previously, our implementation only considered the change in momentum resulting from the shoving, but here we also want to study the space–time picture. We note that the two hadrons receiving a transverse-momentum push would be also pushed in space along the z direction in the parallel frame. This is implemented by simply shifting the production vertices assigned by the PYTHIA8 string

[2]In the parallel frame, the two stings pieces lie in planes parallel to the $x - y$ plane, moving in opposite directions along the z axis (see ref. [6]).

[3]The complexity of our algorithm is already very high, requiring the construction of several millions parallel frames in a single central AA event.

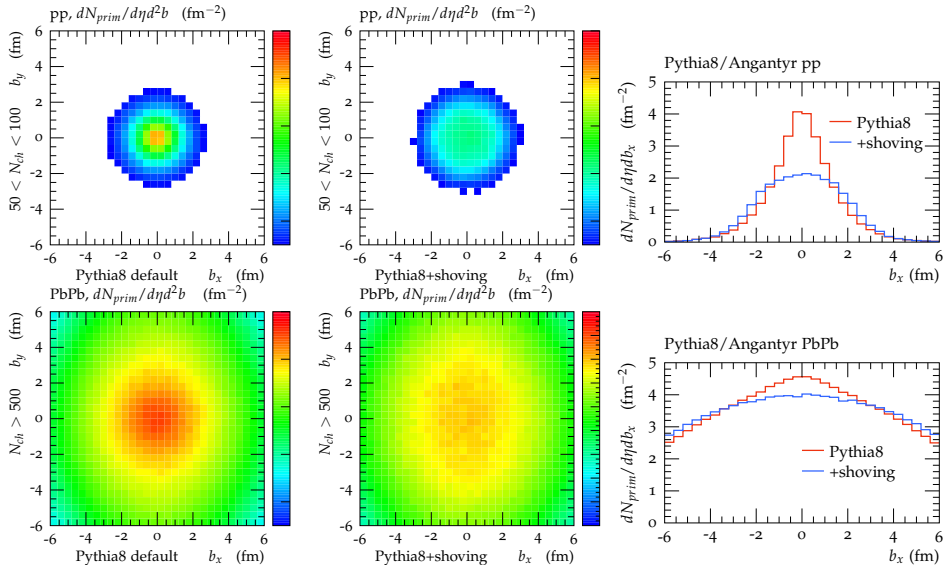

Figure 4: The distribution of vertices for primary hadrons in the shoving model for pp collisions with central charged multiplicity, $50 < dN_{\mathrm{ch}}/d\eta|_{\eta=0} < 100$ (top row), and for PbPb collisions with $dN_{\mathrm{ch}}/d\eta|_{\eta=0} > 500$ (bottom row). The pp events were generated at $\sqrt{s} = 7$ TeV, and the PbPb events at $\sqrt{s_{NN}} = 2.76$ TeV. The left panels show a heat map, giving the number of primary hadrons with $|\eta| < 0.5$ per fm^2 in impact parameter space for PYTHIA8/Angantyr without shoving and the middle panels shows the same with shoving. The right panels compares the distributions with and without shoving in a slice with $|b_y| < 0.5$ fm.

fragmentation (see description in section 3.2 below) by δz. In addition, any hadron produced between these two hadrons along the string will be affected by the push and are also shifted by δz. Note, however, that their momenta are not affected by the push.

String shoving therefore, affects the primary hadronic vertices directly via their z component in each parallel frame. This is what we account for in this implementation and its effect is shown in figure 4. Shoving would have the most effect in the most dense regions in a collision. The correction due to shoving force would "dilute" the distribution of primary hadrons transverse to the beam axis in the lab frame.

To show the effect of the shoving on the position of the primary hadron vertices, we have generated a large sample of pp and PbPb events at 7 TeV and 2.76 TeV respectively, and looked at the positions of the centrally produced ($|\eta| < 0.5$) primary hadrons in impact parameter space. In figure 4, we show in the top row the

resulting distributions with and without shoving[4] for high-multiplicity pp events (with charged multiplicity, $N_{ch]}$ between 50 and 100 in the central rapidity bin), and in the bottom row the same for high-multiplicity ($N_{\rm ch} > 500$) PbPb events.

The first thing to note is that without shoving the high multiplicity pp events reaches almost as high densities of primary hadrons as the very central PbPb ones, which confirms what we already saw in figure 2.[5] With shoving (middle column), we see that the vertices of primary hadrons are more spread out compared to their distribution without shoving (first column). The impact is most apparent for pp collisions in the first row, where the peak at $(0, 0)$ is heavily dampened. This is clearly seen in the right-most column, where for the $|b_y| < 0.5$ fm bins, the number density of primary hadrons are shown as a function of b_x for both with and without shoving. Also for PbPb events the hadronic vertices are more spread out with shoving included, but the effect is not as dramatic. This is because the strings in the centre are shoved from all sides, and therefor do not move as much.

3.2 Rope hadronization

In ref. [7, 8] we presented a new rope hadronization model for HI collisions in Angantyr, based on the parallel frame technique described above. Depending on the transverse separation between two string pieces at the time of hadronization, the partons at the end of the strings combine to form higher colour-multiplets. This would result in a higher effective string tension, following lattice results and as established in our previous works [7, 8, 18]. When the higher colour multiplet transitions to lower colour multiplets in a string breaking, the energy from the higher string tension is released. This results in an effective string tension, $\kappa_{\rm eff}$, which is higher than in a single string, increasing the possibility to produce strange quarks in the tunnelling mechanism responsible for the breaking. This would give rise to higher number of strange particles as well as baryons in the final state. This $\kappa_{\rm eff}$ would, however, also influence the production vertices of primary hadrons in various stages, which we will describe below.

To calculate vertices of primary hadrons in PYTHIA, the relation between the energy-momentum picture and space-time picture is used. In the Lund model, the equation of motion of a string between a pair of massless quark q and antiquark $\bar{q}$,

[4]All basic PYTHIA8/Angantyr parameters have their default values, and the shoving model used a string radius of $R = 0.5$ fm and a shoving strength of $g = 0.25$.

[5]Note that the number of primary hadrons from a string is roughly one per unit rapidity.

results in a linear relation between space-time and energy-momentum:

$$|\frac{dp_{x,q/\bar{q}}}{dt}| = |\frac{dp_{x,q/\bar{q}}}{dx}| = |\frac{dp_{q/\bar{q}}}{dt}| = |\frac{dp_{q/\bar{q}}}{dx}| = \kappa, \tag{2}$$

where κ is the string tension. The location of a break-up point on the string can be given by $v_i = \frac{x_i^+ p^+ + x_i^- p^-}{\kappa}$, where $x_i^\pm$ are the light cone fractions and p^+ (p^-) is the four-momentum of the q ($\bar{q}$). It is to be noted that these equations are not a function of the width of the string from which the hadron is formed. In case of a string with a radius R the uncertainity of a hadronic vertex point will arise in the transverse plane. This effect is accounted for in the vertex calculation using a Gaussian smearing[6]. We will return to this effect while discussing the effect on κ_{eff} on production vertices later.

Since a hadron is formed from two adjacent break-ups, the vertex should be a function of each break-up point, say v_i and v_{i+1}. Since locating a hadronic vertex is not precise due to a hadron's transverse extent, they are somewhat approximated. These space-time locations of a hadronic vertex in PYTHIA8 can therefore be chosen in three different ways. The default definition is the "middle point" in sampling the hadron vertex. This is given by:

$$v_i^h = \frac{v_i + v_{i+1}}{2} \quad \text{middle.} \tag{3}$$

The "early" position is defined as the space-time point where the backward light cones of the partons forming the hadrons cross. The "late" position is where the forward light cones cross:

$$\begin{aligned} v_{l,i}^h &= \frac{v_i + v_{i+1}}{2} + \frac{p_h}{2\kappa} \quad \text{late,} \\ v_{e,i}^h &= \frac{v_i + v_{i+1}}{2} - \frac{p_h}{2\kappa} \quad \text{early.} \end{aligned} \tag{4}$$

For the detailed implementation, we refer the reader to ref. [17].

For the purpose of this paper we have modified the vertex finding in PYTHIA8, to take into account the increased string tension, κ_{eff}, in the rope model. Since κ_{eff} varies along the string this is done locally for each vertex.[7] It should be noted that κ_{eff} also affects the transverse momentum of the of the $q\bar{q}$ pair in the tunnelling

[6] In PYTHIA8, a is called `HadronVertex:xySmear` controls the gaussian smearing and has a default value of 0.5 fm, which is the same value for R.

[7] It should be noted that κ_{eff} is only approximately localised along the string in our current implementation, and also the effects on the vertices are somewhat approximate.

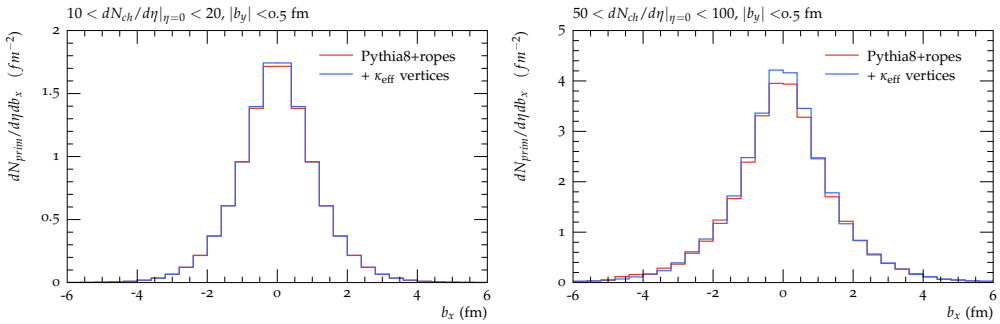

Figure 5: The distribution of vertices for primary hadrons in the rope hadronization model for pp collisions with central charged multiplicity, $10 < dN_{\mathrm{ch}}/d\eta|_{\eta=0} < 20$ (left), and $50 < dN_{\mathrm{ch}}/d\eta|_{\eta=0} < 100$ (right). The events were generated at $\sqrt{s} = 7$ TeV, and the distribution of vertex position along the impact parameter vector (b_x) is shown for a slice with $|b_y| < 0.5$ fm. The blue line includes the effect of κ_{eff} on the vertex calculation in PYTHIA8, while the red line does not.

mechanism, giving $\sqrt{\langle k_\perp^2 \rangle} \propto \sqrt{\kappa_{\mathrm{eff}}}$, and this also results in a corresponding scaling of the transverse momenta of the hadrons. This means that the difference between *early* and *late* for the transverse coordinates in eq. (4) would effectively be smaller than for the longitudinal ones. In the following we will only use the default *middle* option in eq. (3).

When we include the modified κ_{eff} in calculation of the primary hadron production vertices, the impact on the vertices proved to be rather small. In figure 5, we show the effects in pp collisions at $\sqrt{s} = 7$ TeV, for a slice around $|b_y| < 0.5$ fm in impact parameter space, as a function of b_x. We show two multiplicity bins $10 < \frac{dN_{\mathrm{ch}}}{d\eta} < 20$ (left) and $50 < \frac{dN_{\mathrm{ch}}}{d\eta} < 100$ (right). As seen in the figure, the effect is barely visible for the lower multiplicities due to lower density of strings, but also for the higher multiplicities the effect is small compared to the effects of shoving in figure 4.

We have also studied the effect in HI collisions, and there it is even smaller, since the vertex distribution in impact parameter is less peaked than in the pp case. Even for the highest multiplicities in PbPb collisions at 2.76 TeV, the effect (not shown here) is barely visible, even though the densities of strings is larger than in pp.

4 Conclusion and outlook

A correct description of primary hadron vertices in the Lund string picture is essential to arrive at more consistent predictions from string interactions in PYTHIA and Angantyr. This would help us determine the contribution of such non-perturbative QCD effects on the final-state observables both in small and large systems. As already observed in refs. [6,8], both shoving and rope hadronization have non-trivial effects on the final-state in dense systems. The effect is dependent on system size and if accounted for correctly can reproduce QGP-like effects. This would present different underlying mechanisms as origins of QGP-like observations in both small and large systems.

We have shown here that in the Angantyr model, the initial occupancy of colour fields from the MPIs is not large. As the fields grow transversely they start shoving, giving rise to flow, and when they finally hadronize the increased κ_{eff} gives rise to strangeness and baryon enhancement. One should note that the rope hadronization and string shoving models used in this publication is rather distinct to CGC-Glasma picture (see *e.g.* refs. [19–21]). While the Glasma initially contains string-like features, it is assumed to be unstable and will rapidly turn into a QGP. In our picture we instead assume that the strings survive the dense environment and form ropes which then fragments.

In this paper, we have shown that string shoving reduces the string density, resulting in a smaller overlap between the stings forming ropes. This reduces the effective string tension, which is used during rope hadronization. That will in turn cause lower yield of strangeness in dense environments. This would dampen the linear rise in the strangeness yields for AA using only rope effects as observed before [8]. Whether it will produce the saturation behaviour as observed in data remains to be seen.

We have also observed that the increase of κ_{eff} in rope hadronization, mainly affects the flavour of the hadrons and its influence on the primary hadron vertices are small, especially when compared to the effects of string shoving. While there are still some caveats as discussed in the section 1, such as the strings not being pushed in space–time before hadronization, we are working towards a proper combination of both string shoving and ropes. This would enable the string shoving to properly affect the space-time overlaps between string, so that the dilution of strings from the shoving can directly affect the κ_{eff} calculation in the rope hadronization.

The primary hadron vertices are the main input to the hadronic rescattering model in PYTHIA8, hence, one could expect significant effects from the spreading of the vertices due to shoving. Also, the rescattering has effects on the flavour

composition of the final state, and it is reasonable to assume that there would be some interplay with rope model.

String shoving and hadronic rescattering together could provide an enhanced final-state collectivity in both small and large systems. Impact from hadronic rescattering in Angantyr ideally would be additive to that from string shoving, and they would build on each other. This non-trivial effect needs proper correction to the vertices of the primary hadrons, which is the work done in this paper. By consistently combining shoving, ropes and rescattering, we hope to achieve a consistent and complete picture for final-state collectivity in all collision systems.

Acknowledgements

We thank Gösta Gustafson and Christian Bierlich interesting discussions and important input to this work.

This work was funded in part by the Knut and Alice Wallenberg foundation, contract number 2017.0036, Swedish Research Council, contracts number 2016-03291, 2016-05996 and 2017-0034, in part by the European Research Council (ERC) under the European Union's Horizon 2020 research and innovation programme, grant agreement No 668679, and in part by the MCnetITN3 H2020 Marie Curie Initial Training Network, contract 722104.

References

[1] C. Bierlich, G. Gustafson, L. Lönnblad, and H. Shah, "The Angantyr model for Heavy-Ion Collisions in PYTHIA8," *JHEP* **10** (2018) 134, 1806.10820.

[2] B. Andersson, G. Gustafson, G. Ingelman, and T. Sjöstrand, "Parton Fragmentation and String Dynamics," *Phys. Rept.* **97** (1983) 31–145.

[3] **ALICE** Collaboration, S. Acharya *et. al.*, "Centrality and pseudorapidity dependence of the charged-particle multiplicity density in Xe–Xe collisions at $\sqrt{s_{\mathrm{NN}}}$ =5.44TeV," *Phys. Lett. B* **790** (2019) 35–48, 1805.04432.

[4] C. Bierlich, G. Gustafson, L. Lönnblad, and A. Tarasov, "Effects of Overlapping Strings in pp Collisions," *JHEP* **03** (2015) 148, 1412.6259.

[5] C. Bierlich, G. Gustafson, and L. Lönnblad, "Collectivity without plasma in hadronic collisions," *Phys. Lett. B* **779** (2018) 58–63, 1710.09725.

[6] C. Bierlich, S. Chakraborty, G. Gustafson, and L. Lönnblad, "Setting the string shoving picture in a new frame," *JHEP* **03** (2021) 270, 2010.07595.

[7] C. Bierlich, S. Chakraborty, G. Gustafson, and L. Lönnblad, "Jet modifications from colour rope formation in dense systems of non-parallel strings," 2202.12783.

[8] C. Bierlich, S. Chakraborty, G. Gustafson, and L. Lönnblad, "Strangeness enhancement across collision systems without a plasma," 2205.11170.

[9] T. Sjöstrand and M. Utheim, "A Framework for Hadronic Rescattering in pp Collisions," *Eur. Phys. J. C* **80** (2020), no. 10 907, 2005.05658.

[10] C. Bierlich, T. Sjöstrand, and M. Utheim, "Hadronic rescattering in pA and AA collisions," *Eur. Phys. J. A* **57** (2021), no. 7 227, 2103.09665.

[11] R. J. Glauber, "Cross-sections in deuterium at high-energies," *Phys. Rev.* **100** (1955) 242–248.

[12] M. L. Miller, K. Reygers, S. J. Sanders, and P. Steinberg, "Glauber modeling in high energy nuclear collisions," *Ann. Rev. Nucl. Part. Sci.* **57** (2007) 205–243, nucl-ex/0701025.

[13] V. N. Gribov, "Glauber corrections and the interaction between high-energy hadrons and nuclei," *Sov. Phys. JETP* **29** (1969) 483–487.

[14] A. Bialas, M. Bleszynski, and W. Czyz, "Multiplicity Distributions in Nucleus-Nucleus Collisions at High-Energies," *Nucl. Phys. B* **111** (1976) 461–476.

[15] T. Sjöstrand and M. van Zijl, "A Multiple Interaction Model for the Event Structure in Hadron Collisions," *Phys. Rev. D* **36** (1987) 2019.

[16] T. Sjöstrand, "Jet Fragmentation of Nearby Partons," *Nucl. Phys. B* **248** (1984) 469–502.

[17] S. Ferreres-Solé and T. Sjöstrand, "The space–time structure of hadronization in the Lund model," *Eur. Phys. J. C* **78** (2018), no. 11 983, 1808.04619.

[18] G. S. Bali, "Casimir scaling of SU(3) static potentials," *Phys. Rev.* **D62** (2000) 114503, hep-lat/0006022.

[19] T. Lappi and L. McLerran, "Some features of the glasma," *Nucl. Phys. A* **772** (2006) 200–212, hep-ph/0602189.

[20] R. Venugopalan, "From Glasma to Quark Gluon Plasma in heavy ion collisions," *J. Phys. G* **35** (2008) 104003, 0806.1356.

[21] F. Gelis, "Color Glass Condensate and Glasma," *Int. J. Mod. Phys. A* **28** (2013) 1330001, 1211.3327.

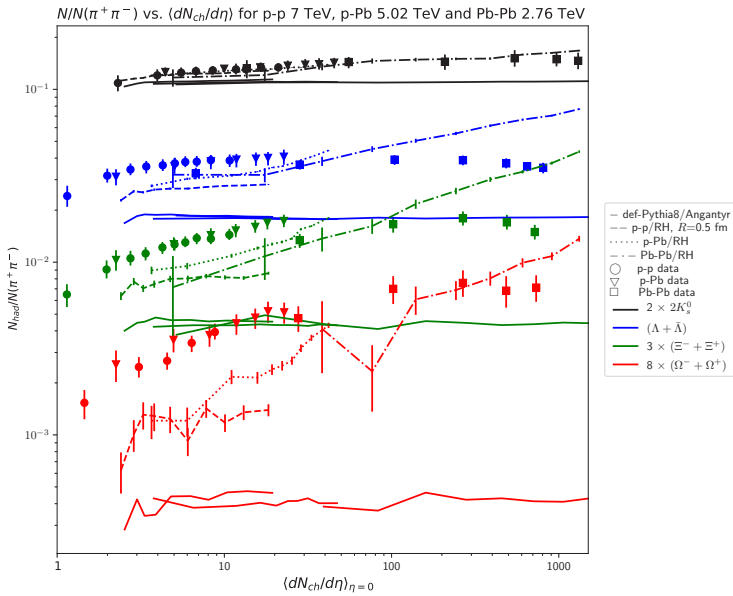

Printed by Media-Tryck, Lund 2022 NORDIC SWAN ECOLABEL 3041 0903

LUND UNIVERSITY

Faculty of Science
Department of Astronomy
and Theoretical Physics

ISBN 978-91-8039-348-5